CHARACTERIZATION OF THE COPPER RESISTANCE MECHANISM IN *STREPTOCOCCUS PNEUMONIAE*

Yue Fu

Submitted to the faculty of the University Graduate School
in partial fulfillment of the requirements
for the Degree
Doctor of Philosophy
in the Department of Molecular and Cellular Biochemistry
Indiana University
February 2015

Accepted by the Graduate Faculty, Indiana University, in partial fulfillment of the requirements for the degree of Doctor of Philosophy.

Doctoral Committee

David P. Giedroc, Ph.D.

Charles E. Dann III, Ph.D.

Michael VanNieuwenhze, Ph.D.

Martha G Oakley, Ph.D.

Date of Oral Defense
December 17th , 2014

© 2015
Yue Fu

Acknowledgements

I would like to thank, first and foremost, my thesis advisor, Dr. Daivd P. Giedroc, for his great help and guidance during the past five years. I have learnt many things from him, which would have significant impact for my future career. I am indebted to my research and thesis committees, Dr. Charles E. Dann III, Dr. Michael VanNieuwenhze, Dr. Carl Bauer and Dr. Martha G. Oakley. Although it is hard to fully express my deep gratitude for their persistent support, I thank all of them for always opening their door for me.

To Dr. Malcolm Winkler. Without his support, the biological study presented in this dissertation won't be possible. To Dr. Hongwei Wu. Without his great effort, it will be really hard for me to calculate the solution structure of apo-sCupA and perform dynamic study. I also appreciate the collaboration with Kevin Bruce, Dr. Ho-ching Tiffany Tsui, Dr. Khadine A. Higgins and John P. Lisher. Their collaborative work makes the CupA story better than I deserved. For the thesis writing, I deeply appreciated all my committees who took time and provided suggestions on my writing. I also express many thanks to Dr. Joseph Braymer for his proof-reading and discussion.

To my wife Yan Yang and my dear parents, my motivation for pursuing this Ph.D. degree is from all of you. Thanks for your support during this five years.

To my friends, colleagues, mentors, and lab members, and many of those who I failed to mentioned in this short page. No matter where you were and where you are, I want you know that I cherish our friendship and will remember each single moment you shed light on my life. I appreciate every meeting and every interaction with each of you.

Yue Fu
CHARACTERIZATION OF THE COPPER RESISTANCE MECHANISM IN *STREPTOCOCCUS PNEUMONIAE*

Pneumococcal related disease is an infection caused by *Streptococcus pneumoniae* (pneumococcus), including but not limited to otitis media, pneumoniae and meningitis. About 40 % of the infections are caused by drug resistant *Streptococcus pneumoniae* (DRSP). The prevalence of DRSP requires identifying novel targets for fighting against pneumococcal related diseases. The bacterial copper homeostasis machinery emerges as one important determinant for survival and virulence for bacteria in human host and serves as one potential drug development target. One cop operon (copY-cupA-copA) has been demonstrated to be essential for copper resistance in *S .pneumoniae* cells. The transcription of the cop operon is induced in *S. pneumoniae* isolated from the lungs and nasopharynx of intranasally infected mice and is required for bacterial growth in nasopharynx. The cop operon encodes three proteins, the copper-specific transcriptional regulator CopY, a protein of unknown function prior to this thesis work CupA and a copper-exporting P_{1B} type ATPase CopA. In my thesis work, CupA has been shown to represent a novel class of copper chaperone widely distributed among lactobacillus and streptococcus, which lack CopZ-like Cu(I) chaperones identified in *Enterococcus hirae* and *Bacillus subtilis*. Subcellular cell fractionation experiment confirms that CupA harbors a single N-terminal membrane-spanning helix, thus is the first identified cell membrane-anchored copper chaperone. The membrane association may facilitate copper loading onto CupA as copper gets into the bacterial cell. Cell growth experiments reveal that a Cu(I)-binding competent, membrane-localized CupA is obligatory for bacterial copper resistance. The crystal structures of the soluble domain of

CupA (sCupA) and N-terminal MBD of CopA ($CopA^{MBD}$) in the Cu(I) bound state reveal isostructural cupredoxin-like folds each harboring a binuclear Cu(I) cluster unprecedented in bacterial copper trafficking. NMR studies reveal unidirectional Cu(I) transfer from the low-affinity site (S2 site) on sCupA to the high-affinity site (S1 site) of $CopA^{MBD}$. NMR solution structure of apo-sCupA adopts the same fold as the crystal structure of Cu(I)-bound sCupA with the exception of a flexible Cu(I) binding loop between β7 and β8. Backbone and side chain NMR dynamic study show the side chains of residues in S1 site are pre-arranged for Cu(I) binding while side chains of residues in S2 site are completely disordered. Cell growth analysis shows that the high affinity S1 Cu(I) site is dispensable for cellular Cu(I) resistance, while the low affinity S2 Cu(I) binding site is essential for bacterial growth under copper stress, which is in consistent with the hypothesis that S2 is more involved in Cu(I) transfer to CopA for efflux. *All above establishes the first Cu(I) chaperone required for copper resistance in bacteria in contrast to the CopZ-like chaperones.*

The study in my dissertation leads to two further important questions which will require additional investigation. One is what the mechanism of a protein-protein interaction is between CupA and CopA and the second one is there any interplay between copper resistance and redox homeostasis systems in *S. pneumoniae* cells. The answers to those two questions may help us to better understand the biology of *S. pneumoniae*, which might shed light on combating the drug resistance issue of DRSP.

David P. Giedroc, Ph.D.

Charles E. Dann III, Ph.D.

Michael VanNieuwenhze, Ph.D.

Martha G. Oakley, Ph.D.

Table of Contents

Acknowledgements iv

Abstract v

Table of Contents viii

List of Figures xi

List of Tables xiii

Table of Abbreviations xiv

CHAPTER I: The functional role of copper in biology and of the host-pathogen interface **1**

1.1 Copper chemistry **1**

1.2 Cellular copper toxicity **2**

1.3 Copper uptake and trafficking in human cells **4**

1.4 The driving force for copper trafficking in cells **9**

1.5 Copper flow in the human host cell can be shifted towards phagolysosome **9**

1.6 Copper homeostasis system in bacterial pathogens **10**

1.6.1 Most bacteria appear to lack a dedicated copper uptake system 10

1.6.2 Copper resistance determinant in the extracellular space of pathogens 12

1.6.3 Cu(I) Sensing in Bacteria 14

1.6.4 Cu buffering by low molecular weight thiols (LMWT) 17

1.6.5 CopZ-like Copper Chaperones 18

1.6.6 Cu(I) delivery to P_{1B}-type ATPase and Cu(I) transport across bacterial cell membrane 21

1.6.7 Cu(I) delivery to the HME-RND complex by periplasmic Cu(I) chaperones and Cu(I) transporting to the extracellular space through heavy metal resistance-nodulation-cell division (HME-RND) complex 25

1.7 Scope of dissertation research **27**

CHAPTER II: CupA is a novel Cu(I) chaperone in *S. pneumoniae* **29**

2.1 Introduction **29**

2.2 Methods **31**

2.2.1 Bioinformatics analysis 31

2.2.2 Protein expression and purification 31
2.2.3 Cu(I) form Protein crystallization 32
2.2.4 X-ray data collection, structure determination and refinement 32
2.2.5 Apo-sCupA backbone and side chain resonances assignments 33
2.2.6 ICP-MS analysis 34
2.2.7 Cu(I) Binding Affinity Measurements 35
2.2.8 Western blotting to quantitate cellular expression levels of CupA and CopA in various *cupA* or *copA* mutants 36
2.3 Results 37
2.3.1 Both CupA and CopA are required for Cu resistance and localize to the plasma membrane 37
2.3.2 Copper binding by sCupA and $CopA^{MBD}$ 46
2.3.3 Crystallographic structures of sCupA and $CopA^{MBD}$ 46
2.3.4 Identification of the high and low affinity Cu(I) sites in sCupA and $CopA^{MBD}$ .. 55
2.3.5 Cu(I) is transferred from the S2 site on sCupA to the S1 site on $CopA^{MBD}$ 60
2.3.6 Cu(I) coordination by CupA but not by $CopA^{MBD}$ is essential for copper resistance of *S. pneumoniae* 61
2.4 Implication of the work 67
CHAPTER III: Solution structure of apo-sCupA and the functional role of each Cu(I) binding site in CupA 75
3.1 Introduction 75
3.2 Methods 77
3.2.1 Measurement of apo-sCupA backbone dynamics 77
3.2.2 Measurement of apo-sCupA side chain dynamics 77
3.2.3 Apo-sCupA structure calculation 78
3.2.4 *In vitro* redox potential measurement 79
3.2.5 CupA oxidation by Cu(II) 80
3.2.6 *In situ* thiol-labeling experiment 80
3.3 Results 81
3.3.1 Resonance Assignments and Solution Structure of apo CupA 81
3.3.2 Dynamics of the Cu(I) Binding β7-β8 Loop. 86
3.3.3 Differential biological functions for each Cu binding site in CupA 91
3.3.4 Oxidation state of CupA in cells 96
3.3.5 A heterologous copper chaperone expressed and localized to the plasma membrane does not provide cellular copper resistance 103

3.3.6 The metal binding site or entry site on CopA is required for Cu resistance at high Cu 105
3.4 Implication of the work 107
Chapter IV: Characterization of Cu(I)-specific regulator CopY in *S. pneumoniae* 112
4.1 Introduction 112
4.2 Methods 113
4.2.1 Protein expression and purification 113
4.2.2 Cu(I) Binding Affinity Measurements 114
4.2.3 Intial NMR study on CopY 115
4.3 Results 115
4.3.1 Copper and Zinc binding affinities of *Spn* CopY 115
4.3.2 Initial NMR study on *Spn* CopY 120
4.4 Summary 120
Chapter V: Future work and Perspectives 123
Appendix 126
Appendix I Assignments of backbone resonances of extracellular loop 1 of FtsX ($FtsX^{ECL1}$) from *S. pneumoniae* 126
Methods 126
Protein expression and purification 126
FtsxECL1 resonance assignment 127
Results 127
Complete backbone assignments of $FtsX^{ECL1}$ construct 127
Appendix II Backbone assignments of each metallation states 129
Appendix III Sample Dyanfit script for Cu(I) binding affinity measurement. 135
BCA binding experiments 135
BCS binding experiments 136
Appendix IV XAS study of Cu(I) coordination geometry 137
Methods 137
X-ray Absorption Spectroscopy (XAS) 137
XAS Data Reduction and Analysis 137
Results 139
Appendix V. Strain used in the work 148
Reference 150
Curriculum vitae

List of Figures

Figure 1:Identified mechanism of copper toxicity for bacterial cell..... 3
Figure 2: Pathways of copper transport, trafficking, sensing and resistance in several well-studied bacterial pathogens..... 7
Figure 3: Cartoon representation of the trimeric structure of hCtr1 derived from cryo-electron microscopy reconstructions..... 8
Figure 4: Molecular structures of Cu(I)/Cu(II) bound CopC..... 11
Figure 5: Molecular structures of (a) Cu(I) and (b) Cu(II)-bound *Candida albicans* SOD5..... 13
Figure 6: Molecular structures of two Cu(I)-specific metalloregulatory proteins..... 15
Figure 7: Structures of periplasmic Cu(I) chaperone CusF, Cu(I) chaperone CopZ, and the apo-structure of the Cu(I)-effluxing P_{1B}-type ATPase CopA..... 19
Figure 8: Cartoon of a mechanistic model of Cu(I) efflux across the bacterial inner membrane..... 20
Figure 9: Multiple sequence alignment of CupA homologs..... 39
Figure 10: Phylogenetic reach of the putative copper chaperone CupA..... 40
Figure 11: Δ*cupA* and Δ*copA Spn* strains are highly sensitive to copper toxicity..... 42
Figure 12: Growth curves of several *cupA* and *copA* mutant strains..... 43
Figure 13: Western blotting of different *cupA* and *copA* strains..... 44
Figure 14: Both CopA and CupA localize to the cell membrane fraction in *S. pneumoniae* D39..... 45
Figure 15: Representative binding curves obtained from anaerobic Cu(I) chelator competition experiments..... 47
Figure 16: Representative binding curves obtained from anaerobic Cu(I)-chelator competition assays..... 48
Figure 17: Structure representations of $Cu(I)_2$-sCupA..... 49
Figure 18: Structure representations of $Cu(I)_2$-$CopA^{MBD}$..... 50
Figure 19: Electrostatic surface potential of (**a**) sCupA and (**b**) $CopA^{MBD}$..... 52
Figure 20: Cu(I) sites of sCupA and $CopA^{MBD}$..... 53
Figure 21: Global superposition of CopAMBD with cupredoxin-fold containing protein..... 54
Figure 22: The Met-rich S2 site is the low-affinity site on both $CopA^{MBD}$ and sCupA and Cu(I) is transferred only from the S2 site of sCupA to the S1 site of apo-MBD..... 56
Figure 23: Cu(I) transfer observed from chemical shift of backbone resonances..... 57
Figure 24: NMR chemical shift perturbation analysis of sCupA and $CopA^{MBD}$ induced by Cu(I) binding..... 59
Figure 25: Apo-sCupA is unable to chelate Cu(I) from $Cu_{0.8}$ $CopA^{MBD}$ when mixed at a molar ratio of 1:1..... 62
Figure 26: Structural characterization of integrity of C74S sCupA..... 64
Figure 27: Mutagenesis of CupA Cu(I) binding residues partly or completely abrogates Cu(I) resistance by *S. pneumoniae*, but not in $CopA^{MBD}$..... 65
Figure 28: Growth rate analysis of *cupA* and *copA* mutant strains..... 66
Figure 29: Cu(I) resistance mechanism proposed based on data in chapter II..... 70
Figure 30: Close-up of the binuclear Cu(I) cluster in Cu_2-bound sCupA..... 82
Figure 31: Solution structure ensemble of apo-sCupA..... 83

Figure 32: Cartoon representation of apo-sCupA solution structure. 84
Figure 33: Structural overlay of apo and $Cu(I)_2$ form sCupA 85
Figure 34: Plot of backbone ^{1}H-^{15}N heteronuclear NOE. 87
Figure 35: Build-up curves as a function of intensity ratio (I_a/I_b) used to determine the intra-methyl ^{1}H-^{1}H dipole-dipole cross-correlated relaxation rate (η). 89
Figure 36: Plot of order parameters of each side chain εCH_3 group (S^2_{axis}) for three ligation states. 90
Figure 37: NMR spectra of apo-sCupA^{C111S} and Cu_1-sCupA^{C111S}. 93
Figure 38: ^{1}H,^{13}C-HMQC spectra of apo-sCupA^{C111SM116AH117A} and Cu_1-sCupA^{C111SM116AH117A} 94
Figure 39: Apo-sCupA is stoichiometrically oxidized by two mol•equivalents Cu(II) concomitant with the binding of Cu(I) to the partially oxidized S2 metal site. 95
Figure 40: Growth rate analysis of strains encoding CupA^{C111S} or CupA^{2MA} in BHI media in various Cu stress conditions. 97
Figure 41: Total cell associated Cu measurement for different cupA WT and mutant strains. 98
Figure 42: Redox potential measurement for (**a**) apo-sCupA and (**b**) apo-CopA^{MBD}. 99
Figure 43: Free thiol labeling with CupA. 101
Figure 44: Growth rate analysis using copper and oxidative stress. 102
Figure 45: Growth rate analysis of *copZ* chimeric strain. 104
Figure 46: Growth rate analysis of copA^{MBS} strain in various Cu stress conditions. 106
Figure 47: Multiple sequence alignment of CopY from different bacteria. 117
Figure 48: Binding curves obtained from anaerobic Cu(I) chelator competition to measure Cu(I) binding affinity of CopY 118
Figure 49: Binding curves obtained from zinc chelator competition to measure Zn(II) binding affinity of CopY 119
Figure 50: ^{1}H, ^{15}N-HSQC spectra of different metallated states of the C-terminal metal bindind domain of CopY (CopY$^{68-131}$). 121
Figure 51: ^{1}H, ^{15}N-HSQC spectra of different states of CopY. 122
Figure 52: Backbone assignments labeled on ^{1}H, ^{15}N-HSQC spectra of FtsXECL1. 128
Figure 53: Backbone assignment labeled on ^{1}H, ^{15}N-HSQC spectra of apo-sCupA. 129
Figure 54: Backbone assignment labeled on ^{1}H, ^{15}N-HSQC spectra of Cu_1-sCupA 130
Figure 55: Backbone assignment labeled on ^{1}H, ^{15}N-HSQC spectra of Cu_1-sCupA 131
Figure 56: Backbone assignment labeled on ^{1}H, ^{15}N-HSQC spectra of apo-CopA^{MBD}. 132
Figure 57: Backbone assignment labeled on ^{1}H, ^{15}N-HSQC spectra of Cu_1-CopA^{MBD}. 133
Figure 58: Backbone assignment labeled on ^{1}H, ^{15}N-HSQC spectra of Cu_2-CopA^{MBD}. 134
Figure 59: X-ray absorption near-edge spectra (XANES) of sCupA and CopA^{MBD}. 140
Figure 60: X-ray absorption spectroscopy for $Cu_{0.8}$ CopA^{MBD} 141

List of Tables

Table 1: Cu(I) binding affinities for sCupA and $CopA^{MBD\ *}$ 71
Table 2: Crystallographic data collection and refinement statistics 72
Table 3: Crystallographically determined copper coordination bond lengths and bond angles for Cu_2 sCupA and Cu_2 $CopA^{MBD\ a}$ 73
Table 4: Total cell-associated copper content (in ng/mg protein) of various *Spn* strains in the absence and presence of 0.2 mM added to the growth medium[a] 74
Table 5: NMR structural statistics for apo_sCupA. 109
Table 6: Cu(I) binding affinities of wild-type sCupA and sCupA mutants[a] 111
Table 7: EXAFS fits for $Cu_{0.8}$-$CopA^{MBD}$. 142
Table 8: EXAFS fits for $Cu_{0.8}$-sCupA. 144
Table 9: EXAFS fits for $Cu_{1.8}$-sCupA in 0.2 M NaBr. 146
Table 10: Strain table 148

Table of Abbreviations

AMS	4-Acetamido-4'-Maleimidylstilbene-2,2'-Disulfonic Acid, Disodium Salt
BCA	Bicinchoninic acid
BCS	Bathocuproine disulfonate
COSY	Correlation spectroscopy
4-DPS	4,4'-dithiodipyridine
ESI MS	Electrospray Ionisation Mass Spectrometry
IPTG	Isopropyl β-D-1-thiogalactopyranoside
GSH	Reduced glutathione
GSSG	Glutathione disulfide
HSQC	Heteronuclear single quantum coherence spectroscopy
HMQC	Heteronuclear multiple quantum correlation spectroscopy
MBD	Metal Binding Domain
NMR	Nuclear Magnetic Resonance
NOE	Nuclear overhauser effect
NOESY	Nuclear overhauser effect spectroscopy
PAGE	Polyacrylamide Gel Electrophoresis
TCEP	Tris-2-carboxyethyl phosphine
TOCSY	Total correlated spectroscopy

CHAPTER I: The functional role of copper in biology and of the host-pathogen interface

1.1 Copper chemistry

Streptococcus pneumoniae (*S. pneumoniae*) is a major bacterial pathogen in children and adults. It is normally a commensal bacteria for the upper respiratory tract of human and may invade other parts of human host under certain conditions. Depending on the infected tissues, pneumococcus can cause various diseases, from localized disease such as otitis media and sinusitis, to more serious cases like pneumonia and meningitis.[1] The health care cost for pneumococcus-related disease is tremendous and mostly comes from pneumococcus caused pneumonia. Drug resistance *S. pneumoniae* is another major cause of pneumococcus-related disease and is held responsible for causing more 7000 deaths annually in the U.S (data from CDC).

General mechanism of copper homeostasis systems from both prokaryotes and eukaryotes will be discussed in this chapter, serving as a foundation to introduce my work presented in the following chapters, which is focusing on studying copper homeostasis system in *S. pneumoniae*.

Copper in biological systens can exist in either the reduced, cuprous or Cu(I) ($3d^{10}$) state or the oxidized, cupric or Cu(II) ($3d^{9}$) state. The reduction potential of +150 mV for the one-electron reduction of Cu(II) to Cu(I) reveals that Cu(I) is the major oxidation state of copper in the reducing environment of the cellular cytosol or cytoplams (≈–220 mV).[2] Cu(I) is a soft acid while Cu(II) is borderline acid as classified by the Hard and Soft Acids and Bases (HSAB) principle.[3] As such, the metal binding sites in copper-utilizing or transporting proteins are formed primarily by cysteine, methionine and

histidine residues as first coordination shell ligands. Cu(I) is relatively unique in biological systems in that it can adopt thermodynamically very stable complexes characterized by a low coordination number (*n*) of 2-4. In contrast, Cu(II) adopts higher coordination number complexes, with *n*=4-6, with a preference for four-coordinate, distorted square planar complexes. Cu(II) complexes are also thermodynamically stable, since Cu(II) sits at the apex of the Irving-Williams series of divalent cation-small molecule chelate complex stabilties.[4,5] The abilities of copper to cycle between two oxidation states and to form thermodynaically stable and ligand exchange labile coordination complexes establish the foundation for understanding copper transport, sensing, trafficking, and utilization in biological systems.

1.2 Cellular copper toxicity

The mechanism by which copper impacts cell viability is a subject of ongoing investigation and may well involve a combination of effects depending on the microenvironmental niche of the organism. The original proposal posted protein and DNA damage caused by hydroxyl radical (OH•) derived by a Cu(I)-catalyzed Fenton reaction with hydrogen peroxide (H_2O_2) with concomitant formation of Cu(II); this reaction becomes then catalytic in the reducing milieu of the cytoplasm.[6] Indeed, the analogous reaction driven by Fe(II) has long been known to damage DNA and cause cell death.[7] Although exogenous H_2O_2 clearly potentiates the ability of copper to kill intracelllar bacterial pathogens within macrophages,[8] low molecular weight thiols (LMWTs) such as glutathione will chelate any free copper, rendering it incapable of cycling between Cu(I) and Cu(II) states[6] thus attenuating its capacity to perform Fenton-like chemistry. As a result, the ability of Cu(I) to catalyze the Fenton reaction within the

bacterial cytoplasm seems increasing unlikely; in contrast, there is some evidence to suggest that copper-mediated hydroxyl radical formation occurs in the periplasm of *E. coli* and by extension other Gram (–) bacteria.[6,9]

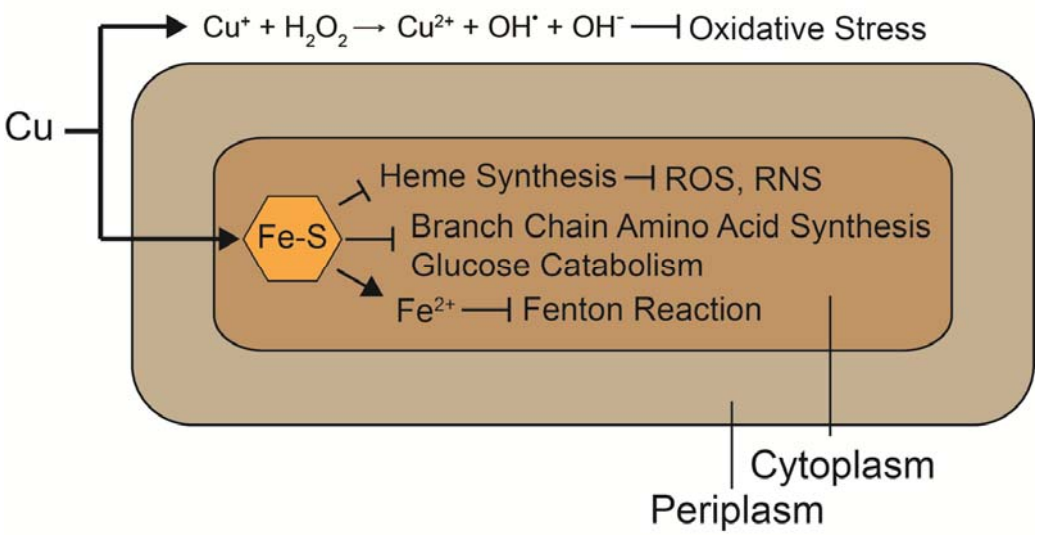

Figure 1: Identified mechanism of copper toxicity for bacterial cell.
The primary target to date intracellularly is [Fe-S] cluster, an important co-factor for enzymes involved in important biological pathways. [11–13]

More recent studies reveal that the exposed iron-sulfur clusters in metalloenzymes involved in branch-chain amino acid synthesis are primary targets of copper toxicity in *E. coli* (**Fig. 1**).[10] Cu(I) can inactivate the enzymes by displacing the iron atoms from the cluster in a reaction that does not require molecular oxygen. The displaced iron is then postulated to overload the cell and accelerate the Fe(II)-based Fenton chemistry if oxygen is present (**Fig. 1**).[10] Similar mis-metallation by excess copper of Fe sites in other iron-sulfur-containing enzymes has been demonstrated to occur in other bacteria affecting key metabolic pathways including glucose catabolism and heme biosynthesis (**Fig. 1**).[11–13] However, more work must be done to validate this model as a general mechanism of Cu toxicity, particularly in those organisms that lack iron-sulfur cluster-containing enzymes and in others, *e.g.*, lactic acid bacteria and *S. pneumoniae*, that thrive under conditions of considerable hydrogen peroxide generation.[14]

1.3 Copper uptake and trafficking in human cells

A cartoon representation of copper transport and trafficking from outside of the vertebrate host cell, *e.g.,* a macrophage, to a bacterial pathogen that has been engulfed by that macrophage is shown (**Fig. 2)**. In eukaryotes from yeast to mammalian cells, the acquisition of cellular copper requires a conserved plasma membrane-localized Cu(I) importer, Ctr1 (**Fig. 3**).[15] In the extracellular space, free copper is in the oxidized Cu(II) state; thus, for Ctr1 to transport Cu(I) across the cell membrane, Cu(II) must be reduced to Cu(I) by yet unidentified Cu(II) reductase in humans (**Fig. 2**). The mechanism by which human Ctr1 (hCtr1) transports Cu(I) has received considerable attention. Since Ctr1 lacks an identifiable ATP-hydrolysis domain, Cu(I) transport is ATP-independent.[16] hCtr1 has three transmembrane (TM) domains and exists as a symmetrical all α-helical

homotrimer in a native phospholipid bilayer[17] with the proposed Cu(I) translocating channel in the center of the trimer (**Fig. 3**). Four consecutive sets of methionine triads in the channel region contributed by residues from each monomer (Met43, Met45, Met150 and Met154) are proposed to be involved in Cu(I) capture and shuttling.[18] The fours triads span from the extracellular N-terminal "capture" domain to the transmembranous region. The organization of the triads suggests a stepwise transport model of Cu(I) across the plasma membrane via transient "bind-and-release" mechansim mediated by ligand exchange by the methionine triads within the channel.[18] The cytosolic C-terminus of Ctr1 harboring a His188-C189-H190 sequence has been shown to bind four Cu(I) as a Cu_4L_6 cuprous-thiolate polynuclear cluster[19] and is thought to be required to facilitate Cu(I) transfer to downstream cellular Cu(I) binding proteins, but plays no role in the kinetics of Cu(I) permeation.[20,21]

The copper trafficking hypothesis[22] posits that there is no free copper present in the cytosol and that Cu(I) is shuttled to different cellular targets by dedicated Cu(I) chaperones. The human Cu(I) chaperone Atox1/HAH1 has been characterized as a small cytosolic protein with the ferredoxin-like fold and the conserved Cys-xx-Cys Cu(I) binding motif (where x stands for any residue).[23,24] There are two models for Cu(I) loading onto Atox1 from Ctr1: (1) Atox1 receives Cu(I) from the Cu(I) binding sites in cytosolic C-terminal domain of Ctr1 directly via specific protein-protein interaction[20] or (2) glutathione functions as an intermediate between the cytosolic C-terminal domain of Ctr1 and Atox1 by receiving Cu(I) from Ctr1 and then delivering it to Atox1[25]. Both models assume that the Cu(I) chaperone is evenly distributed in the cytosol. Although Atox1 is constitutively expressed in *S. cerevisiae* and is present at ≈10 μM[22], there is

some question as to how the cell ensures that Atox1 is capable of sequestering all Cu(I) as soon as it enters the cytosol. Rather than a 3D-random search model, a recent study reveals that Atox1 can bind to liposomes, which function as mimic of plasma membrane, through interaction between the positively charged protein surface residues and the negatively charged moiety of the membrane *in vitro*[26]. Association with the plasma membrane would signficantly reduce the 3D-random search to two-dimensional search along the inner leaflet of the plasma membrane, which would facilitate Atox1 Cu(I) loading. Consistent with this hypothesis, although the copper binding of the membrane-binding deficient mutants of Atox1 remains the same *in vitro*, these mutants show decreased copper loading *in vivo*[26].

Identified targets for Cu(I) loaded Atox1 to transfer Cu(I) are Cu(I) transporting P_{1B}-type ATPase ATP7A and ATP7B, which are primarily located in the trans-Golgi network (TGN). P_{1B}-type ATPases transport metal ions, such as Cu(I) and Ag(I), across biological membranes.[8] The mechanism of Cu(I) transport by P_{1B}-type ATPase will be discussed in detail later. Upon reaching ATP7A and ATP7B, Cu(I) can be imported into TGN to be supplied to the maturation of different cuproproteins. Excess Cu(I) would cause the relocalization of ATP7A and ATP7B to intracellular vesicles. Cu(I) then can be exported out of the cytosol via vesicle-mediated fusion.

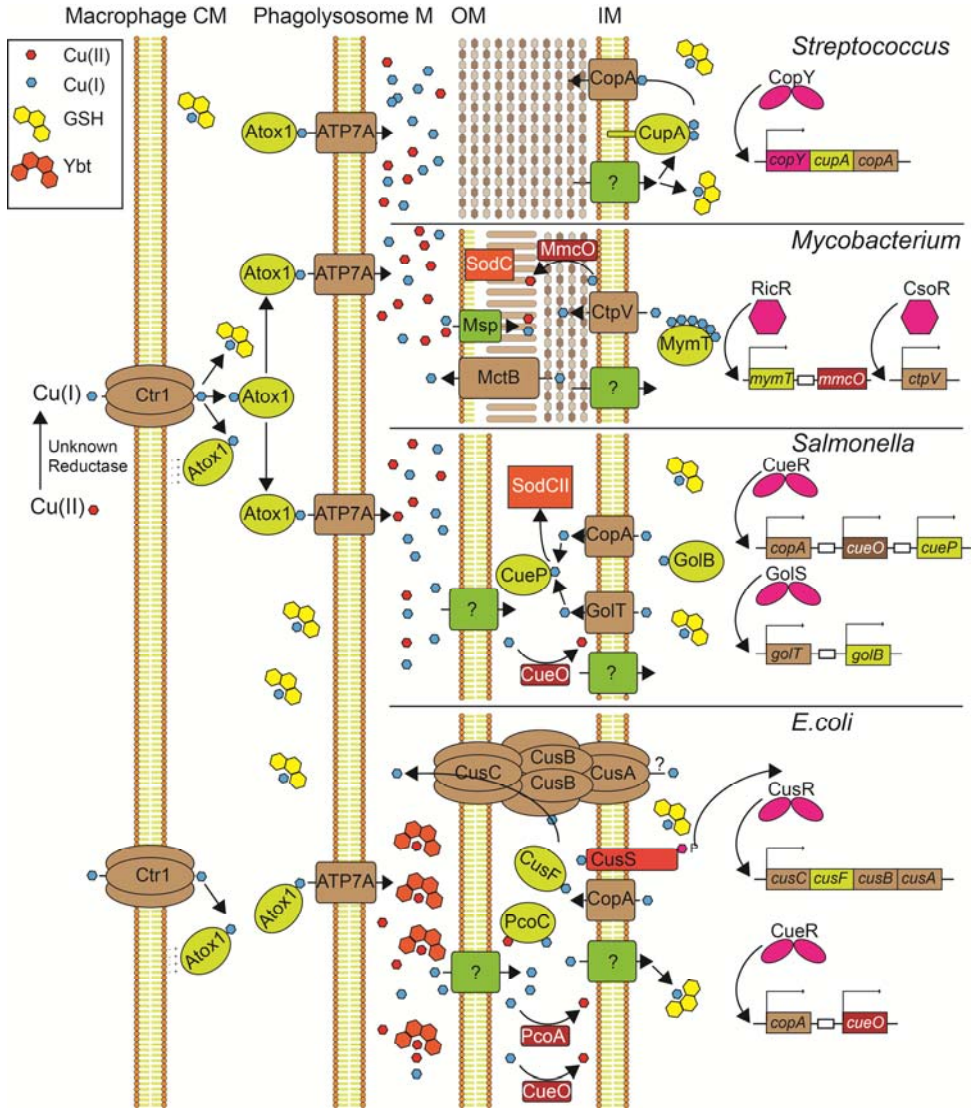

Figure 2: Pathways of copper transport, trafficking, sensing and resistance in several well-studied bacterial pathogens.

These include the Gram (+) pathogen, *S. pneumoniae*, *M. tuberculosis*, and two similar Gram (–) pathogens, *E. coli*, and *Salmonella spp*., at the host-pathogen interface. CM, cell membrane; M, membrane; OM, bacterial outer membrane; IM, bacterial inner membrane. *E. coli* CueO, plasmid-encoded PcoA and mycobacterial MmcO[151] are multi-copper oxidases (MCOs).[37] Both MmcO and an outer membrane channel MctB[31] are required for mycobacterial copper resistance. CtpV is a copper exporting ATPase that is required for full virulence of *M. turberculosis* in murine models of infection.[152] while Msp is a porin on the outer membrane of *M. tuberculosis*.[153] Over-expression of Msp genes induces copper stress in *M. turberculosis*, consistent with a role in Cu uptake.[153] The major components of bacterial copper homeostasis systems, including Cu(I) exporting P_{1B} type ATPases, copper chaoerones, and metalloregulatory proteins, are also shown (see text for details).[1,46,48,56,154]

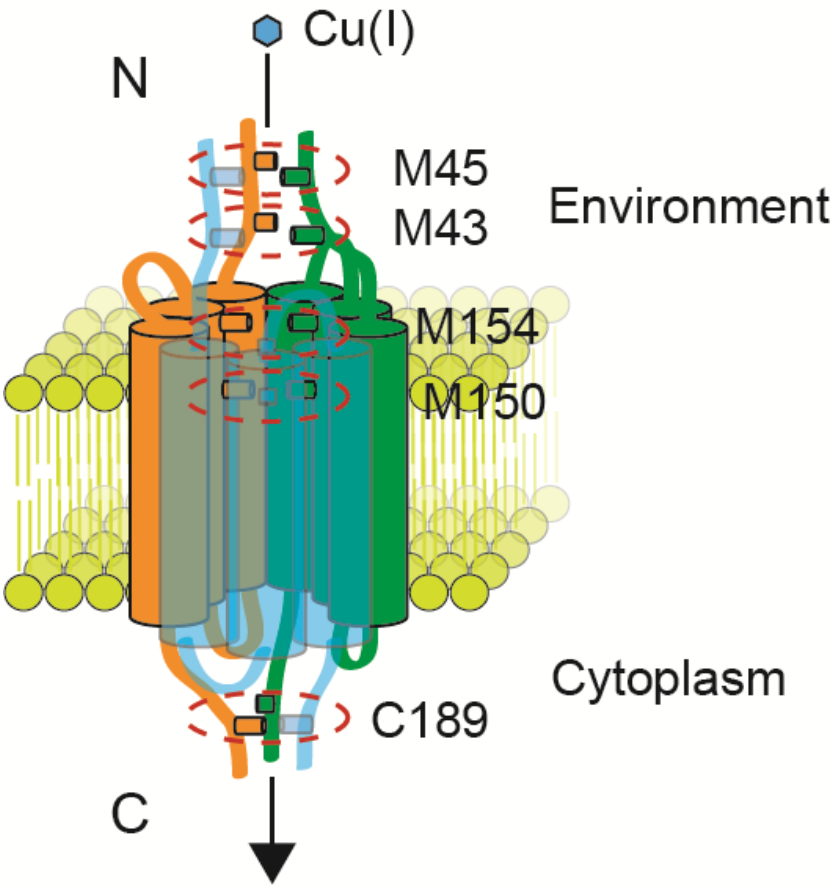

Figure 3: Cartoon representation of the trimeric structure of hCtr1 derived from cryo-electron microscopy reconstructions.[17]

1.4 The driving force for copper trafficking in cells

Thermodynamic gradient is proposed to be the driving force for directing the copper flow in human cells, which is exemplified by the increasing Cu(I) binding affinities along the copper flow pathway. Several efforts have been made to measure the Cu(I) binding affinities of Atox1 and the metal binding domains (MBD) of ATP7A and ATP7B.[27–29] MBD is the soluble, cytoplasmic domain of P_{1B}-type ATPase, which shares structural similarity with the copper chaperones and is postulated to be involved in Cu(I) transport. Based on an electrospray ionization mass spectrometry (ESI-MS) approach[27], Atox1 has lower affinity compared with MBDs of ATP7A, which is consistent with the thermodynamic gradient model. It should be noted that the Cu(I) binding affinities determined by ESI-MS are 3-4 magnitudes lower than the affinities determined by competition titration[28,29]. However, the general increasing trend of Cu(I) binding affinities along the pathway remains the same.

1.5 Copper flow in the human host cell can be shifted towards phagolysosome

A study using X-ray microprobe analysis has demonstrated that there is ~ 10 fold increase of Cu(I) within the mycobacteria-containing phagosomes in interferon-γ (IFN-γ) stimulated macrophages[30]. Using RAW264.7 macrophage as a model, proinflammatory signals (IFN-γ and lipopolysaccharide from bacteria) induce the expression of IFN-γ in macrophages, stimulating Cu(I) uptake and the trafficking of ATP7A to vesicles overlapping with phagosomal compartments.[8] The increased uptake of Cu(I) and relocation of ATP7A contribute to the accumulation Cu(I) in pathogen-containing phagosomes and the increased Cu(I) is proposed to facilitate bacterial killing through

copper toxicity mechanism that we have discussed. Indeed, copper resistance has been shown to be necessary for the virulence of mycobacteria[31]. To fight against the overloading of Cu(I), bacteria have to divert the copper flow out of their cellular environment through their copper homeostasis system.

1.6 Copper homeostasis system in bacterial pathogens

1.6.1 Most bacteria appear to lack a dedicated copper uptake system

The copper importing mechanism for bacteria is largely unknown, with several isolated reports on potential candidates to be the copper importer. In the copper-requiring cyanobacterium Synechocystis PCC 6803, a P_{1B}-type ATPase CtaA has been demonstrated to be responsible for copper uptake[32]. For Gram-negative bacteria, the work on CopABCD operon from *Pseudomonas syringae* indicates CopC, a periplasmic copper-binding protein and CopD, a probable inner membrane protein, function together for copper uptake into cytosol[33]. CopC has been shown to have two distinct copper-binding sites: Cu(II) site and Cu(I) site, which are 30 Å apart and oxidation of Cu(I)-CopC or reduction of Cu(II)-CopC results in the translocation of copper to different site (**Fig. 4**). [34]

For Gram-positive bacteria, the study on YcnJ protein from *Bacillus subtilis* suggests YcnJ may be involved in copper uptake.[35] Sequence alignment reveals that the N-terminal region of YcnJ shares sequence similarity with CopC from *P. syringae*, with all the Cu(II) binding residues conserved and the C-terminal region shares similarity with CopD. Under extracellular copper deplete condition, an eight-fold up-regulation of *ycnJ* gene was observed and under extracellular copper replete condition, a 2-fold downregulation was observed.[35] The Δ*ycnJ* strain also shows growth phenotype in copper-limited growth media, revealing that YcnJ may well function in copper uptake.

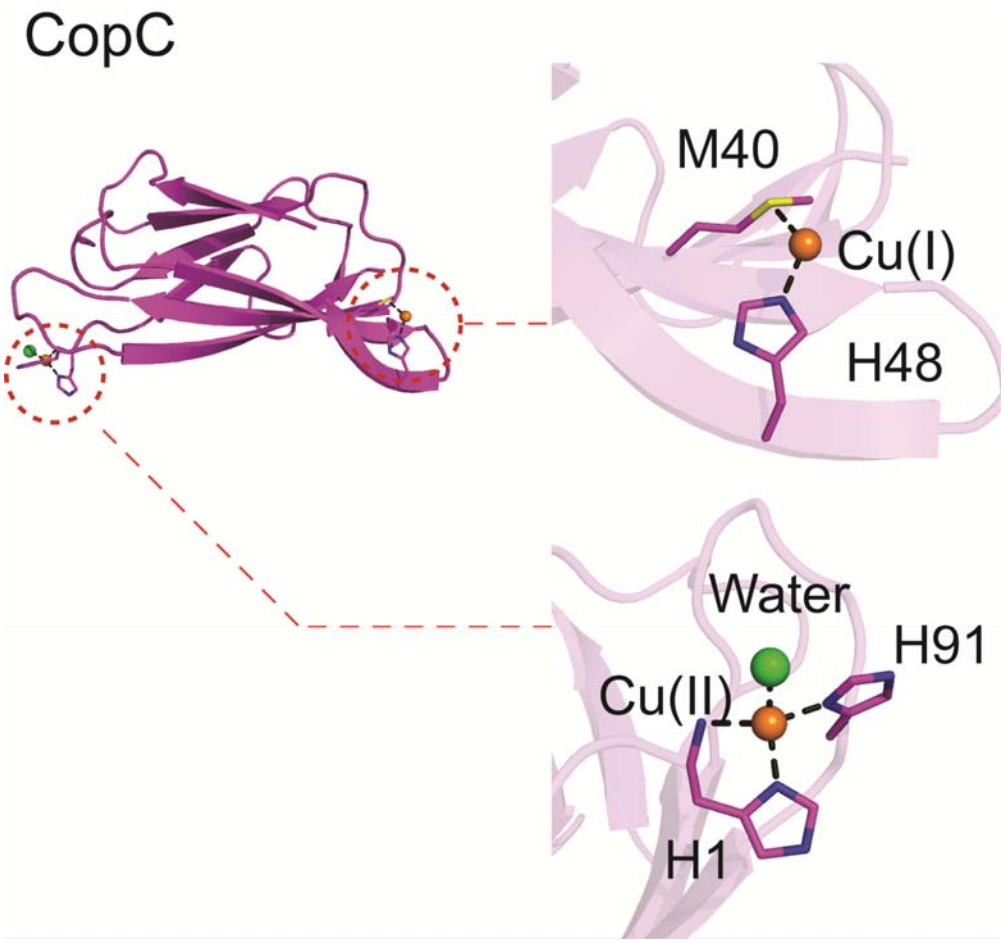

Figure 4: Molecular structures of Cu(I)/Cu(II) bound CopC.
Both copper sites are highlighted showing the coordination geometry for bound copper ions. [155]

The lack of dedicated copper uptake system in most bacteria is consistent with the limited copper utilization in bacteria. The predicted copper-binding proteins accounts for less than 0.3% of the annotated proteome in bacteria.[36] Of the few bacterial copper-binding proteins, most of them are either localized in the periplasmic space in Gram-negative bacteia, which is more oxidizing or are tethered to the plasma membrane and facing the extracellular space. For most human pathogens, copper may pose more as a threat than useful nutrition, especially in fighting against human host immune system as discussed above. The multi-level and well-regulated copper resistant systems to divert the copper flow out of bacterial cellular environment ensure the survival and virulence of the pathogens.

1.6.2 Copper resistance determinant in the extracellular space of pathogens

The extracellular space represents the dynamic environment in which bacterial cells reside. Bacteria secrete certain chelators into the extracellular space to lower free copper ion concentration before it reaches the bacterial cell. A copper binding siderophore, yersiniabactin (Ybt), with previously unappreciated superoxide dismutase-like (SOD) activity has recently been characterized in uropathogenic *E. coli* (UPEC).[37] Yersiniabactin serves as a bacterial extracellular Cu(II) sequester by binding to Cu(II) and Cu(II)-Ybt has been demonstrated to have SOD-like activity while apo-Ybt has no such activity. The dual function of Ybt gives the bacteria survival advantage once they are internalized into macrophages, where they encounter a toxic cocktail of elevated copper and superoxide during the human immune response.[8,38]

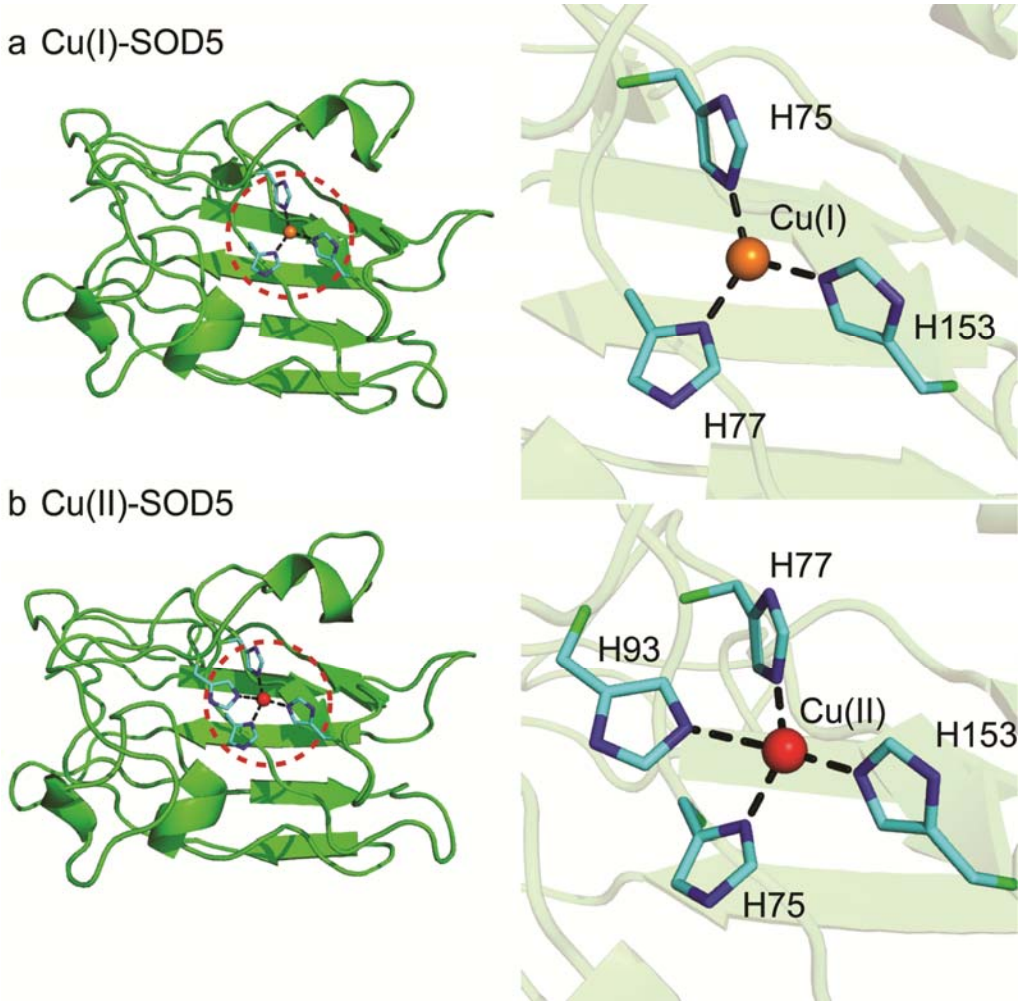

Figure 5: Molecular structures of (a) Cu(I) and (b) Cu(II)-bound *Candida albicans* SOD5.[39]

In the most prevalent human fungal pathogen *Candida albicans*, a novel SOD has been characterized (SOD5) (**Fig. 5**).[39] SOD5 from *C.albicans* represents a class of GPI-anchored extracellular SOD that is the Cu-only homologue to the classic Cu/Zn SODs. Structural studies on SOD5 have shown that although it retains the overall structure of Cu/Zn SODs, SOD5 is a monomeric copper protein lacking a zinc-binding site and the electrostatic loop proposed to function as superoxide guidance to catalyze the SOD activity (**Fig. 5**).[39] Cell culture experiments of *C. albicans* have revealed SOD5 is secreted as disulfide-oxidized apo-protein and can be readily metallated by extracellular copper ion due to the solvent exposed copper site.[39] Despite all the structural difference, the copper bound SOD5 has been shown to disproportionate superoxide with the kinetics similar to Cu/Zn SODs, approaching diffusion limits.[39] The open copper site makes this class of SOD well adapted to the challenges of the increased copper level at the host-pathogen interface. The bacterial homologous protein of SOD5 has not been identified, however, this might still be a strategy bacterial pathogens employ to fight against copper stress.

1.6.3 Cu(I) Sensing in Bacteria

The transcription and expression of the proteins involved in copper flow in bacteria are controlled by a group of proteins designated metalloregulators. Seven families of prokaryotic metalloregulator proteins have been characterized with distinct structural features as summarized in another review.[40] Three other families are characterized with only a subset associated with metal sensing (TetR[41,42], MarR[43] and LysR[44]).

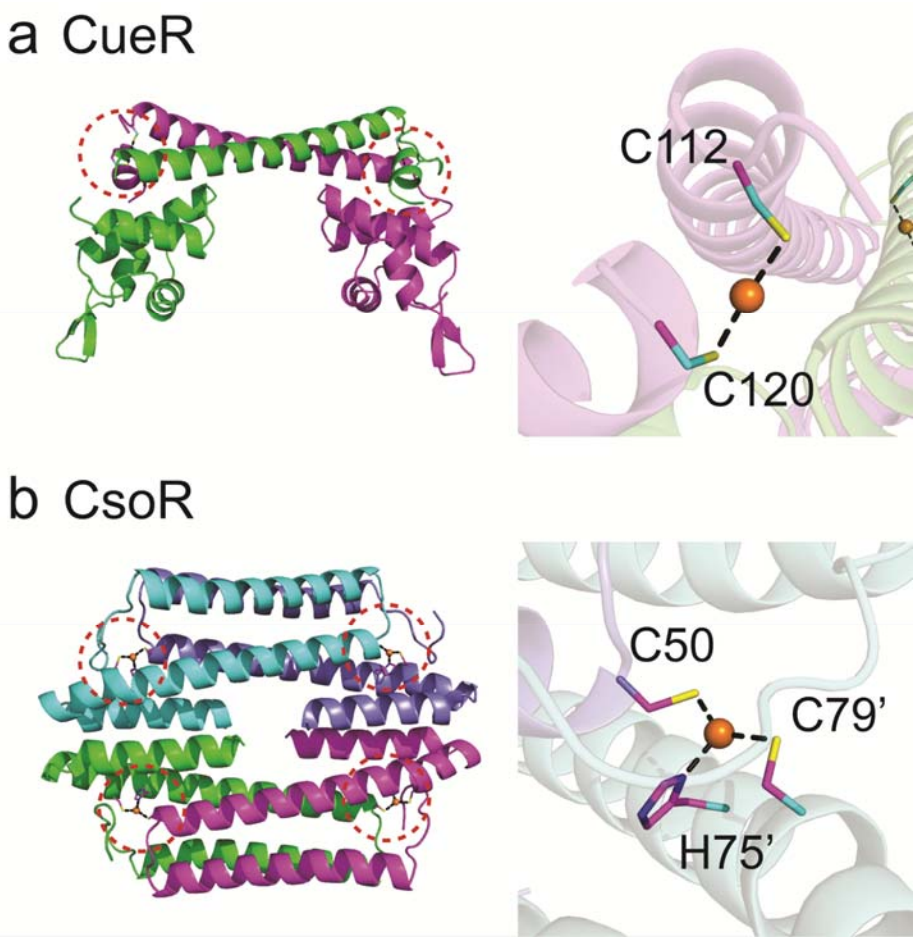

Figure 6: Molecular structures of two Cu(I)-specific metalloregulatory proteins. (a) Cu(I)-bound *E. coli* CueR;[46] (b) Cu(I)-bound CsoR from *Geobacillus thermodenitrificans*.[49] Protomers are differentially shaded with the Cu(I) binding sites *circled* and expanded (*right*).

There are no direct linkages between metals and the family of metalloregulators. The same family of metalloregulators has been shown to sense different metals while the same metal can be sensed by distinct family proteins. This is consistent with the "mix and match" approach in the evolution of metal sensing genes which could be mediated by horizontal gene transfer.[45] There are several identified Cu(I)-responsive metalloregulator in bacteria, including CueR in *E. coli*, CopY in *E. hirae* and *S. pneumoniae*, and CsoR in *M. tuberculosis and Geobacillus thermodenitrificans,* respectively.[1,46–49]

The interaction between Cu(I)-responsive metalloregulators and the cognate DNA serves as the basis in understanding metalloregulator mediated gene regulation. The different DNA-binding properties between Cu(I) and apo form of Cu(I)-responsive regulators are exploited to activate or repress the transcription of the downstream genes. CueR, the Cu(I)-responsive regulator in *E.coli*, binds to DNA with high affinity in both apo and Cu(I) states.[46] In the apo form, CueR binds DNA, suppressing transcription. The Cu(I)-CueR binds and unwinds DNA, activating the transcription.[50,51] There is no evidence that CueR undergoes a mechanism similar to the thiol ligand exchange process as observed for Cu(I) chaperones[52] to facilitate the transition between apo and Cu(I) states. So the high Cu(I) binding affinity[46] would pose a high energy barrier for the transition between apo and Cu(I) bound CueR, which is in contrast to the efficient regulation. The emerging field of applying single molecular technique to study the mechanism of protein-DNA interaction of CueR has provided one possible approach to switch off the transcription activation by replacing the incumbent Cu(I)-CueR with apo-CueR on the DNA.[53]

Other than Cu(I) sensing in cytoplasm by Cu(I)-responsive regulators, Gram-negative bacteria has to respond to elevated copper level in the periplasm and initiate transcriptional regulation of periplasmic copper resistance system (CueO[54] and CusCBA[55]) in the cytoplasm. A CusRS two-component system was identified and has been demonstrated to be essential for the induction of the *cusCFBA* operon, including the periplasmic Cu(I) chaperone CusF (**Fig. 7a**).[56] The histidine kinase CusS is predicted to be a membrane protein, with a periplasmic sensor domain. The sensor domain has been shown to bind Ag(I), which has similar chemical property as Cu(I), with micromolar affinity and the Ag(I) binding causes conformational change and dimerization of the sensor domain, which may be responsible for initiating the signal transduction across the cytoplasm membrane.[56]

1.6.4 Cu buffering by low molecular weight thiols (LMWT)

The tripeptide glutathione (GSH) is proposed to be one of the most abundant LMWT inside the bacterial cell with high affinity for Cu(I)[27]. Based on the high affinity for Cu(I) through the sulfhydryl group of the cysteine moiety, reduced glutathione (GSH) is proposed to form GSH:metal complex, which can effectively sequester toxic copper from the bulk cytosolic environment. In Gram-negative bacteria *E. coli*, the deletion of the glutathione synthesis machinery has no effect on the growth of cells under copper stress.[57] Gram-positive bacteria have a different story. Based on genome sequence analysis, *Streptococcus pneumoniae* does not encode glutathione synthesis machinery and the major source of glutathione is imported from the environment facilitated by the ABC transporter substrate binding protein, GshT. The Δ*gshT* strain, which fails to accumulate cytosolic glutathione, shows severe growth defect under copper stress.[58]

1.6.5 CopZ-like Copper Chaperones

CopZ from *Enterococcus hirae* is the first identified bacteria Cu(I) chaperone.[59] Structural studies reveal CopZ represents the bacterial Atox1-like copper chaperone with a ferrodoxin-like fold and conserved CXXC Cu(I) binding motif.[60] In cyanobacteria, a Atox1-like copper chaperone scAtx1 has also been discovered. The CopZ and CopZ-like proteins represent one of the major classes of Cu(I) in bacteria. Although some data suggests CopZ may transfer Cu(I) to the copper responsive regulator CopY,[59] the major function of CopZ-like chaperones is still proposed to be delivering Cu(I) to the exporting P_{1B}-type ATPases.[61]

The copper coordination chemistry of CopZ-like Cu(I) chaperones receives special attention (**Fig. 7b**). NMR solution structures of *Bacillus subtilis* CopZ suggest the S-Cu-S bond angle is ~ 120 °.[60] That raises the question whether there is a third solvent ligand. EXAFS studies on Atox1/HAH1 suggest it is possible to reconstruct Cu(I)-HAH1 with a S-Cu-S bond angle ~ 180 ° in a buffer containing no thiol ligand.[24] In cyanobacteria, one extra histidine is also involved in the coordination of Cu(I).[62,63] The low coordination number for Cu(I) is proposed to be important for copper transfer to happen between Cu(I) chaperones and metal binding domain (MBD) of copper transporting P_{1B}-type ATPase. It should be noted that despite the proposed central role of CopZ-like chaperones in Cu(I) delivery to P_{1B}-type ATPases, there is no experiment evidence in support of CopZ-like copper chaperone dependent protection against copper-mediated cell damage, nor there is no copper sensitivity in any of the CopZ mutants under copper stress.

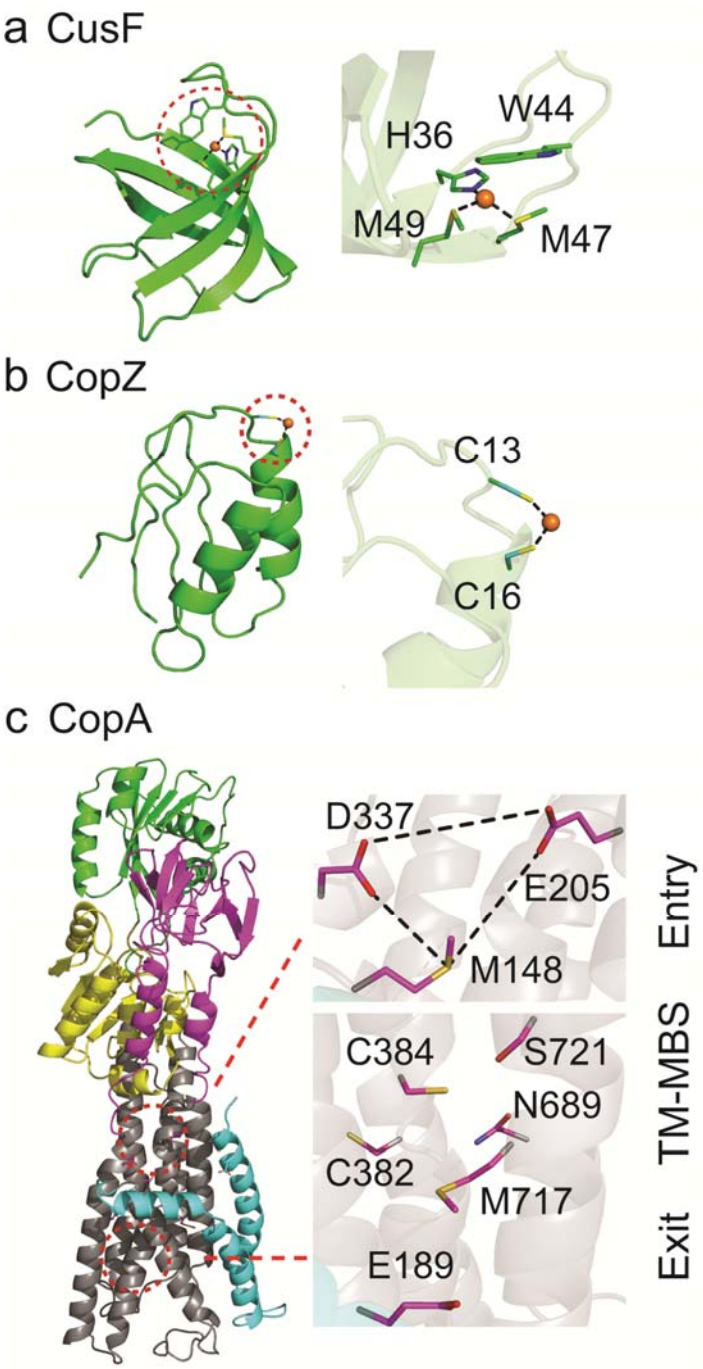

Figure 7: Structures of periplasmic Cu(I) chaperone CusF, Cu(I) chaperone CopZ, and the apo-structure of the Cu(I)-effluxing P_{1B}-type ATPase CopA.
(**a**) *E.coli* CusF, a periplasmic Cu(I) chaperone in the *cusCFBA* operon. (**b**) *B. subtilis* CopZ, representative of the Atox1-like ferredoxin-like fold metallochaperones. (**c**) *L. pneumophila* CopA with the proposed copper entry, transmembrane (TM-MBS) and exit sites indicated.[67,73] The MA and MB helices are shaded *cyan*, with the actuator (A, *yellow*), nucleotide-binding (N, *magenta*) and phosphorylated (P, *green*) domains also highlighted.

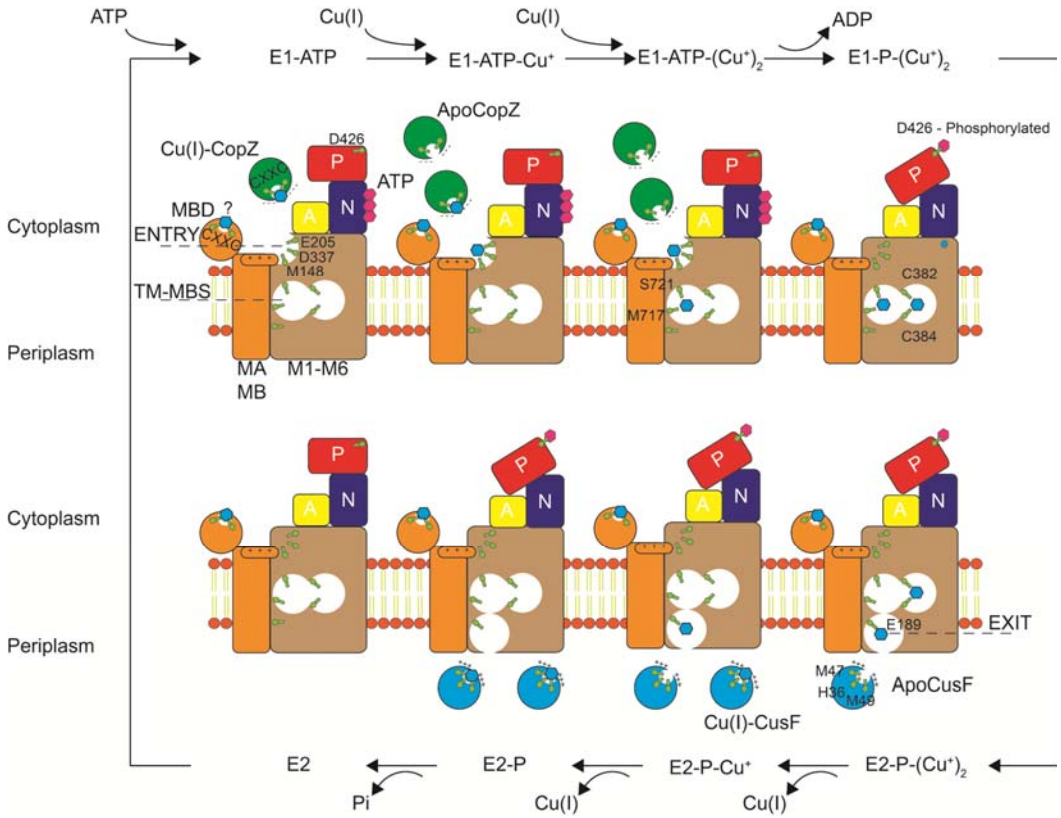

Figure 8: Cartoon of a mechanistic model of Cu(I) efflux across the bacterial inner membrane.

This figure summarizes recent structural and biochemical studies on CopA from *E. coli*, *A. fulgidus* and *L. pneumophila*. CopA is postulated to transport two Cu(I) ions per ATPase cycle. *E. coli* CusF has been shown to be metallated upon Cu(I) release from CopA through a protein-protein interaction.[77]

1.6.6 Cu(I) delivery to P_{1B}-type ATPase and Cu(I) transport across bacterial cell membrane

The work on copper transfer from copper chaperone to P_{1B}-type ATPase focuses primarily on the direct copper transfer between copper chaperone and the MBD of ATPase, the formation of the protein-protein complex and the ligand exchange transfer mechanism. The copper chaperone from cyanobacteria scAtx1 has been shown to form heterodimer with N-terminal MBD of PacS, the Cu(I) importing ATPase for thylakoid in a Cu(I) dependent manner.[64] Further NMR studies identified a protein-protein complex formed by yeast copper chaperone Atx1 and MBD of CCC2a, with a dominant species being a Cu(I) tri-coordinated by cysteines from both proteins.[52] This species is proposed to be the intermediate step for copper transfer, which establishes the ligand exchange model for protein-interaction-dependent Cu(I) transfer.

The copper transporting P_{1B}-ATPase is the most abundant P_{1B}-ATPase[65] and is recently classified into 1B-1 subclass of P_{1B}-ATPase using combined bioinformatics and biochemical data[66]. The core structure of P_{1B-1} ATPase consists of 6 transmembrane helices (TM), designated M1-6, starting from N-terminus to C-terminus (**Fig. 7c**).[67] The core α-helix bundle usually has two flanking N-terminal TMs (MA and MB) that are specific of the P_{1B-1} ATPase class and one or several N- and/or C-terminal metal binding domains (MBD). A conserved Cys-Pro-Cys (CPC) motif in TM4[59,68] is proposed to be involved in copper binding. The proposed general mechanism for P-type ATPase is based on the Albers-Post model (**Fig. 8**).[69,70] The E1 state of the enzyme has high affinity for substrate and marks the beginning of copper transporting cycle. ATP binding and hydrolysis results in substrate bound phosphoenzyme intermediate E1P and subsequent

E2P state. During E2P state, substrate is released to the extracellular space. The enzyme is then cycled back through E2 state to E1 state.[71]

Most of the work on P_{1B-1} ATPase has been carried out using *Archaeoglobus fulgidus* CopA (*Af*CopA) and *Legionella pneumophila* CopA (*Lp*CopA). The first high resolution x-ray crystallographic structure of metal-free apo *Lp* CopA has been used to model a candidate copper transport pathway within the transmembrane domain of CopA (**Fig. 8**).[67] This Cu(I)-translocation pathway is proposed to involve three spatially resolved Cu(I) binding sites termed entry, transmembrane and exit. The entry site is the first site that Cu(I) might encounter and consists of the conserved residues M148, E205 and D337 (**Fig. 7c**). The entry site is butressed by a cluster of positively charged residues, which constitute a platform helix as part of the linked P_{1B}-specific MB helix. The positively charged platform is believed to provide the docking site for the electronegative surface of the N-terminal MBD or the cognate copper chaperone dictated by charge complementarity. The MB helix has a pronounced kink induced by two consecutive and highly conserved Gly residues, G129 and G130 in *Lp* CsopA, with the C-terminal region of the MB helix hosting three of the positively charged residues of the platform.[67]

The mechanistic importance of the proposed copper entry site and the positive charge of the platform helix has been experimentally tested in *Af* CopA.[72] *Af* CopA exhibits approximately 50% amino acid similarity with the *Lp* CopA and the proposed copper entry site and docking platform are conserved. The copper chaperone *Af* CopZ contains a predicted electronegative patch which is complementary to the positively charged platform on *Af* CopA as judged by a homology model of *Af* CopA based on the structure of *Lp* CopA. Three major groups of mutations were characterized: (1) mutations

in the kink region of the MB helix designed to alter the local structure of the platform helix (kink mutant); (2) mutations designed to eliminate the positively charged residues in the platform (charge mutant) and (3) mutations to replace the coordination residues of the copper entry site (coordination mutant). If free Cu(I) is utilized as the copper donor (which is highly unlikely in the cytoplasmic environment) there is no observed difference in the kinetics of Cu(I)-stimulated ATP hydrolysis between among three mutants and the wild-type enzyme *in vitro*. This suggests that the platform and copper entry site are not required for chaperone-independent copper delivery to CopA. However, if Cu(I)-*Af* CopZ was used as copper donor, both the charge mutant and the MBS entry site mutant result in a loss of Cu(I)-stimulated ATPase activity. In striking contrast, the kink mutant has no impact on ATP hydrolysis. This latter observation is interesting because this Gly-Gly sequence is the site of a number of Menkes and Wilsons disease-causing mutations in ATP7A and ATP7B, respectively. That might suggest that the kinked MB helix is required for the structural integrity of the transporter in cells or otherwise attenuates metal transport rates via uncoupling of ATP hydrolysis and metal efflux, which is not typically measured in these assays. An analogous charge substitution mutant of *Af* CopZ in which candidate negatively charged residues predicted to physically interact with the platform helix were mutated to postively charged residues shows the same degree of attenuation in ATPase activity as the charge mutant of *Af* CopA. These data taken collectively are strongly consistent with the charge complementation model of Cu(I) chaperone-mediated Cu(I) transfer to CopA and might suggest that the local structure is of comparatively lesser importance in ATPase stimulation. Given the high Cu(I) binding affinity of copper chaperones, the copper is postulated to transfer from the chaperone to

the entry site via a mechanism similar to the proposed ligand exchange model.[52] However, further studies are required to obtain coordination chemistry details on the transfer process and there is as yet no evidence for a Cu(I)-trapped CopZ-CopA complex, a presumed intermediate on the Cu(I)-transfer pathway.

The binding of copper at the copper entry site of CopA is proposed to be transient.[67,73] Copper would be further delivered to the high affinity transmembrane copper binding site (TM-MBS).[74] The first report on the TM-MBS of *Af*CopA proposed two sites, both with femtomolar copper binding affinity.[74] Based on EXAFS, site I contains two cysteine residues from the conserved CPC motif in M4 helix and the tyrosine residue from the conserved IYNV motif in M5 helix. Site II is rather unique, formed by one asparagine residue from M5 helix and methionine and serine residues in M6 helix. The structural and further molecular dynamics (MD) studies give us a much deeper understanding of the TM-MBS.[67,73] Four of the six coordinating residues proposed based on *Af* CopA data were found to be positioned in the putative site I and II in the first crystal structure of the *Lp* CopA[67] while the tyrosine and asparagine residues from M5 helix require side-chain rearrangement to be close to the putative sites. Based on MD simulation, the site I formed by the two cysteine residues Cys382 and Cys384 from the CPC motif may be more important in transporting copper.[73]

The high affinity of TM-MBS for copper poses an energy barrier for releasing copper into the extracellular bulk solvent.[74] The presence of a putative Cu(I) exit site involving conserved glutamate and methionine residues may facilitate the copper release (**Fig. 7c**). Based on MD simulations of the *Lp* CopA structure, extracellular solvent was observed entering the TM domains from the periplasmic side. Solvent reaches the Glu189

in the exit site, outlining a putative Cu(I) release pathway. This solvent filled pathway is predicted to be wide enough for copper ion to be delivered from TM-MBS to the exit site. The Cys382 and Met717 residue from TM-MBS are found to be along the solvating channel and are proposed to be important in shuttling copper ion to the exit site. One conserved Pro residue involved in the structural rearrangement of MA and M5 helices is predicted to be important for the opening of the release pathway to the extracellular space. All the residues proposed based on MD simulation were tested by both *in vitro* ATPase activity assay and *in vivo* complementation of LpCopA into CopA deficient *E. coli*. Substitution of the Met in the TM-MBS and the Pro involved in the structural rearrangement are found to be detrimental in both types of experiments while mutations on other residues only show significant effects only in the *in vitro* experiment, which may be traced to the redundancy of the copper resistance system in *E. coli*.

1.6.7 Cu(I) delivery to the HME-RND complex by periplasmic Cu(I) chaperones and Cu(I) transporting to the extracellular space through heavy metal resistance-nodulation-cell division (HME-RND) complex

The periplasmic space in Gram-negative bacteria is a more oxidizing environment compared to the cytosolic space. The deletion of periplasmic copper resistance protein CusF has been shown to result in a more copper sensitive phenotype.[75] Structural and spectroscopic studies on CusF reveal a methionine rich copper site, which consists of two methionine residues, one histidine residue and the site is stabilized by cation-π interaction with a nearby tryptophan residue (**Fig. 7a**).[76] Recent evidence suggests that CusF gets Cu(I) loaded through interaction with cytosolic membrane copper exporting P_{1B}-type ATPase CopA were reported. The Cu(I) transfer from CopA to CusF has been shown to

be unidirectional and dependent upon the ATP hydrolysis. The transfer requires specific protein-protein interaction between CopA and CusF, since the replacement of either component by CusFs from other species results in undetectable Cu(I) transfer. Through immunoprecipitation experiments, the authors reveal preferred interaction between Cu(I)-CopA with apo-CusF when holo-CopA is in the E1.Cu(I) form, which is consistent with the model of Cu(I) movement during the CopA ATPase cycle.[77] Metallated CusF has been shown to deliver copper to CusB in the CusCBA HME-RND complex through specific protein-protein interaction with CusB.[78] Although the *in vitro* data suggests the Cu(I) transfer occurs in both direction between CusF and CusB and is distributed equally between these two proteins, it is possible the equilibrium would be shifted by translocating Cu(I) to the extracellular space by CusCBA complex as a whole and the net flow of Cu(I) is towards the extracellular space.[79]

CusCBA is a tripartite complex that spans both inner and outer membrane, which consists of CusA, a RND efflux pump, CusB, a periplasmic membrane fusion protein (MFP) and CusC, an outer membrane channel protein, with a 3:6:3 polypeptide ratio (**Fig. 2**).[80,81] The crystal structure of CusA suggests CusA exists as a homodimer and each monomer contains 12 TM helices and a periplasmic domain formed by two loops. A three methionine residues cluster (Met573, Met623 and Met672) is proposed to be the Cu(I) binding site receiving Cu(I) from periplasmic CusB protein, which may be delivered by CusF as discussed above. A more recent tri-element X-ray absorption spectroscopy (XAS) study exploiting protein-specific selenomethione labeling and Se, Ag and Cu XAS suggests that Cu(I)-CusB activates Cu(I) transfer from CusF to CusA into novel S_2(O/N) Cu(I) site formed by two Met and one Glu.[82] CusA, CusB and CusF

continue the theme of Met-rich Cu(I) coordination complexes in the more oxidizing periplasm as they are less susceptible to oxidation than the Cys-rich coordination sites that dominate in the cytoplasm.[82] There are two methionine residues (Met271 and Met755) in the periplasmic domain together with 3 pairs of methionine residues in the TM domain (Met391 and Met1009, Met486 and Met403, Met410 and M501) forming a potential copper ion relay network[83] to transport copper in a stepwise fashion. The existence of a periplasmic copper binding site and the spanning of the methionine relay network make it tempting to propose CusA transport the copper ion from both the cytoplasm and periplasm to the outer membrane channel for exporting.[54] The electronegative channel formed by CusB and CusC may facilitate copper export through negative potential gradient.[83]

1.7 Scope of dissertation research

Since the original discovery of Atx-1 like copper chaperone in 1999, there is considerable amount of work dedicated to characterize the copper chaperone and the copper transfer between copper chaperones and cellular metalloproteins or Cu(I) transporting P_{1B} type ATPase. Despite these progresses, it remains unclear the functional role of copper chaperone in bacterial cells. This is exacerbated by the fact that Atx-1 like copper chaperones are not obligatory for copper resistance in known organisms.

The two major questions that the work presented in this dissertation is designed to address are: (1) What is the molecular mechanism of copper resistance in bacterial pathogens to prevent copper overdose by human host? and (2) what is the functional role of copper chaperone in copper resistance system in bacteria? Studies are focused on the

novel copper chaperone protein CupA discovered in S. *pneumoniae*, which has not been found prior to this work.

In chapter II, efforts were made to characterize CupA from *S. pneumoniae*. CupA was characterized to be a novel membrane-anchored copper chaperone. The Cu(I) binding affinities and membrane localization of CupA are essential for the survival of bacterial cells under copper stress. In Chapter III, NMR solution structure of apo-sCupA and NMR dynamic studies revealed a flexible Cu(I) binding loop in CupA. S2 Cu(I) binding site in CupA was shown to be essential for copper resistance. In chapter IV, studies on the transcriptional regulator CopY were presented. Chapter V focuses on the future directions followed by the work discussed in previous chapters.

CHAPTER II: CupA is a novel Cu(I) chaperone in *S. pneumoniae*

2.1 Introduction

For *S. pneumoniae* to survive and cause disease in different host environments, it has to adapt to various conditions in the environments, including extracellular metal ion concentration. The concept of "nutritional immunity"[84] refers to host withholds essential metal, such as Fe and Zn, away from engulfed pathogens in the macrophages. Contrary to this, elevated Cu has been linked to efficient pathogen removal in macrophages. Thus, the bacterial metal homeostasis systems might serve as novel drug targets for combating drug-resistant pathogens with demonstrated examples from *Salmonella*.[85] *S. pneumoniae* has no known copper containing proteins, thus it is crucial for the bacterial cells to deal with copper toxicity. Copper resistance in *S. pneumoniae* is mediated by a single operon encoding the winged helix Cu(I)-dependent repressor, CopY[86], CupA,,of unknown function prior to this thesis work, and Cu(I)-effluxing P_{1B}-type ATPase CopA.[1] *S. pneumoniae* also encodes the TIM-barrel Cu(I)-binding protein CutC[87] previously shown to play a role in copper homeostasis in *Enterococcus faecalis*[88], but its expression is not induced by Cu in *Spn*[1]. *Spn* CopY is functionally equivalent to *Enterococcus hirae* CopY[89] and performs the role played by the copper metalloregulatory protein CsoR and CsoR-like regulators found in other Gram-positive human pathogens including *M. tuberculosis*[48,90], *S. aureus*[91] and *Listeria monocytogenes*[92]. Although the intracellular requirement for Cu(I) in *S. pneumoniae* is unknown[93], *S. pneumoniae* contains significant cell-associated copper[94], and adaptation to a high Cu(I) environment may be important for invasive disease. Total Cu(I) is replete in the nasopharynx and in lung tissues and *copA* expression is induced in *S. pneumoniae* residing in these tissues in intranasally

infected mice[1]. Deletion of *copA* leads to poor kinetics of colonization in the nasopharynx and delayed appearance and reduced bacterial loads in the lung[1]; consistent with this, signature-tagged mutagenesis reveals that strains inactivated in *cupA* and *copA* are attenuated in a murine model of lung infection and pneumonia[95].

However, the function of CupA was still unknown prior to this thesis work. In this chapter, a structurally novel copper chaperone-copper effluxer pair jointly mediates resistance to copper toxicity was characterized in *S. pneumoniae* D39 strain. CupA is a plasma membrane-anchored copper binding protein whose membrane localization and high Cu(I) binding affinity are required for cellular copper resistance. The crystallographic structures of sCupA and $CopA^{MBD}$ reveal a new functional twist on the common cupredoxin fold firmly associated with iron uptake in yeast and cytochrome *c* oxidase assembly and electron transfer.[96–98] Although I establish that the soluble domain of CupA (sCupA) is capable of transferring bound Cu(I) to N-terminal metal binding domain of CopA ($CopA^{MBD}$) in a thermodynamically favorable and kinetically facile reaction, the Cu(I) transfer between CupA and $CopA^{MBD}$ is not required for cellular copper resistance under conditions of acute copper stress. These data suggest that the primary function of membrane anchored CupA under these conditions is to chelate Cu(I) as soon as it enters the cytoplasm, rather than function as an obligatory chaperone to the MBD of CopA.

2.2 Methods

2.2.1 Bioinformatics analysis

The protein sequence of CupA from pneumococcus was subject to protein-BLAST search in NCBI. The multiple sequence alignment of CupA homologs from different bacteria were done using ClustalW algorithm.

2.2.2 Protein expression and purification

The pHis plasmid[99] was used to subclone sCupA (residues 29-123 of full-length CupA) and the $CopA^{MBD}$ (residues 1-99 of CopA). This vector encodes a His6 tag and TEV protease cleavage site at the N terminus to yield, following cleavage, three non-native N-terminal amino acids of the sequence GAM for sCupA (denoted residues 26-28 in the structure) and a single non-native N-terminal Gly in the case of CopAMBD(denoted Gly0). BL21 (DE3) competent cells were transformed with the resultant plasmids. For unlabeled proteins, an overnight culture of *E. coli*. cells was inoculated into Luria Broth (LB) media containing 100 μg/mL ampicillin. For the $^{15}N/^{13}C$ labeled proteins, an overnight culture of *E .coli*. cells was inoculated into M9 minimal media (pH 7.4) containing 100 μg/mL ampicillin, supplemented with $15NH_4Cl$ (1 g/L) (Cambridge Isotope Laboratories) and [$^{13}C_6$]-D-glucose (2.5 g/L) (Cambridge Isotope Laboratories). For both media, the cells were grown at 37 °C to OD600 = 0.6. Isopropyl β-d-thiogalactopyranoside (IPTG) was then added to a final concentration of 0.4 mM and cultures were continued at 16 °C for 20 h. The cells were harvested by centrifuging and kept at -80 °C. All the buffers in the purification were degassed and refilled with Argon using a Schlenk line right before use. To break the cells, the cells were resuspended in buffer R (25 mM Tris, pH 8.0, 200 mM NaCl, 5 mM TCEP). The resuspended cells were

lyzed by a sonic dismembrator (Fisher). The recombinant proteins were purified using HisTrap FF columns (GE Healthcare) using a gradient of imidazole from 10 mM to 300 mM in buffer R. The appropriate fractions were pooled and subjected to TEV protease cleavage at for 16 °C for 36 h. The proteins were further purified using HisTrap FF columns (GE healthcare) and Superdex 75 16/60 column (GE healthcare). The purity of the proteins was estimated to be >95 % as judged by SDS-PAGE and ESI-MS. Protein concentration was determined by A280 with an extinction coefficient of 4595 $M^{-1}cm^{-1}$ on an UV-visible spectrometer (HP/Agilent8453). The number of reduced thiols was 1.9 for sCupA and 1.7 for $CopA^{MBD}$ (both expected to be 2.0) as determined by anaerobic DTNB colorimetric assay. Mutants of sCupA and $CopA^{MBD}$ were generated using site-directed mutagenesis strategy (Stratagene), and mutant proteins were purified similarly.

2.2.3 Cu(I) form Protein crystallization

Cu(I)-sCupA was crystallized by hanging drop vapor diffusion at 20 °C against a well buffer of 30 % (w/v) PEG 3350, 0.1 M sodium citrate tribasic dihydrate pH 5.0 and Big CHAP Deoxy. Cryosolvent was prepared by using 35 % (w/v) polyethylene glycerol 3350 in the well solution. Cu(I)-$CopA^{MBD}$ was crystallized by hanging drop vapor diffusion at 20 °C against a well buffer of 28 % (w/v) polyethylene glycerol monomethyl ether 2000, 0.1M Bis-Tris pH 6.5. Cryosolvent was prepared by using 35 % (w/v) polyethylene glycerol monomethyl ether 2000 in the well solution.

2.2.4 X-ray data collection, structure determination and refinement

For $CopA^{MBD}$, diffraction data for the native data set were collected at -160 °C on an R-AXIS IV+ detector at Indiana University, Bloomington. The space group of the crystal was $P2_12_12_1$ with one monomer in the asymmetric unit. All data were processed

with the program HKL2000[100]. Diffraction data for the initial phase determination were collected on ALS 4.2.2 (Advance Light Source, Lawrence Berkley National Lab).

Initial phases for the structure of $CopA^{MBD}$ were determined by single-wavelength anomalous dispersion (SAD) techniques from a dataset collected on ALS 4.2.2 source with Cu(I) as the heavy atom. The structure of $CopA^{MBD}$ was solved and auto-built with PHENIX[101]. Two Cu(I) atoms were found in the structure. Iterative rounds of model building and refinement were carried out in Coot[102] and PHENIX, respectively.

For sCupA, diffraction data were collected at -160 °C on an R-AXIS IV+ detector at Indiana University Bloomington. The space group of the crystal was $P2_12_12$ with one monomer in the asymmetric unit. All data were processed with the program HKL2000.

Initial phases for the structure of sCupA were determined by using a portion of the crystal structure of $CopA^{MBD}$ as molecular replacement search model in PHENIX. The structure of sCupA was solved and auto-built with PHENIX. Two Cu(I) atoms were found in the structure. Iterative rounds of model building and refinement were carried out in Coot and PHENIX, respectively. Atomic coordinates and structure factors have been deposited to the Protein Data Bank with accession codes: sCupA (4F2E) and $CopA^{MBD}$ (4F2F). All structure related figures were prepared using PyMOL (Delano Scientific).

2.2.5 Apo-sCupA backbone and side chain resonances assignments

Typical NMR sample solution conditions were 300-600 μM, $^{15}N/^{13}C$-labeled sCupA, pH 6.0, 50 mM sodium phosphate, 50 mM NaCl, 0.02% (w/v) NaN3 and 10% (v/v) ^2H_2O. All the NMR samples were prepared in an anaerobic glove box. Apo-sCupA was prepared with 5 mM TCEP. Varian DDR 800 and 600 MHz spectrometers equipped with cryogenic probes in the METACyt Biomolecular NMR Laboratory were used to

acquire data for sCupA samples at 298 K. NMR spectra were referenced to H_2O. NMR data were processed using NMRPipe[103] and was analyzed using Sparky[104] and CcpNmr Analysis[105]. Chemical shift is referenced relative to 2,2-dimethyl-2-silapentene-5-sulfonic acid (DSS). Sequential resonance assignments of apo-sCupA were obtained using ^{1}H-^{15}N heteronuclear single quantum coherence (HSQC), HADAMAC[106], along with triple resonance CBCA(CO)NH, CBCANH, HNCO and Best-HNCA[107] spectra. Automatically backbone assignment server PINE[108] was employed to help with the assignment. Assignments of side chain resonances were made using three-dimensional C(CO)NH-TOCSY[109], H(CCO)NH-TOCSY[109,110], HCCH-TOCSY[111] and HCCH-COSY[112] experiments.

2.2.6 ICP-MS analysis

1.5 mL aliquots of *S. pneumoniae* strains were centrifuged and washed once with BHI containing 1 mM nitrilotriacetic acid (Aldrich), then twice with PBS that had been treated overnight with Chelex-100 (Biorad) according to the manufacturer's protocol. The cell pellets were dried overnight in a rotary evaporator. 400 µL of 2.5% v/v nitric acid (Ultrapure, Sigma- Aldrich) containing 0.1% v/v Triton-X 100 was added to solubilize the cell pellets which were then lysed for 10 min at 95 ºC with shaking at 500 rpm followed by vigorous vortexing for 20 s. 200 µL of the lysed cell solution (equivalent to 0.75 mL total cell culture) was added to 2.8 mL of 2.5% v/v nitric acid for ICP-MS analysis. Analyses were performed using a Perkin Elmer ELAN DRCII ICP-MS essentially as described earlier.[94] The instrument was equipped with a Microflow PFA-ST concentric nebulizer with a 100 µL/min self-aspiration capillary, a cyclonic spray chamber, a quartz torch and nickel sampler/skimmer cones. Germanium at 50 ppb was

added as an internal standard using an EzyFit glass mixing chamber. Metal concentration per mg protein were determined in the following way. ICP-MS gave [metal] in μg/L * 0.003 L sample equals total μg metal in 0.75 mL of cell culture. The μg metal * 1000 * 2 gave the ng metal in the original 1.5 mL of culture. Protein samples were resuspended in 100 μL buffer and concentrations were determined in mg/mL using a Bradford assay (Biorad). Total protein in 1.5 mL was calculated multiplying by 0.1 to correct for the resuspension volume. The final copper concentration as expressed by ng metal/mg protein determined by dividing those two values (ng/1.5 mL)/(mg/1.5 mL) = ng/mg protein.

2.2.7 Cu(I) Binding Affinity Measurements

Bathocuproine disulfonate (BCS) and bicinchoninic acid (BCA) were used for Cu(I) binding affinity determination of sCupA and $CopA^{MBD}$. All proteins for binding experiments were buffer exchanged from protein stock to the degassed buffer B (25 mM HEPES, pH 7.0, 200 mM NaCl) in an anaerobic glove box. Cu(I) stock was prepared by taking the supernatant from the mixture of CuCl powder with fully degassed buffer B (25 mM HEPES, pH 7.0, 200 mM NaCl). The accurate concentration of Cu(I) stock was determined by Atomic Absorption Spectroscopy with a general concentration around 10 mM. The final titration solution contained 20 or 30 μM sCupA or $CopA^{MBD}$ and 30 or 40 μM BCA (BCS) in Buffer B. Each 120 μL aliquot of titration solution was mixed with increasing Cu(I) titrant. Optical spectra of BCA or BCS were recorded from 200 nm to 900 nm. Corrected spectra were obtained by subtracting apo-sCupA ($CopA^{MBD}$) spectrum from each Cu(I)-addition spectrum and then corrected for dilution. A_{483} was used to determine the concentration of Cu_2-BCS complex with an extinction coefficient of 13500

$M^{-1}cm^{-1}$. A_{562} was used to determine the concentration of Cu_2-BCA complex with an extinction coefficient of 7700 $M^{-1}cm^{-1}$. All the data were fitted to the appropriate competition model using Dynafit[113]. The Cu(I) concentration of all Cu(I) titrants used in individual experiments was quantified by atomic absorption spectroscopy on a Perkin Elmer AAS-400 instrument.

2.2.8 Western blotting to quantitate cellular expression levels of CupA and CopA in various *cupA* or *copA* mutants

Whole cell lysates were prepared from strains IU1781 (D39 non-FLAG negative control), IU6041 (*cupA*-(C)-FLAG), IU6216 (Δ*cupA*-(33-aa remnant)-(C)-FLAG)), IU6086 (*cupA* (Δ(2-28)-(C)-FLAG), IU6215 (*cupA* (C74S,3A)-(C)-FLAG), IU6210 (*cupA* (C74S)-(C)-FLAG) and IU6212 (*cupA* (3A)-(C)-FLAG). To detect CopA-FLAG alleles, whole cell lysates were prepared from stains IU1781 (D39 non-FLAG negative control), IU6044 (*copA* (C)-FLAG), IU6260 (Δ*copA* (C)-FLAG), IU6245 (*copA* (C49S)-(C)-FLAG), IU6240 (*copA* (D442A)-(C)-FLAG), IU6307 (*cupA* (C74S)-*copA* (C)-FLAG), and IU6308 (Δ*cupA*-*copA* (C)-FLAG). In order to obtain sufficient cell mass to prepare lysates with the FastPrep method, cell cultures were grown overnight in BHI and then diluted to 0.0035 (*cupA* (C)-FLAG and WT, as well as *copA* (C)-FLAG and *copA* (C49S)-(C)-FLAG) or 0.005 (all other mutant strains) in 30 mL BHI, and allowed to grow to an OD_{620} of 0.04 (*cupA* (C)-FLAG and WT, as well as *copA* (C)-FLAG and *copA* (C49S)-(C)-FLAG) or 0.06 (all other strains) or ≈3 doublings, at which time $CuSO_4$ was added to a final concentration of 0.2 mM. 2.5 h after addition of Cu, at an OD_{620} of ≈0.25 for *cupA*-FLAG strains (≈2 doublings for Cu-sensitive mutant alleles and ≈3 doublings for WT and *cupA* (C)-FLAG) and at an OD_{620} of ≈0.5 for *cop*A-FLAG strains (≈2

doublings for Cu-sensitive mutant alleles and ≈3 doublings for WT, *copA* (C)-FLAG and *copA* (C49S)-(C)-FLAG), cells were centrifuged at 14,500 x *g* for 5 min at 4 °C in a chilled rotor. Supernatants were removed and pellets were placed on ice and suspended in 1.0 mL of cold 20 mM Tris pH 7.0 and 8 µL of protease inhibitor cocktail set III (Calbiochem) and transferred to chilled Lysing Matrix B tubes (MP Biomedicals). Matrix tubes were secured in a 24 x 2 mL-tube adapter in a FastPrep-24 instrument (MP Biomedicals) stored at 4 °C. Cells were disrupted by three consecutive runs of 40 sec each at a speed setting = 6.0 m/s. Lysed cell mixtures were placed on ice and centrifuged at 10,000 x *g* for 1 min at 4 ºC. 100 µL of supernatant was transferred to a tube containing 100 µL of cold 2x Laemmli sample buffer (containing 5% (vol/vol) of freshly added β-mercaptoethanol), boiled for 5 min and placed on ice. Gel loading volumes were calculated to adjust for the slightly different cell culture densities so that the equivalence of 200 µL (*cupA*-FLAG strains) or 312 µL (*copA*-FLAG strains) of OD_{620} = 0.2 culture of each sample (corresponding to 16 and 25 µL of the final lysates for CupA and CopA strains, respectively) was loaded on each lane of a 15% (*cupA*-FLAG strains) or 10% (*copA*-FLAG strains) SDS-PAGE gel. Visualization and relative quantitation of FLAG-tagged proteins were achieved with Western blotting with primary anti-FLAG polyclonal antibody (Sigma, F7425) and an IVIS imaging system as described[1].

2.3 Results

2.3.1 Both CupA and CopA are required for Cu resistance and localize to the plasma membrane

Although the core domain of CopA looks to be a prototypical bacterial Cu(I)-effluxing CopA of known structure that is evolutionarily related to Menkes and Wilson's

disease copper transporters ATPA and ATP7B[67], an approximate 100 residue domain that exhibits high sequence similarity to CupA is found at the N-terminus of CopA. Notably, both domains contain a number of conserved cysteines and methionines that are excellent candidate ligands for Cu(I) and are found in a Cys….Cys-x-Met-x-Met (where x, any amino acid) primary structural arrangement (**Fig. 9**). Furthermore, the N-terminus of CupA is predicted to contain a single transmembrane helix between residues 5-22. The high sequence similarity of CupA and the N-terminal region of CopA is a hallmark of a cognate copper chaperone-metal binding domain (MBD) pair found in many other bacterial species.[114] *S. pneumoniae* does not encode an Atx1 or a CopZ and a bioinformatics analysis reveals that CupA is nearly always found in genomes that lack a recognizable gene encoding CopZ or Atx1. Furthermore, CupA is widely distributed, perhaps more so that of CopZ/Atx1, but clearly clustered in *Lactobacillus* and *Streptococcus*; CupA is also present on at least one extrachromosomal plasmid pCT0018 in *Listeria monocytogenes* (**Fig. 10**).

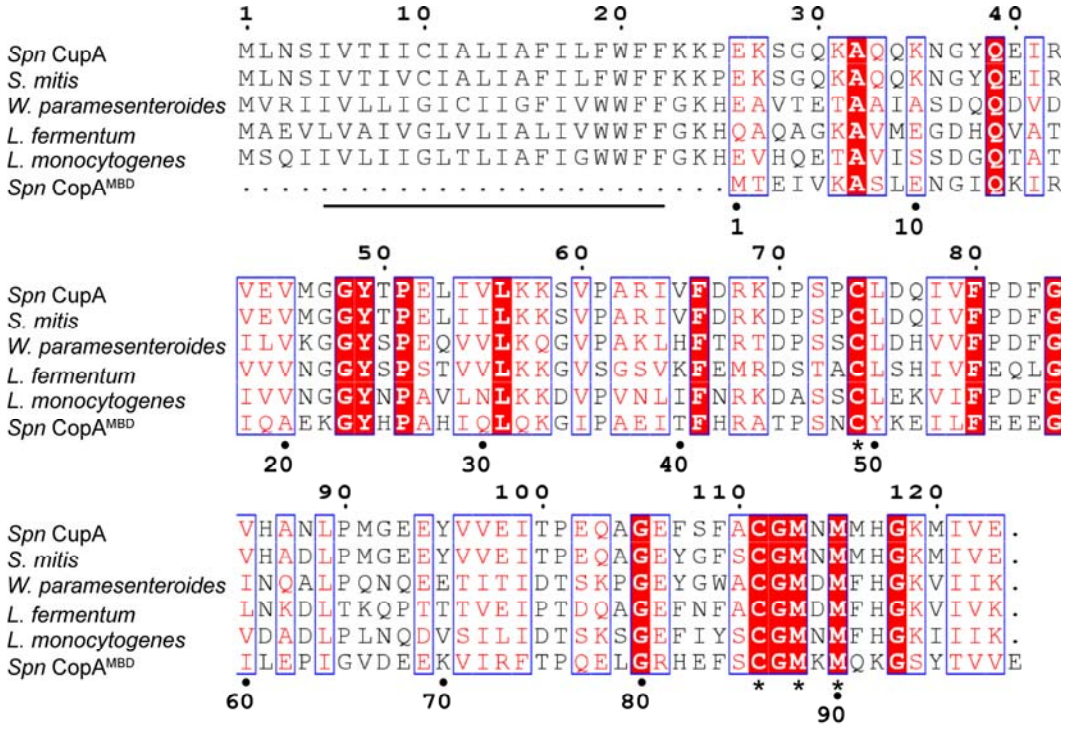

Figure 9: Multiple sequence alignment of CupA homologs.
(a) *S. pneumoniae* D39 CupA (SPD_0634) with the N-terminal 99 residues of CopA (SPD_0635) and (b) putative CupAs from a number of bacterial sources illustrates conservation of a putative transmembrane domain (underlined) and candidate Cu(I)-binding ligands (asterisks).

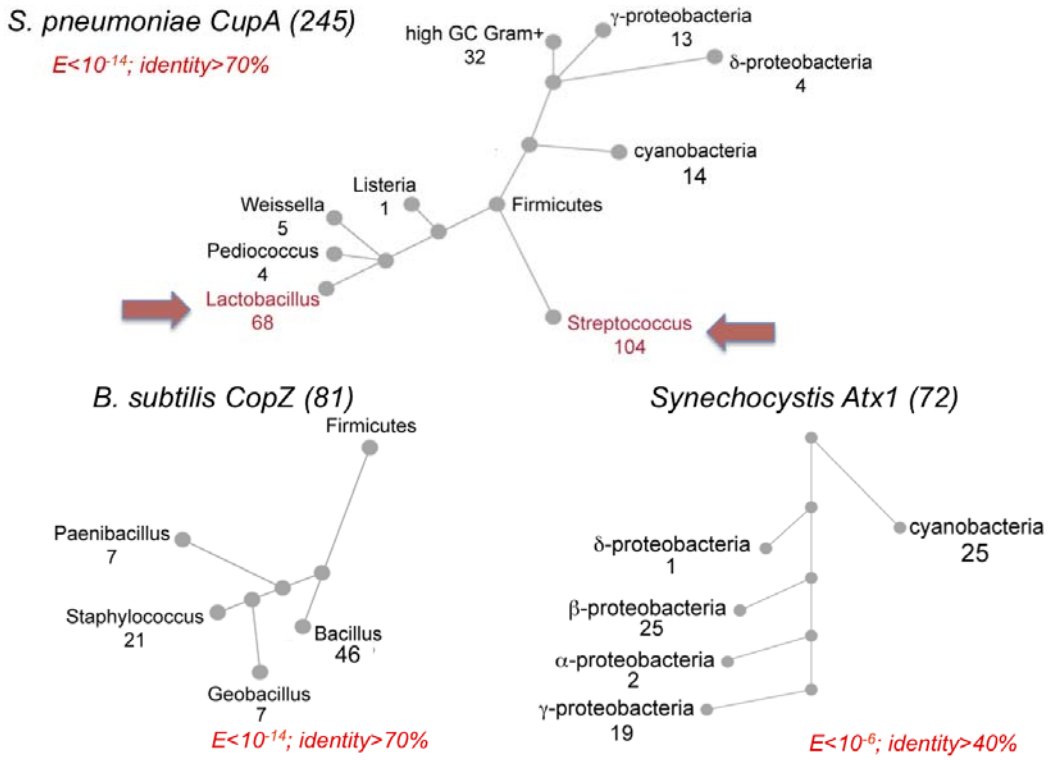

Figure 10: Phylogenetic reach of the putative copper chaperone CupA.
Shown here is the distribution of CupA relative to previously structurally characterized bacterial chaperones, *B. subtilis* CopZ and *Synechocystis* Atx1 as of 2012. Each sequence was used to pBLAST a bacterial genome collection, and those sequences with ≥70% identity with C…CxMxM (where x is any amino acid) sequence conserved are shown. Indicated criteria for CopZ and scAtx1 are also shown, with the total number of nonredundant sequences meeting these criteria indicated.

All CupAs are predicted to harbor a single transmembrane helix that anchors CupA to the plasma membrane. To test this, we created Δ*cupA* and Δ*copA Spn* D39 deletion strains and tested growth on a rich (BHI) medium under microaerophilic conditions in the presence of 0.2 or 0.5 mM added Cu(II) (see **Appendix IV** for strain details). Both strains show a marked growth inhibition phenotype relative to the wild-type strain (**Fig. 11a** and **Fig. 12a-b**), which can be rescued by ectopic expression of CupA from a heterologous promoter positioned elsewhere in the chromosome (**Fig. 11b**). This result rules out any unintended polar effect on the expression of the downstream *copA* gene due to deletion of *cupA*; in fact, the Δ*cupA* strain accumulates CopA protein to high levels (**Fig. 13b**). Strains expressing C-terminally FLAG-tagged CupA or CopA are characterized by a wild-type growth in the presence of 0.2 or 0.5 mM Cu (**Fig. 12c-d**). In contrast, a strain expressing a D442A CopA in which the predicted catalytic Asp residue in the ATPase domain of the CopA transporter (based on a structural alignment with *Legionella* CopA) is replaced with Ala, is indistinguishable from the Δ*copA* strain (**Fig. 12d**). More importantly, a strain expressing CupA lacking the N-terminal transmembrane domain, Δ(2-28) CupA (denoted hereafter sCupA), *i.e., cupA*(Δ(2-28)) or *cupA*(Δ(2-28)-(C)-FLAG) (**Fig. 11c**), is also unable to grow under these conditions. These experiments establish that a C-terminal FLAG-tag does not interfere with CupA and CopA function thus allowing us to determine the subcellular localization of both CopA and CupA using a standard fractionation scheme followed by Western blotting with anti-FLAG antibody (**Fig. 14**). These data reveal that both CupA and CopA localize exclusively to the plasma membrane in *S. pneumoniae* D39; furthermore, plasma membrane localization of CupA is required for full copper resistance.

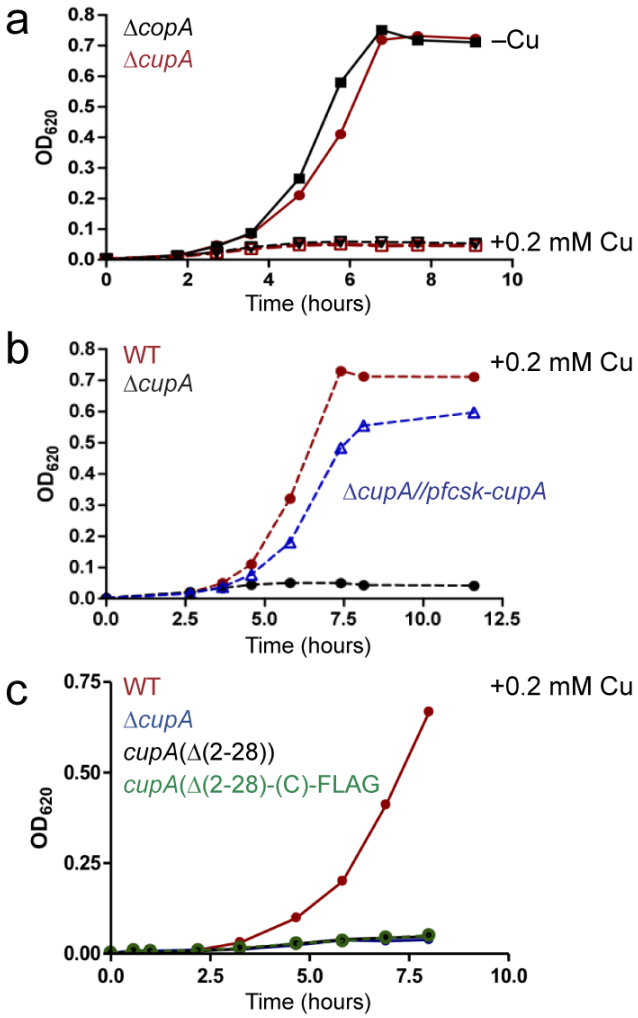

Figure 11: Δ*cupA* and Δ*copA Spn* strains are highly sensitive to copper toxicity. (**a**) which can be reversed by expression of *cupA* from a heterologous promoter (**b**). (**c**) Deletion of the single putative transmembrane helix abrogates copper resistance to an extent comparable to inactivation of CopA(D442A) (compare to **Fig. 12d**). The strains used for these experiments are wild-type (WT, IU1781), Δ*copA* (IU5975), Δ*cupA* (IU5971), Δ*cupA*//P_{fcsk}-*cupA* (IU6017), *cupA*(Δ(2-28)-(C)-FLAG (IU6086) and *cupA*(Δ(2-28) (IU6084). Experiment was carried out by Ho-Ching Tiffany Tsui and Kevin Bruce from Winkler Lab in the Department of Biology.

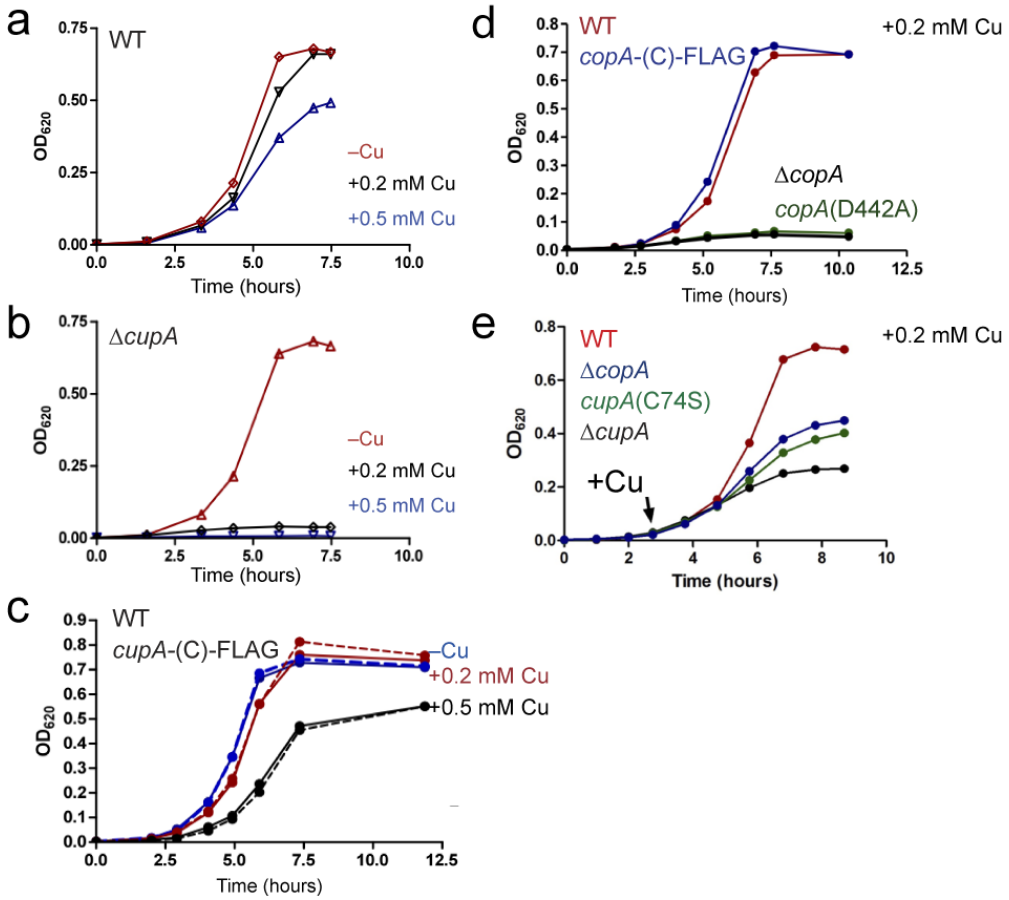

Figure 12: Growth curves of several *cupA* and *copA* mutant strains.
(**a**) wild-type (IU1781), (**b**) Δ*cupA* (IU5971), (**c**) C-terminally FLAG-tagged *cupA, cupA*-(C)-FLAG (IU6041) (open symbols, dashed line) vs. WT (solid symbols, continuous line), (**d**) C-terminally FLAG-tagged *copA, copA*-(C)-FLAG (IU6044), Δ*copA* (IU5975) and *copA* (D442A) (IU6054) *S. pneumoniae* D39 strains in BHI in the absence of added copper sulfate (–Cu) or in the presence of 0.2 mM or 0.5 mM Cu(II) as indicated. Overnight cultures were diluted to OD_{620} = 0.002 at the beginning of the growth curves for panels (a) to (d). (**e**) Representative growth curves of WT, Δ*cupA* (IU5971), *cupA*(C74S) (IU6050), and Δ*copA* (IU5975) strains with the addition of Cu(II) at the indicated time. Strains were diluted from overnight cultures to OD_{620} = 0.002 in BHI at the start of growth curve. $CuSO_4$ was added to the cultures at a final concentration with 0.2 mM at $OD_{620} \approx 0.03$ (arrow), and the growth of the strains was monitored in the presence of Cu(II). Cells obtained from these growth curves were used for whole cell Western blotting (**Fig. 13**) and ICP-MS measurements (**Table 4**). Experiment was carried out by Ho-Ching Tiffany Tsui and Kevin Bruce from Winkler Lab in the Department of Biology.

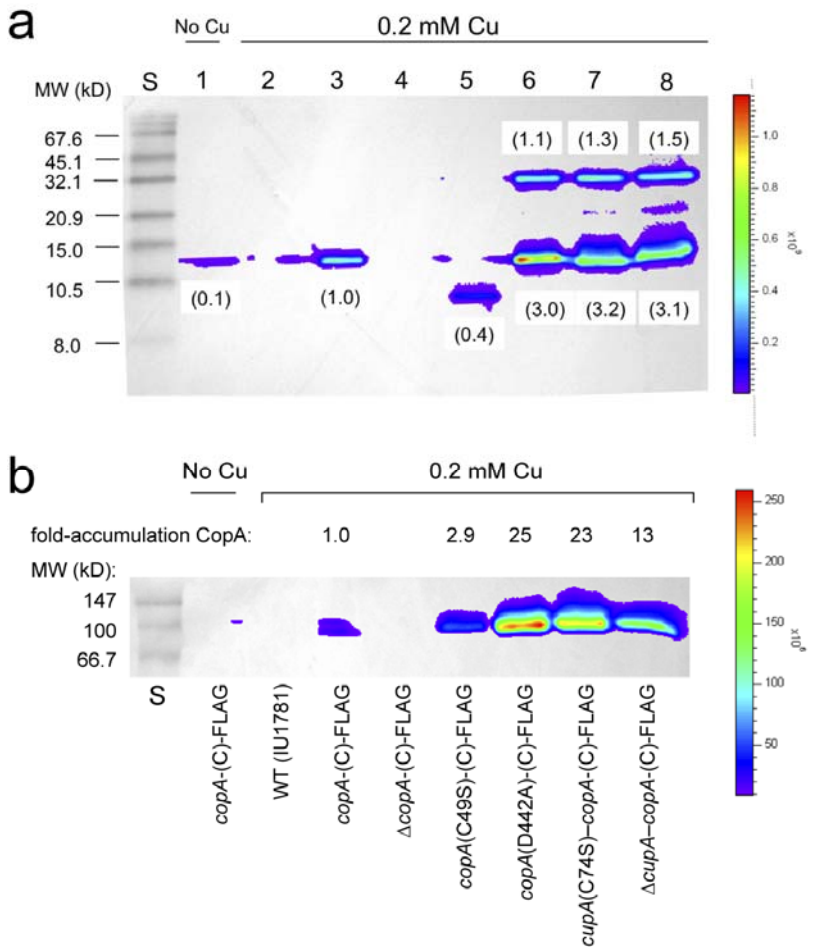

Figure 13: Western blotting of different *cupA* and *copA* strains.
(a) Quantitative Western blotting using an anti-FLAG antibody and whole cell extracts (0.2 mL of ≈0.25 OD_{620} units) of C-terminally FLAG-tagged sCupA and various missense mutants of CupA which show greatly reduced copper tolerance. The numbers in parentheses show the signal intensity relative to lane 3 (*cupA*-(C)-FLAG strain treated with 0.2 mM Cu). S, protein standard; lane 1, *cupA*-(C)-FLAG (IU6041), no Cu added; lanes 2-8, cultures collected after the cells were grown in BHI containing 0.2 mM Cu for 2.5 h: lane 2, $cupA^+$, no FLAG; lane 3, *cupA*-(C)-FLAG (IU6041); lane 4, Δ*cupA*-(33-aa remnant)-(C)-FLAG) (IU6216); lane 5, *cupA* (Δ(2-28)-(C)-FLAG) (IU6086); lane 6, *cupA(*C74S,3A)-(C)-FLAG (IU6215); lane 7, *cupA*(C74S)-(C)-FLAG (IU6210); lane 8, *cupA*(3A)-(C)-FLAG (IU6212). See **Fig. 12e** for a representative growth curve for this experiment. The detected band at ≈30 kD has a mobility approximately consistent with dimeric CupA-(C)-FLAG but its identity is unknown. (**b**) CopA-(C)-FLAG (≈81 kD) Western blotting of various missense *copA* and *cupA* strains. Cells were prepared as described for panel (a). Experiment was carried out by Ho-Ching Tiffany Tsui and Kevin Bruce from Winkler Lab in the Department of Biology.

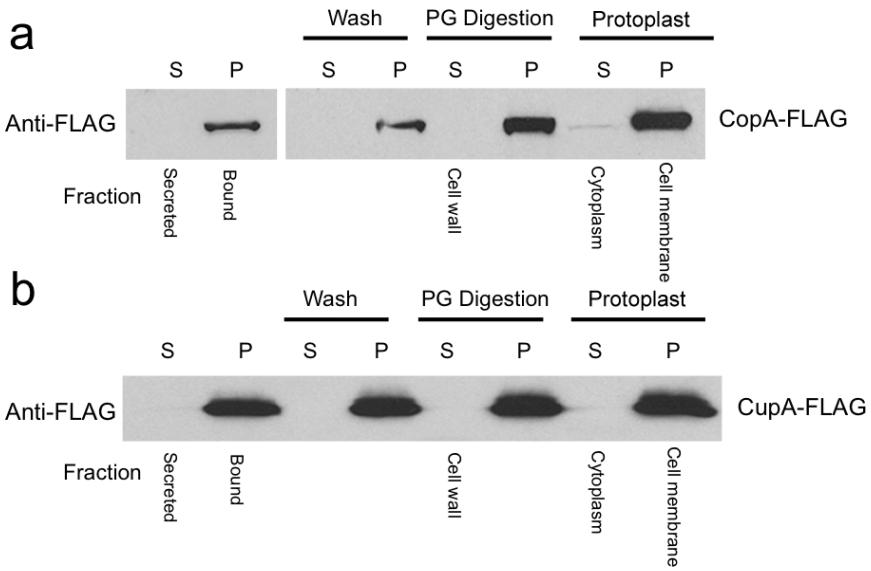

Figure 14: Both CopA and CupA localize to the cell membrane fraction in *S. pneumoniae* D39.

The results of a subcellular fractionation of *copA*-(C)-FLAG (IU6044) **(a)** and *cupA*-(C)-FLAG (IU6041) (**b**) with visualization by anti-FLAG Western blotting. Supernatants (S) or pellets (P) are marked for centrifugation steps, and cell fractions are indicated below the blots. Strains IU6044 and IU6041 were grown exponentially in the presence of 0.3 mM $CuSO_4$ to OD620 ≈ 0.2 and fractionated as described[60]. Cultures were centrifuged to obtain secreted and cell-bound fractions, which were washed with 1X SMM buffer used for peptidylglycan (PG) digestion (Wash). The resulting pellets were subjected to enzymatic digestion of the PG layer with mutanolysin and lysozyme to obtain protoplasts (P of PG digestion) and cell wall (S of PG digestion). Protoplasts were lysed by adding hypotonic buffer (Protoplast), with the resulting pellets as cell membrane fraction and supernatants as cytoplasmic fraction. Experiment was carried out by Lok-To Sham from Winkler Lab in the Department of Biology.

2.3.2 Copper binding by sCupA and CopA^{MBD}

The experiments described above suggest that sCupA and CopA^{MBD} bind Cu(I) directly as a means to effect copper resistance. To test this, I carried out a series of anaerobic titration experiments in which CuCl was added to apo-sCupA or apo-CopA^{MBD} in the absence and presence of one of two specific Cu(I) chelators, bathocuprione disulfonate (BCS) (logβ2=19.8 for Cu^{I}:BCS_2) or bicinchoninic acid (BCA) (logβ2=17.2 for Cu^{I}:BCA_2), thus allowing us to access a range of K_{Cu} between 10^{12} and 10^{19} M^{-1}. A global analysis of two representative titrations at two protein concentrations is shown (**Figs. 15-16**) with parameter values compiled in **Table 1**. These titrations reveal that the stoichiometry of Cu(I) binding in both cases to be ≈2 per monomer. sCupA is characterized by stepwise affinity constants (K_{Cu1}, K_{Cu2} at pH 7.0, 0.2 M NaCl) of 7.4 x10^{17} M^{-1} and 6.2 x 10^{14} M^{-1}, while the CopA^{MBD} binds Cu(I) with 2.1 x 10^{16} M^{-1} and 2.7 x 10^{13} M^{-1} stepwise affinities (**Table 1**). Thus, the putative chaperone sCupA binds Cu(I) 20- to 30-fold more tightly than the putative Cu acceptor CopA^{MBD} to each of the high affinity and low affinity sites.

2.3.3 Crystallographic structures of sCupA and CopA^{MBD}

In order to understand the structural basis for the Cu(I) binding stoichiometry, affinity and resistance, the x-ray crystallographic structures of sCupA and CopA^{MBD} were solved to 1.45 Å and 1.50 Å resolution, respectively (**Fig. 17-18**; **Table 2** for structural statistics).

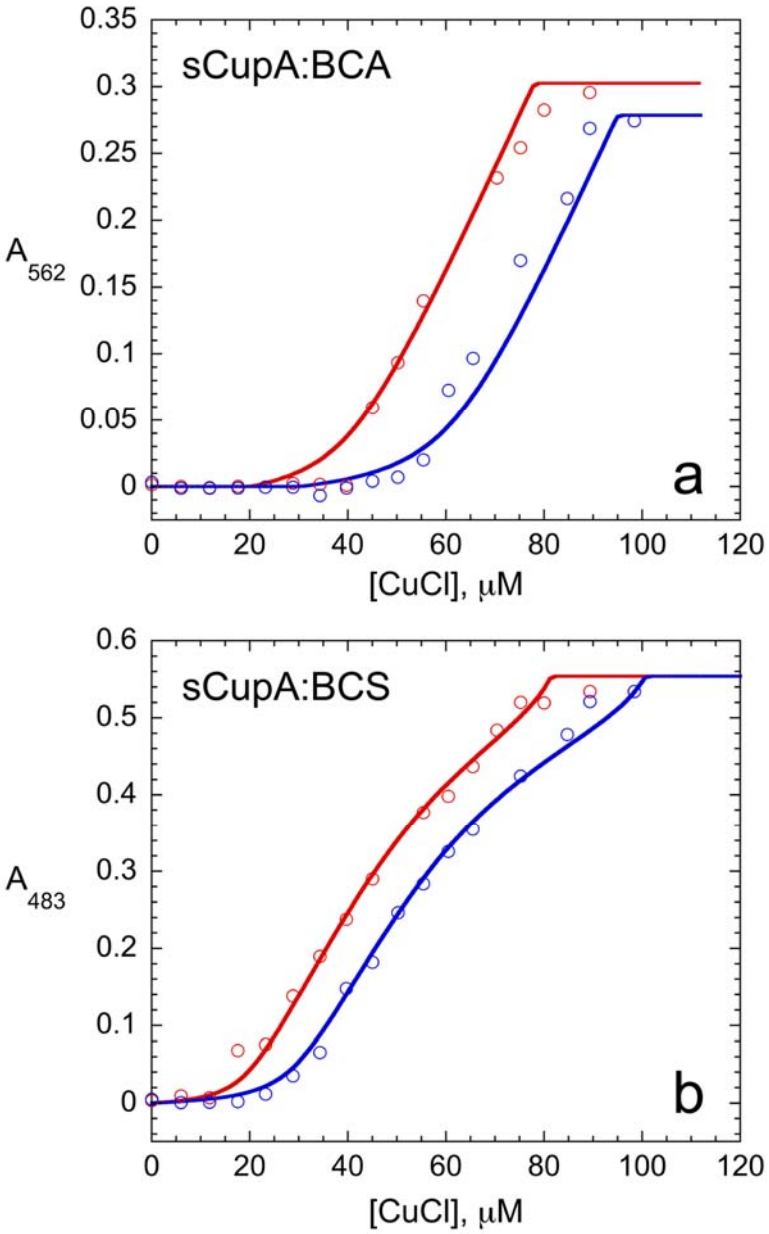

Figure 15: Representative binding curves obtained from anaerobic Cu(I) chelator competition experiments.

Experiments were carried out with a mixture of apo sCupA and BCA (or BCS) at pH 7.0. Two individual experiments were carried out for BCS or BCA assay. (**a**) BCA competition assay for sCupA. Open symbols represent A_{562} values for the Cu(I)-$(BCA)_2$ complex. The continuous line represents the results of a global analysis of both experiments to a two-step binding, direct competition model. *Red*: 20 μM sCupA and 76 μM BCA. *Blue*: 30 μM sCupA and 76 μM BCA. (**b**) BCS competition assay for sCupA. Open symbols represent A_{483} values for the Cu(I)-$(BCS)_2$ complex. The continuous line represents the results of a global analysis of both experiments to the same model. *Red*: 20 μM sCupA and 86 μM

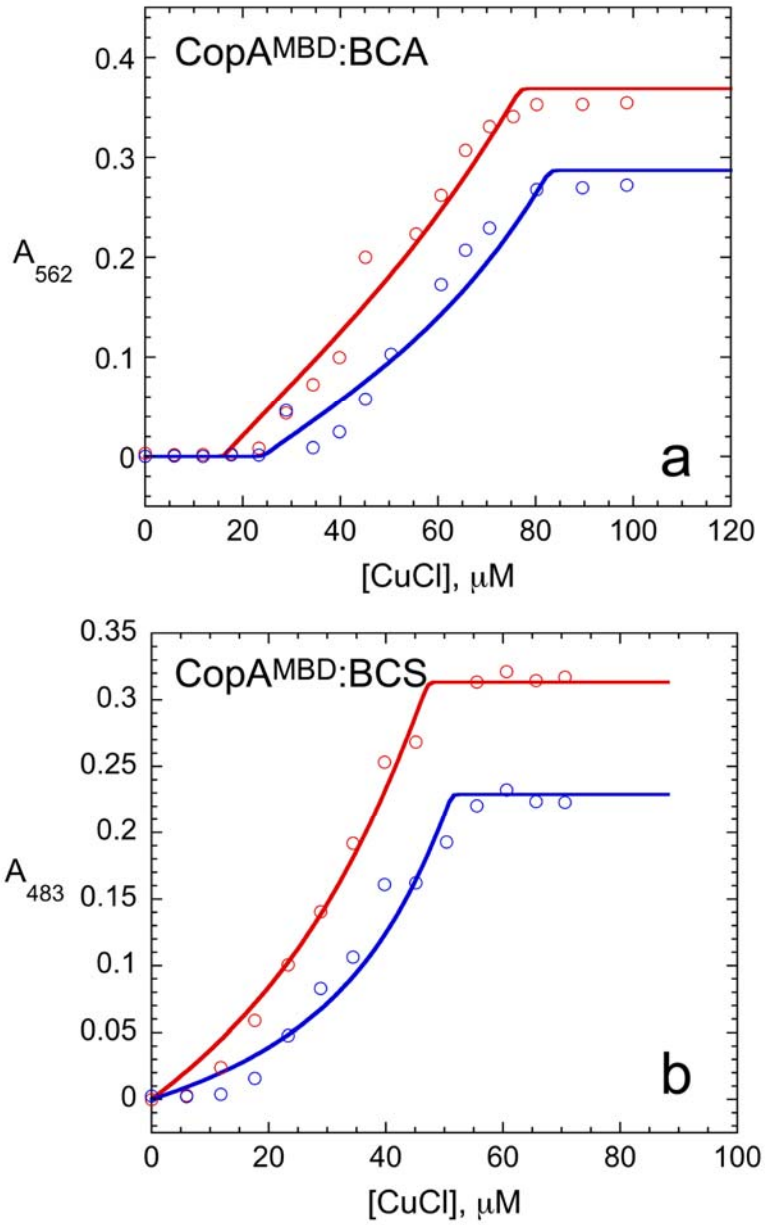

Figure 16: Representative binding curves obtained from anaerobic Cu(I)-chelator competition assays.

The experiments were carried out with a mixture of apo $CopA^{MBD}$ and BCA (or BCS) at pH 7.0. Two individual experiments were carried out for BCS or BCA assay. (**a**) BCA competition assay for $CopA^{MBD}$. Open symbols, A_{562} for the Cu(I)-$(BCA)_2$ complex. The continuous line represents a global fitting of both experiments to a two-step, competition binding model. *Red*: 16 μM $CopA^{MBD}$ and 90 μM BCA; *Blue*: 24 μM $CopA^{MBD}$ and 70 μM BCA. (**b**) BCS competition assay for $CopA^{MBD}$. Open symbols represent A_{483} values for the Cu(I)-$(BCS)_2$ complex. The continuous line represents the results of a global analysis of both experiments to a single-site binding, direct competition model. *Red*: 20 μM $CopA^{MBD}$, 52 μM BCS; *Blue*: 30 μM

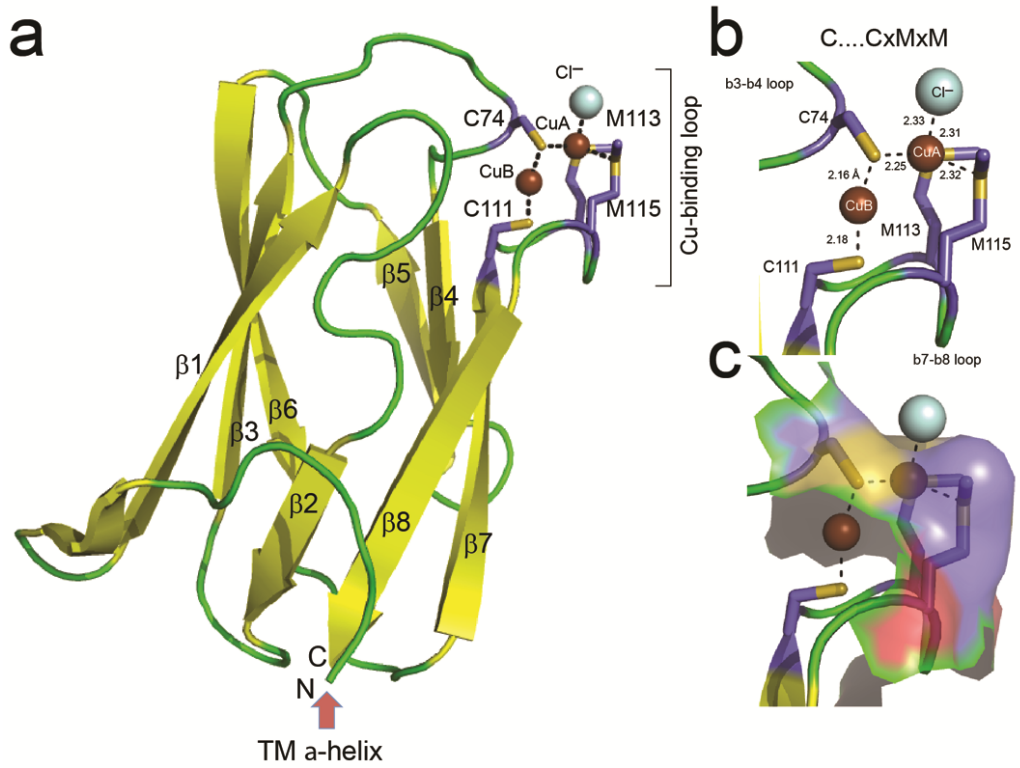

Figure 17: Structure representations of $Cu(I)_2$-sCupA.
Close-up views of the Cu(I) coordination geometries of protein are shown (**b**) as are solvent-accessible surface areas (colored based on solvent accessibility) (**c**) around the binuclear Cu(I) chelate. Structure statistics compiled in **Table 2**.

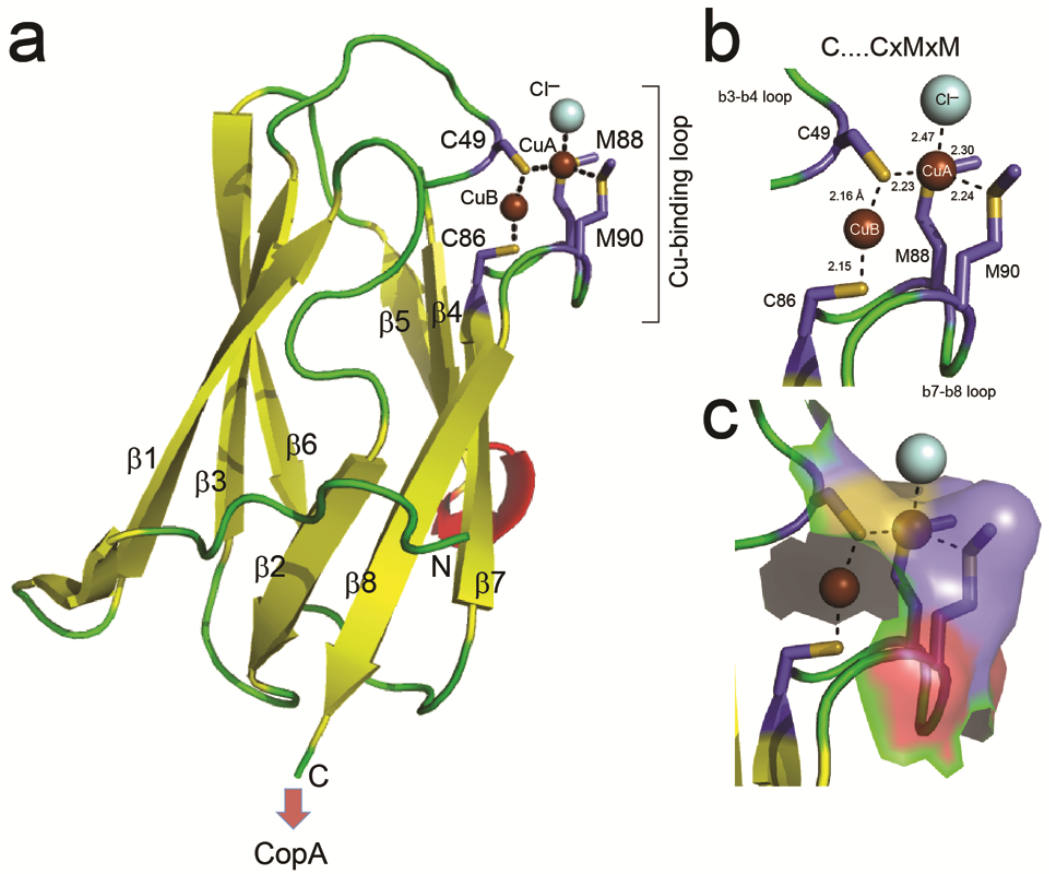

Figure 18: Structure representations of $Cu(I)_2$-$CopA^{MBD}$.
Close-up views of the Cu(I) coordination geometries of protein are shown (**b**) as are solvent-accessible surface areas (colored based on solvent accessibility) (**c**) around the binuclear Cu(I) chelate. Structure statistics compiled in **Table 2**.

Each structure reveals an eight-stranded β-barrel harboring a binuclear Cu(I) cluster with a single Cys from the β2-β3 loop (Cys49 in $CopA^{MBD}$ and Cys74 in sCupA) functioning as a bridging ligand to each Cu site, denoted S1 and S2. The S1 site is digonal *bis*-thiolato while the more solvent-exposed S2 site is best described as distorted trigonal planar coordination by the three protein-derived ligands, with a long axial coordination bond to a Cl^- anion from solution (or distorted trigonal pyramidal) (**Fig. 20 and Table 3**). A conserved **Cys**-gly-**Met**-asp/asn-**Met** motif position in the β7-β8 loop in each protein provides three of the four donor atoms to the Cu(I) ions. The Cu-Cu distance is 3.15 Å in each case. Both sCupA and $CopA^{MBD}$ adopt a well-known cupredoxin fold, with Dali *z*-scores ranging from 10-12 for cupredoxins of known structure, including plastocyanin, nitrosocyanin, nitrous oxide reductase, the CueO multicopper oxidase and the Cu_A site of bacterial cytochrome ba3-type cytochrome c oxidase (**Fig. 21**). [115] However, the metal-ligand disposition is completely novel, evidence that nature has adapted this ancient fold to perform Cu(I) trafficking rather than electron transfer.

Despite adopting identical folds with identical Cu(I) coordination chemistries, sCupA and $CopA^{MBD}$ possess contrasting electrostatic surface potentials around the Cu(I) binding sites, with the sCupA largely negatively charged and the $CopA^{MBD}$ largely positively charged in the vicinity of the Cu(I)-binding sites (**Fig. 19**). Electrostatic complementarity is an established feature of copper chaperone-MBD pairs, which would allow the Cu(I) chelates of each protein to transiently dock and undergo ligand exchange and Cu transfer, without dissociation of bound Cu(I) into solvent[116]. These disparate surface potentials may also explain the weaker overall Cu(I) binding affinity for

CopA^{MBD} vs. sCupA (**Table 1**). In CopA^{MBD}, Lys22, Lys89 and Lys92 are in close proximity of the Cu site and may electrostatically repel the positively charged Cu(I) cation; in contrast, Glu52 in sCupA is in a position to electrostatically attract the Cu(I) cation.

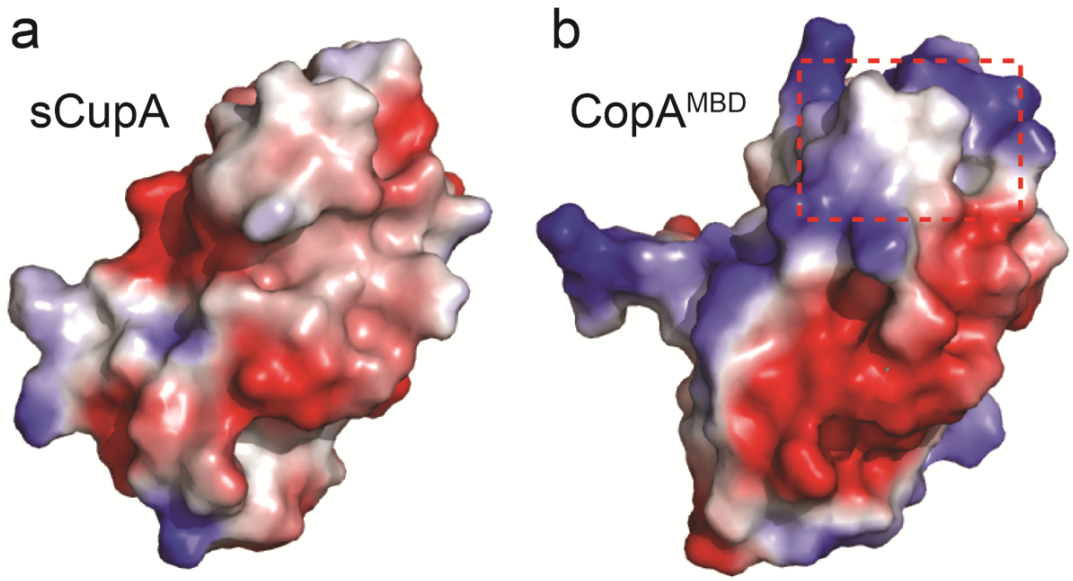

Figure 19: Electrostatic surface potential of (**a**) sCupA and (**b**) CopA^{MBD}.
The potential was generated from Cu_2 form crystal structure of each protein. The binuclear Cu(I) cluster is highlighted using a red box showing the charge complementarity between this pair proteins.

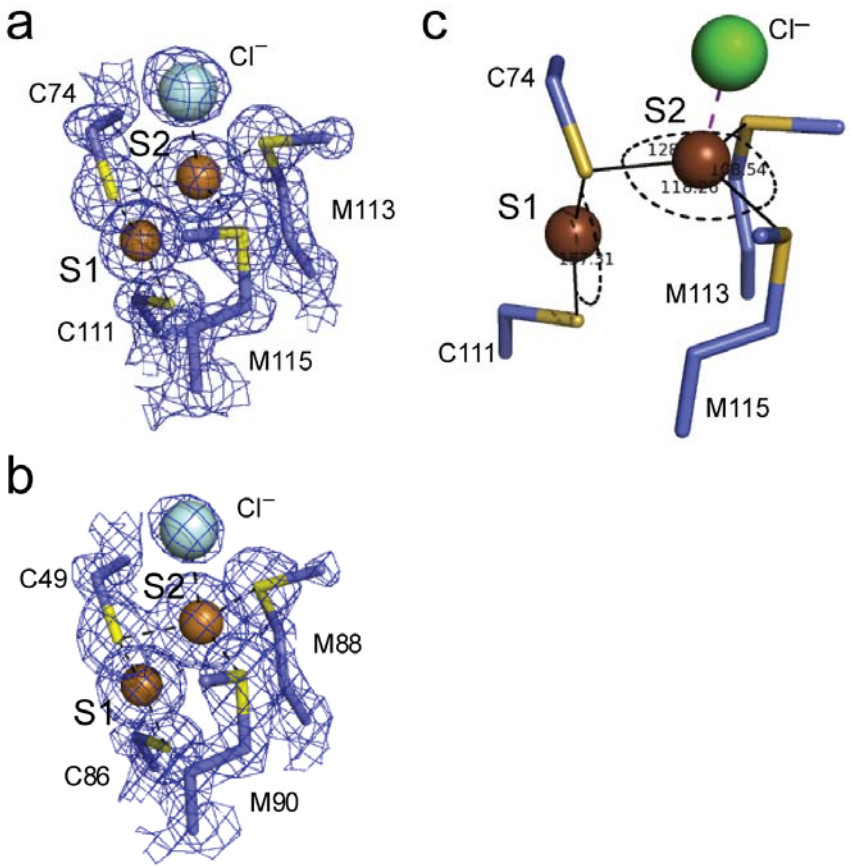

Figure 20: Cu(I) sites of sCupA and CopA^{MBD}.
Close-up of the Cu(I) coordination complex in sCupA, with dihedral angles shown. (**a**) Cu(I) site residues of sCupA (C74, C111, M113, M115) with 2*mFo* - *DFc* map contoured at 2 σ. (**b**) Cu(I) site residues of CopA^{MBD} (C49, C86, M88, M90) with 2*mFo* - *DFc* map contoured at 2 σ. (**c**) The S1 Cu(I) ion is digonal and is very close (157º) to a linear coordination complex (180º), while the S2 Cu(I) ion is best described as distorted trigonal planar (expected 120º dihedral angles) with an axial coordination bond to a Cl^- anion from solution, *i.e.,* distorted trigonal pyramidal. See **Table 3** for metal-ligand bond distances and angles.

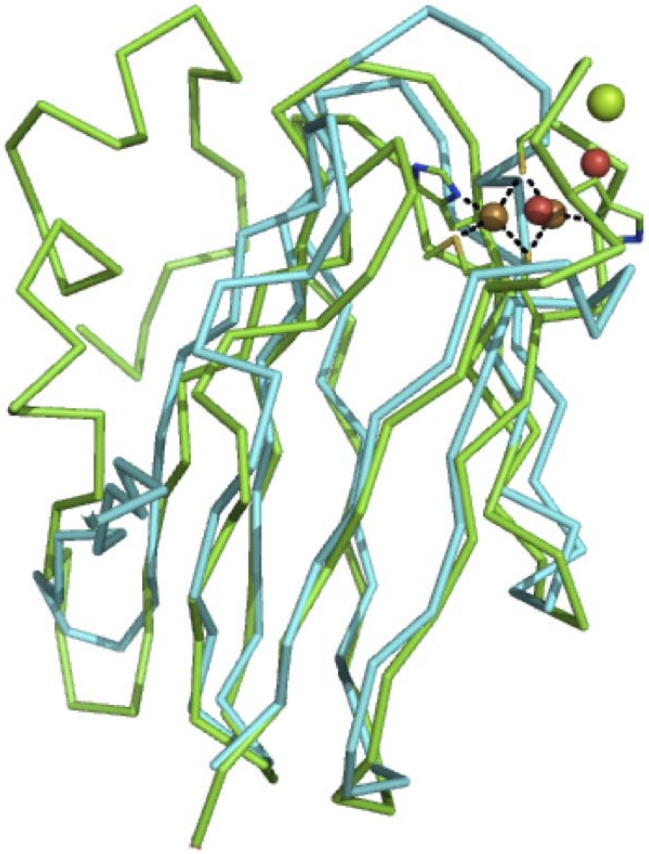

Figure 21: Global superposition of CopAMBD with cupredoxin-fold containing protein.
$CopA^{MBD}$ (*cyan;* Cu ions, *red*, Cl^-, *green*) with the soluble CuA domain from *T. thermophilus* ba3-type cytochrome c oxidase (PDB code 1cua) (*green;* Cu ions, *brown*)[115]. Cyt_{ba3} harbors a CuA binding motif of His…Cys-x_3-Cys-x_3-His-x_2-Met (coordinating residues are shown), with the His derived from the β3-β4 loop and the remaining residues derived form the β7-β8 loop which is analogous to the Cys….Cys-*x*-Met-*x*-Met sequence in sCupA and $CopA^{MBD}$. One Cu ion, the S1 Cu in $CopA^{MBD}$ is identically positioned with one of the Cu ions of Cyt_{ba3}; however, the cytochrome lacks the more solvent-exposed S2 Cu site. The DALI[156] *z*-score is 10.9, with 1.8 Å heavy atom RMSD.

2.3.4 Identification of the high and low affinity Cu(I) sites in sCupA and CopA^{MBD}

The copper trafficking hypothesis[117] states the copper transfer moves from donor chaperone to target protein with or against a relatively shallow thermodynamic gradient as defined by K_{Cu} measured with purified proteins[27,118]. For sCupA and the CopA^{MBD}, the situation is complicated by the presence of two bound Cu(I) ions in each case, with no insight as to which site defines the high and low affinity Cu(I) sites in each case. therefore NMR spectroscopy was employed to define the sequence of Cu(I) binding, exploiting the fact that the stepwise Cu(I) affinities differ by about ≈1000-fold for both sCupA and CopA^{MBD} (**Table 1**).

Cu(I) binding to the apoproteins was examined by monitoring perturbations in the amide chemical shifts of uniformly ^{15}N,^{13}C-labeled samples of sCupA and CopA^{MBD} upon sequential filling each of the two Cu(I) sites (**Fig. 22**). In each case, the β3-β4 and β7-β8 metal binding loops in the apoproteins are conformationally exchange broadened indicative of substantial μs-ms dynamics in this region (**Fig. 24**), as recently established for other apo-cupredoxins involved in electron transfer[119]. Stepwise addition of Cu(I) quenches this line broadening with the addition of the first Cu(I) inducing measurable perturbations beyond these loops and into nearby β-strands, *e.g.,* the β7 strand; addition of the second Cu(I) gives rise to significant perturbations in the metal binding loops only (**Fig. 24**). These perturbation maps are fully consistent with C49 (CopA^{MBD}) and C74 (sCupA) functioning as a bridging ligand since filling of both S1 and S2 sites in each induces backbone perturbations in both β3-β4 and β7-β8 loops.

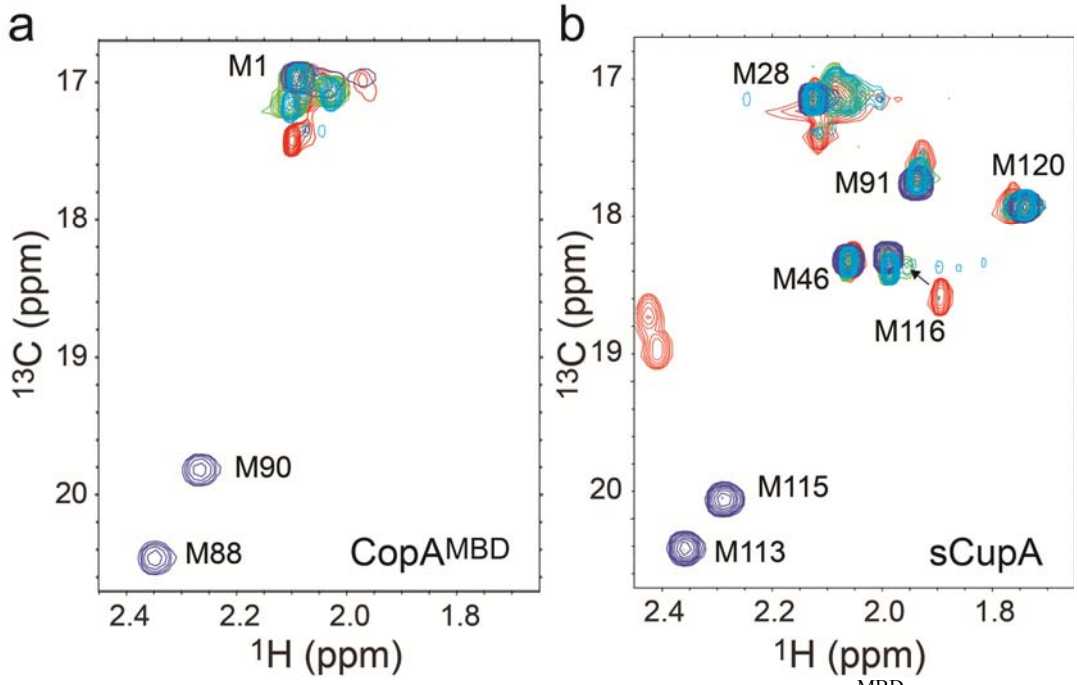

Figure 22: The Met-rich S2 site is the low-affinity site on both $CopA^{MBD}$ and sCupA and Cu(I) is transferred only from the S2 site of sCupA to the S1 site of apo-MBD. Overlay of the Met thioether methyl ($^{13}C\varepsilon$-$^{1}H\varepsilon$) region of an ^{1}H,^{13}C-HSQC spectrum for $CopA^{MBD}$ (**a**) and sCupA (**b**) acquired in the apo-state (*red* crosspeaks), Cu_1 state (*green* crosspeaks; *italics* type) and Cu_2 states (*blue* crosspeaks; *bold-face* type). *Cyan* crosspeaks result when apo-MBD is mixed with 2.0 mol equiv of Cu_2 sCupA (panel **a**) or 1.0 mol equiv of Cu_2 sCupA (panel **b**).

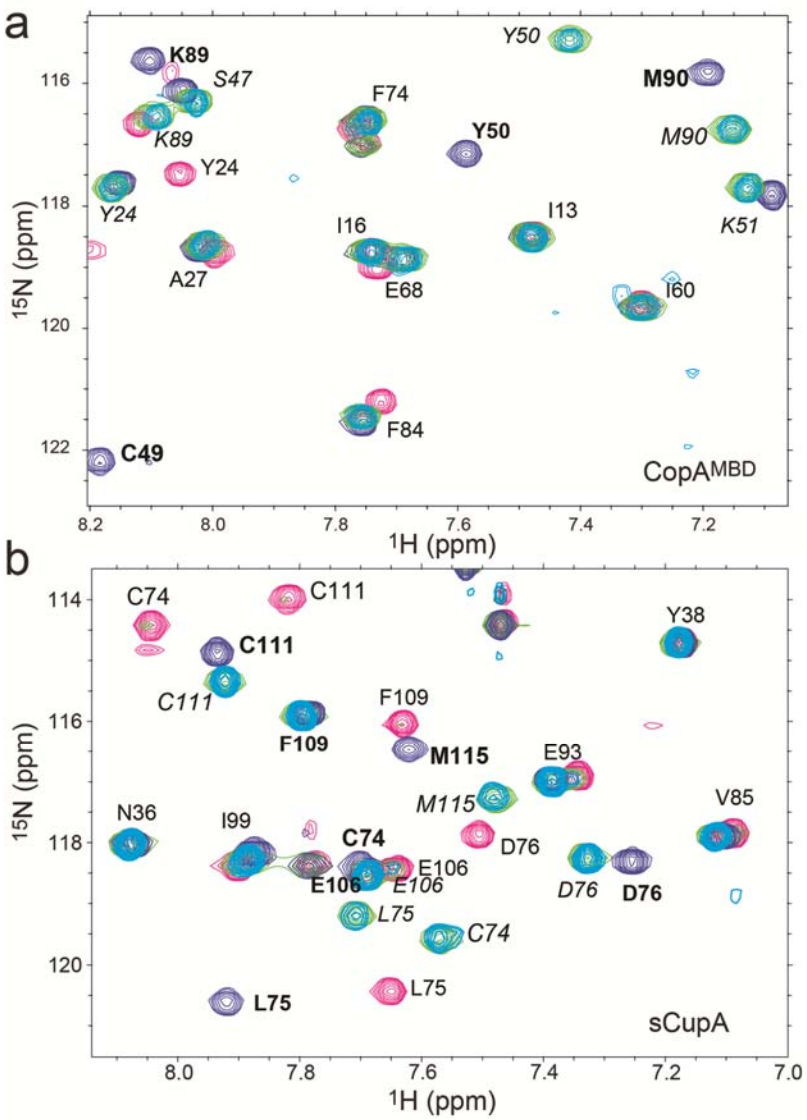

Figure 23: Cu(I) transfer observed from chemical shift of backbone resonances. The Met-rich S2 site is the low-affinity site on both $CopA^{MBD}$ and sCupA and Cu(I) is transferred only from the S2 site of sCupA to the S1 site of apo-$CopA^{MBD}$. Overlay of the backbone $^{1}H,^{15}N$-HSQC spectra of $CopA^{MBD}$ (**a**) and sCupA (**b**), with the same crosspeak color pattern as in panels c-d. The superposition of *cyan* and *green* crosspeaks (panels c-f) reveals that incubation of Cu(I)-saturated sCupA with apo-MBD results in movement of S2 on sCupA to the S1 site of $CopA^{MBD}$.

Although the Cu_1 and Cu_2 states of both sCupA and $CopA^{MBD}$ are readily distinguished from one another (**Appendix III, Fig. 1-6**) they cannot be used to assign the high- and low-affinity sites. The methionine $^{13}C\varepsilon$–Hε groups of both sCupA and $CopA^{MBD}$ were assigned by ^{13}C-edited NOESY spectroscopy. Direct Met-Cu(I) coordination expected to induce a strong downfield shift of the $^{13}C\varepsilon$ chemical shift as revealed by a $^{1}H,^{13}C$-HSQC spectrum (**Fig. 22**)[120]. Only upon addition of the second mol•equiv Cu(I) is there a strong downfield shift of the $^{13}C\varepsilon$-$^{1}H\varepsilon$ methyl crosspeaks of M88 and M90 of $CopA^{MBD}$ indicative of direct ligation (**Fig. 22a**). For sCupA, addition of the first mol•equiv of Cu(I) results in a slight *upfield* shift of the M116 $^{13}C\varepsilon$–Hε with few other changes in the spectrum; only upon addition of the second mol•equiv of Cu(I) is there a strong downfield shift of the methyl resonances of M113 and M115. Inspection of the sCupA structure reveals that M116 is quite close to the S1 site ion, and thus reports on filling the digonal *bis*-thiolato S1 site (**Fig. 22b**). I conclude that the high affinity Cu(I) site on both $CopA^{MBD}$ and sCupA is the *bis*-thiolato S1 site, with the more solvent-exposed Met-rich S2 site the low affinity Cu(I) site in each case.

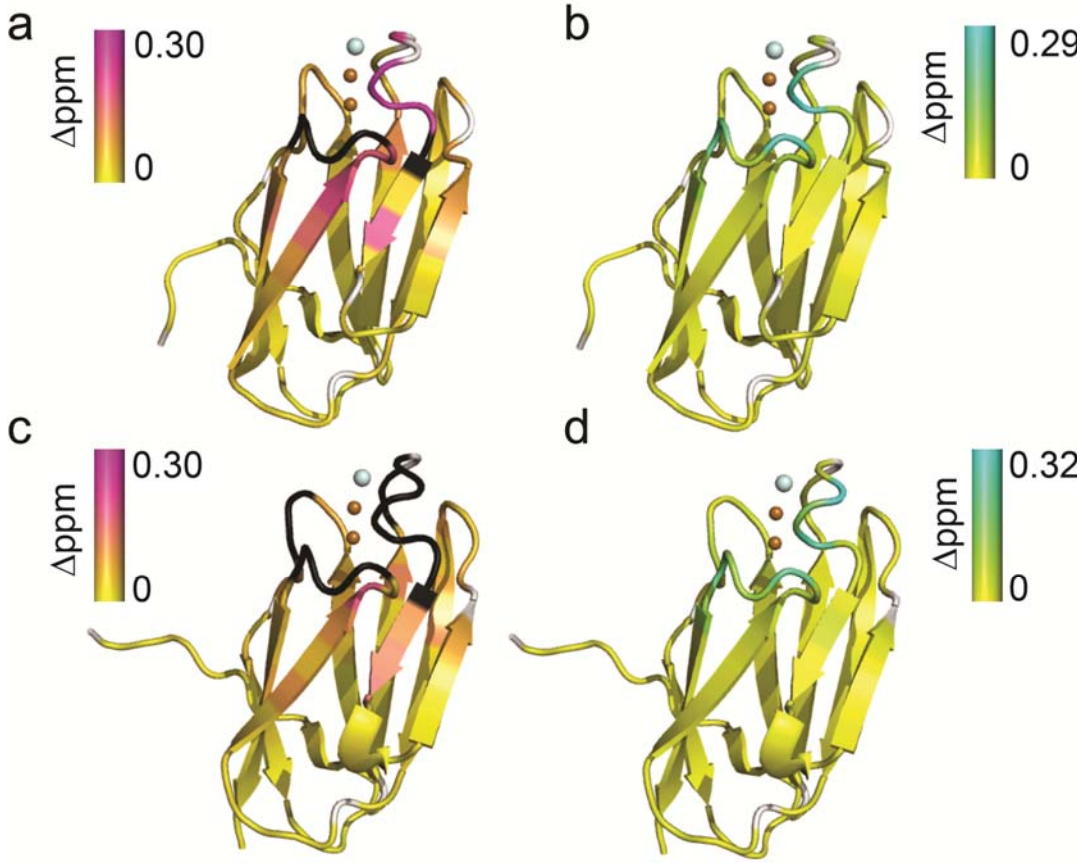

Figure 24: NMR chemical shift perturbation analysis of sCupA and $CopA^{MBD}$ induced by Cu(I) binding.

Ribbon representation of the changes in backbone amide chemical shift upon Cu(I) binding by sCupA (**a**, **b**) and $CopA^{MBD}$ (**c**, **d**). Panels a and c represent Δppm (Cu_1–apo) while panels b and d represent Δppm (Cu_2–Cu_1). The ribbon is painted *white* for Pro residues and *black* for those resonances broadened beyond detection in the apo-state in each case.

2.3.5 Cu(I) is transferred from the S2 site on sCupA to the S1 site on CopA^{MBD}

Next whether Cu(I) bound to the putative donor sCupA could be transferred to acceptor CopA^{MBD} was examined, by taking advantage of the distinct spectroscopic signatures of Cu(I) bound to each of the two Cu(I) sites (**Fig. 22a-b**). This experiment was performed using an NMR-based strategy[98] by mixing $^{13}C,^{15}N$-sCupA with unlabeled CopA^{MBD} or unlabeled sCupA with $^{13}C,^{15}N$-CopA^{MBD}, with sCupA loaded with two mol•equiv of Cu(I) as copper donor. When unlabeled apo-CopA^{MBD} is mixed with stoichiometeric Cu_2 $^{13}C,^{15}N$-sCupA, one Cu(I) is lost, specifically from the low-affinity Met-rich S2 site as evidenced by a return of the $^{13}C\varepsilon$-$^{1}H\varepsilon$ crosspeaks of M113 and M115 to their positions in Cu_1 sCupA (**Fig. 22b)**; the same is evident on inspection of the $^{1}H,^{15}N$-HSQC spectrum of sCupA, with the blue (Cu_2) resonances lost, and concomitant superposition of the green (*bona fide* Cu_1 sCupA) and cyan (Cu_2 sCupA mixed with apo-CopA^{MBD}) crosspeaks (**Fig. 23b**). There is no trace of apo-sCupA in these spectra. Monitoring the same reaction with excess (2:1) unlabeled Cu-saturated sCupA and $^{13}C,^{15}N$-apo-CopA^{MBD} reveals formation of only the *bona fide* Cu_1 CopA^{MBD} with the S1 sites filled (**Fig. 22a**), with no evidence of the Cu_2 or apo-MBD in these mixtures (**Fig. 23a**). Thus, even in the presence of excess Cu bound to sCupA, only the high affinity S1 site on the CopA^{MBD} is capable of accepting the Cu(I) from sCupA, and that Cu(I) is donated from the more solvent-exposed lower affinity S2 site on sCupA.

The reverse experiment was also done in which stoichiometric $^{13}C,^{15}N$-labeled Cu_1 CopA^{MBD} was mixed with unlabeled apo-sCupA. There is no change in the spectrum (**Fig. 25**), thus revealing that despite the higher affinity, the S1 site on sCupA is unable to strip the MDB of its bound Cu(I). Only when excess apo-sCupA is added or Cu(I) is

available from the low affinity S2 site does any Cu(I) move to sCupA. Thus, efficient Cu(I) transfer is preferentially unidirectional, but likely depends on the molar ratio of CupA and CopA in the membrane.

2.3.6 Cu(I) coordination by CupA but not by $CopA^{MBD}$ is essential for copper resistance of *S. pneumoniae*

In order to further understand the essentiality of *cupA* for mediating copper resistance we characterized allelic replacement strains using our structures as a guide (**Fig. 17-18**) in which the *cupA* gene was replaced with a mutant *cupA* allele wherein all Cu-coordinating β7-β8 loop residues (C111, M113 and M115) were substituted with Ala (*cupA*(3A)), and/or the bridging ligand C74 was replaced with Ser (*cupA*(C74S); *cupA*(C74S,3A)). Biochemical experiments reveal that C74S sCupA binds a single mol•equiv of Cu(I) with a low affinity as measured by a BCA competition assay ($K_{Cu} \approx 10^{12}$ M^{-1}) but adopts a fold identical to that of wild-type sCupA with only local structural perturbations around the site of the substitution (**Fig. 26**). In the absence of added copper, all metal-liganding mutant strains grow similarly to that of the *cupA*-(C)-FLAG strain (**Fig. 27a**). However, in the presence of 0.2 mM Cu(II), growth of the *cupA*(3A) strain is significantly inhibited while the *cupA*(C74S) and *cupA*(C74S,3A) both fail to grow significantly (**Fig. 27b**), despite the fact that all CupAs accumulate to level greater than that of wild-type CupA (**Fig. 13a**). At 0.5 mM Cu(II), under conditions where the wild-type strain is somewhat affected, neither strain is able to grow (**Fig. 28**). In fact, the behavior of *cupA*(C74S) strain is indistinguishable from a *copA*(D442A) strain expressing a catalytically inactive CopA (**Fig. 27c**). Interestingly, Western blotting reveals that C-terminally FLAG-tagged CopA accumulates to very high levels in both strains, as well as in the Δ*cupA* strain

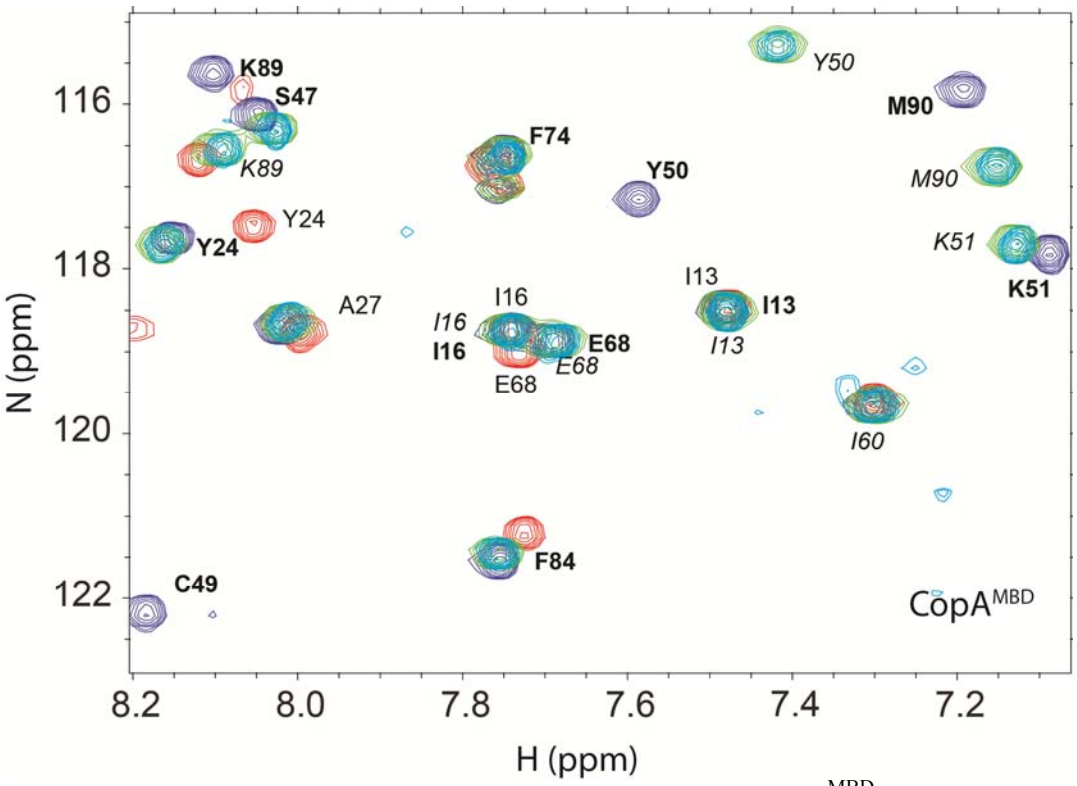

Figure 25: Apo-sCupA is unable to chelate Cu(I) from $Cu_{0.8}$ $CopA^{MBD}$ when mixed at a molar ratio of 1:1.

Overlay of a selected region of an $^{1}H,^{15}N$-HSQC spectrum of $CopA^{MBD}$ acquired in the apo-state (*red* crosspeaks), following addition of 0.8 Cu(I) (*green* crosspeaks; *italics* type) and 1.8 Cu(I) (*blue* crosspeaks; ***bold-face*** type) and after mixing $Cu_{0.8}$ $CopA^{MBD}$ with unlabeled apo-sCupA (*cyan* crosspeaks). The superposition of *cyan* and *green* crosspeaks reveals that apo sCupA is unable to strip the Cu(I) from S1 Cu-ligated $CopA^{MBD}$, despite its higher affinity at equilibrium. Incubation of stoichiometric $Cu_{1.8}$ $CopA^{MBD}$ with apo-sCupA results in the low affinity S2 Cu moving to the high affinity S1 Cu site on sCupA, which is thermodynamically favorable. The S1 Cu on $CopA^{MBD}$ does not transfer under these conditions.

(**Fig. 13b**). Analysis of the total cell-associated metal content of these strains by ICP-MS reveals a substantial increase in total cellular Cu, which reaches a level ≈5-fold higher than WT cells 3 h after addition of 0.2 mM Cu in the Δ*cupA* and *cupA*(C74S) strains (**Table 4**). In contrast, when a substitution that is analogous to C74S in CupA is introduced into the $CopA^{MBD}$ in the *copA* gene (*copA*(C49S)), copper resistance is unaffected at both 0.2 mM (**Fig. 27c**) and 0.5 mM Cu(II) (**Fig. 28c**). Consistent with this, FLAG-tagged C49S CopA accumulates to a level similar to that of wild-type CopA rather than to that of Cu-sensitive mutants (**Fig. 13b**). Thus, these experiments establish that the major function of the CupA in copper stress resistance in *Spn* is not to chaperone Cu(I) to the $CopA^{MBD}$ but is instead required for direct copper delivery to the transmembrane Cu(I) binding sites in CopA for efflux and/or to sequester Cu(I) during copper stress in an effort to mitigate the effects of cellular Cu toxicity (**Table 4**).

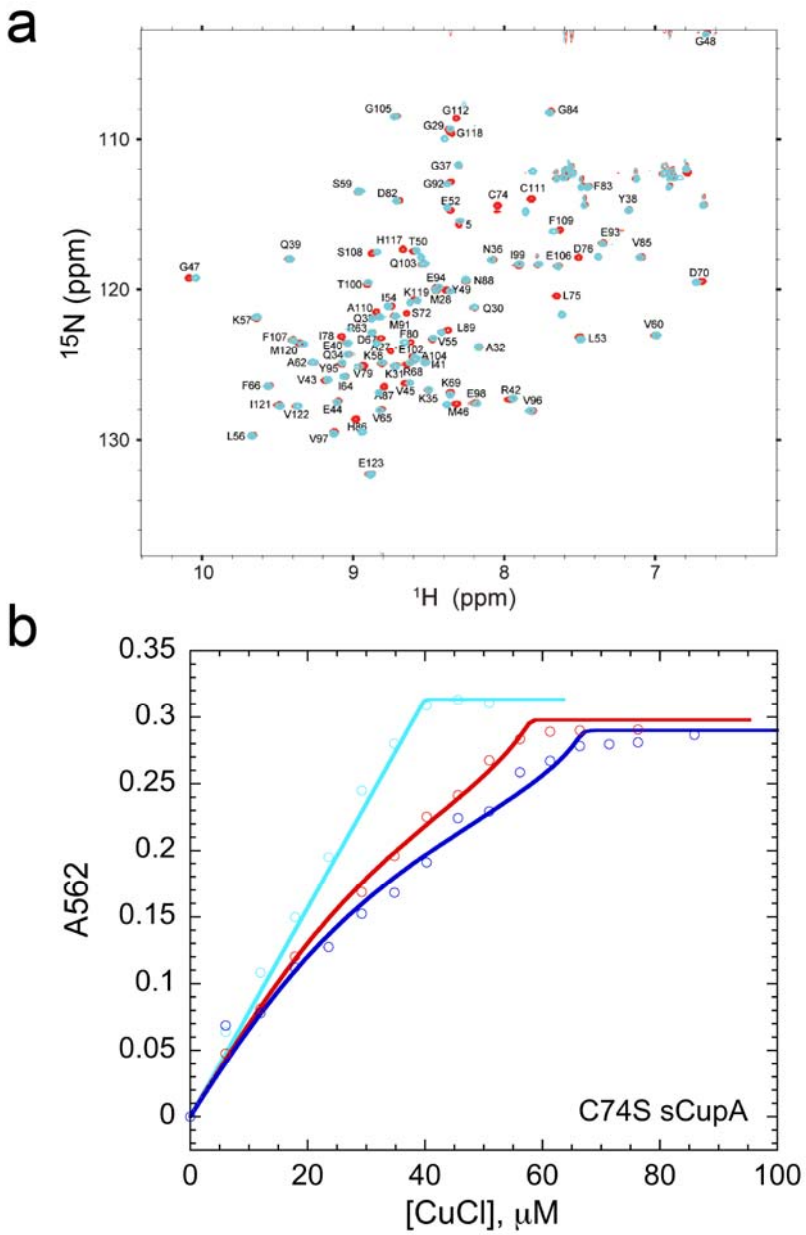

Figure 26: Structural characterization of integrity of C74S sCupA.
(**a**) Superposition of the $^{1}H,^{15}N$-HSQC spectra of apo-C74S sCupA (*cyan* crosspeaks) and the wild-type apo-sCupA (red crosspeaks). Spectral perturbations are structurally near the site of the substitution localized to the β3-β4 and β7-β8 loops, revealing that C74S adopts a wild-type like fold. (**b**) BCA competition experiment. Titration of Cu(I) into 80 μM BCA alone (*cyan*) or in the presence of 76 μM BCA and 20 μM apo-C74S sCupA (*red*) or 74 μM BCA and 30 μM apo-C74S sCupA (*blue*). The continuous lines through the data represent the results of a global analysis of all experiments to a single site, direct competition model with K_{Cu}= 3.6 (±0.6) x 10^{12} M^{-1}, or ≈200-fold weaker than the low-affinity Met-rich S2 Cu site of sCupA.

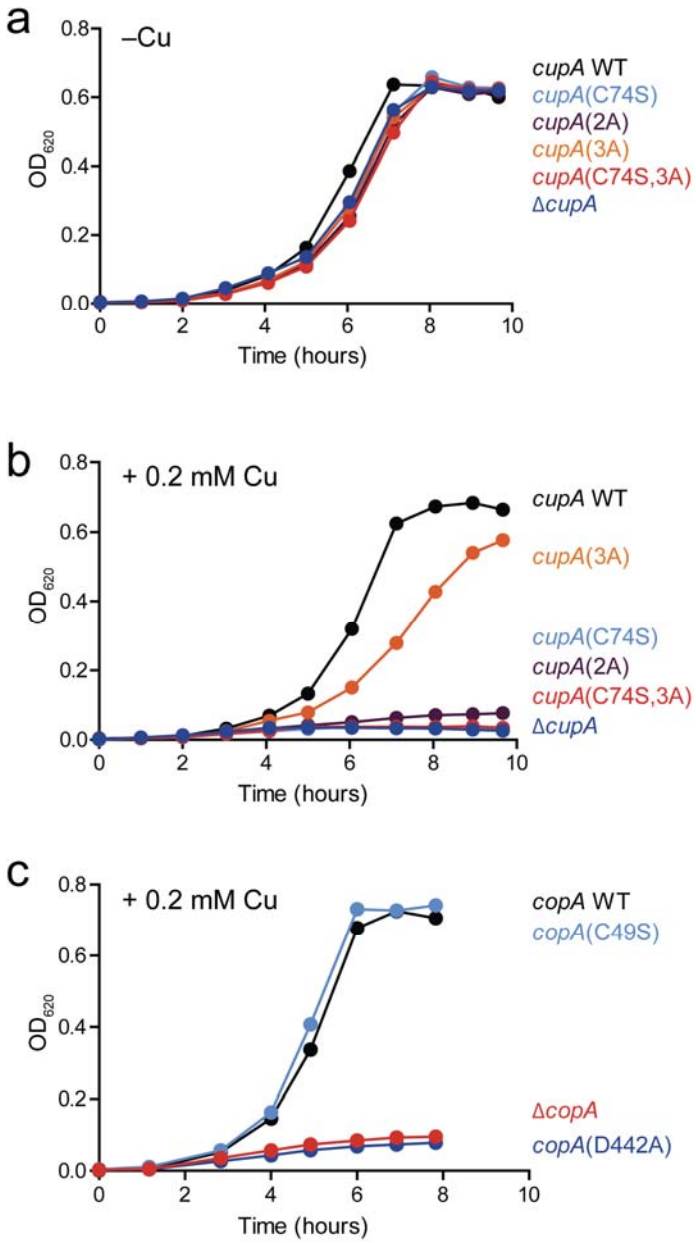

Figure 27: Mutagenesis of CupA Cu(I) binding residues partly or completely abrogates Cu(I) resistance by *S. pneumoniae*, but not in $CopA^{MBD}$.
Representative growth curves for the indicated *S. pneumoniae* strains in BHI in the absence (**a**) or presence (**b**, **c**) of 0.2 mM Cu(II) added to the growth medium. In all cases, two independent isolates of the same strain designation were constructed and duplicate (or more) growth experiments were carried out with each of the two strains. Experiment was carried out by Ho-Ching Tiffany Tsui and Kevin Bruce from Winkler Lab in the Department of Biology.

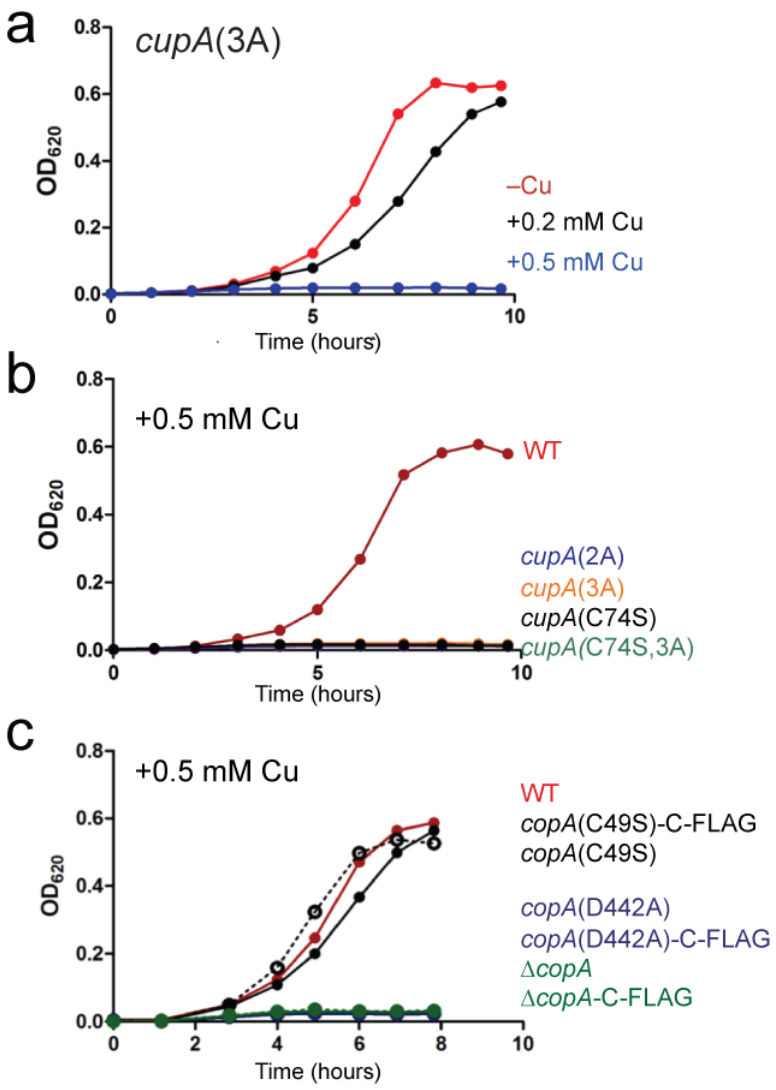

Figure 28: Growth rate analysis of *cupA* and *copA* mutant strains.
Mutation of the Cu(I) ligands in the β7-β8 loop in CupA (C111A/M113A/M115A; designated 3A) gives rise to an intermediate copper sensitivity phenotype, in contrast to a M113A/M115A mutant (designated 2A*) cupA* strain. (**a**) *cupA*(3A) (IU6015) strain grown in the absence and presence of 0.2 mM or 0.5 mM Cu(II) added to the growth media (compare to WT and *cupA*(C74S) growth curves, Supplementary Fig. 4a and Fig. 5b, main text). (**b**) Growth curves of wild-type (WT) (IU1781), *cupA*(2A) (IU6585), *cupA*(3A) (IU6015), *cupA*(C74S) (IU6050), and *cupA*(C74S,3A) (IU6052) strains in 0.5 mM Cu(II). (**c**) The *copA*(C49S) MBD mutant grows like WT, compared to *copA*(D442A) and Δ*copA* and *cupA* mutant strains which do not grow under these conditions (panel b). Growth curves for indicated *copA* mutants are compared to the WT (IU1781) strain in 0.5 mM Cu(II). Experiment was carried out by Ho-Ching Tiffany Tsui and Kevin Bruce from Winkler Lab in the Department of Biology.

2.4 Implication of the work

In this work, a new structural paradigm for copper trafficking and resistance was characterized in the Gram-positive respiratory pathogen *S. pneumoniae*. Soluble CupA and $CopA^{MBD}$ are isostructural and of opposite electrostatic surface potentials, and each harbors a binuclear Cu(I) cluster in the context of a novel architecture not previously observed in bacterial copper trafficking. The Cu(I) binding affinities of sCupA and $CopA^{MBD}$ differ significantly from one another, and although sCupA binds Cu(I) more tightly overall than $CopA^{MBD}$, copper transfer is preferentially down a thermodynamic gradient from the low affinity S2 site of sCupA to the high affinity S1 site of $CopA^{MBD}$ ($\Delta\Delta G$=–2.0 ±0.3 kcal mol^{-1}), as found in other, but not all, Cu(I) chaperone systems[27,118,121]. CupA therefore satisfies all established criteria for designation as a copper chaperone for a copper transporter[122], but is the first one known to be inserted into the plasma membrane. Remarkably, deletion of the transmembrane helix reduces copper resistance to level equivalent to that of a catalytic site mutant in CopA, thus revealing that membrane localization is uniquely essential for copper resistance in *S. pneumoniae*.

This is the first instance to our knowledge where biological studies clearly establish that deletion or functional inactivation of the copper chaperone reduces copper resistance to a level identical to deletion or inactivation of the copper transporter. This is particularly striking when one considers that metallation of metalloproteins is generally thought to require a chaperone when bioavailable Cu(I) is limiting; at excess copper levels, the classic "chaperone" function can be nominally bypassed[116]. The obligatory requirement of the CupA chaperone in Cu resistance in *Spn* was missed in the previous report, which suggested that a *Spn* strain encoding a translationally terminated *cupA* gene

gave rise only to a more modest copper sensitivity phenotype[1]. We show here that CupA protein levels in all *cupA* missense strains that express CupA with diminished Cu(I)-binding affinities accumulate to a level *greater* than that in a wild-type background; furthermore, CopA accumulates to even higher levels relative to a WT strain under conditions of Cu stress (**Fig. 13**). Selected mutant strains that exhibit greatly diminished copper resistance (Δ*cupA*, *cupA*(C74S) and Δ*copA*) accumulate far more cell-associated Cu (**Table 4**). A hyperaccumulation of both CupA and CopA in these cells may be reporting on hypersensitivity or continued derepression of CopY-mediated transcription of the *cop* operon in a failed effort to resist the effects of increased cytoplasmic copper.

Two pieces of evidence suggest that the observed ability of sCupA to donate Cu to the N-terminal MBD of CopA is not strongly correlated with cellular Cu resistance under the growth conditions examined here. First, the *cupA*(3A) strain, which encodes a CupA which likely lacks Cu(I) binding to the low affinity S2 donor site, gives rise only to an intermediate Cu-sensitivity phenotype at 0.2 mM Cu (**Fig. 2**). Secondly, inactivation of the S1 acceptor site in *copA*(C49S) is functionally silent (**Fig. 27**). Thus, although Cu transfer from the S2 site of CupA to the S1 site of $CopA^{MBD}$ occurs spontaneously, we suggest that this may occur only under non-stressed or "housekeeping" conditions since it is not strongly relevant to the cellular response of *Spn* to acute Cu toxicity. Other functional roles for CupA are possible, particularly so given that the metallochaperone for the Cu_A subunit of a bacterial cytochrome *c* oxidase is itself a membrane-anchored cupredoxin-fold protein that binds a single Cu(I) ion.[96,98] However, CupA is not performing this role in *S. pneumoniae* since this bacterium lacks cytochrome *c* oxidase and an electron transport chain.[14]

Recent structural studies of the apo metal-free bacterial CopAs[67,115] support a model in which the N-terminal MBD (not visualized in the crystallographic structure of *Legionella* CopA) plays a regulatory role. The MBD likely docks against the actuator cytoplasmic domain (**Fig. 29**) and inhibits ATP hydrolysis by the pump in the absence of Cu(I); metal binding by the MBD is hypothesized to disrupt this interaction and allosterically activate ATP hydrolysis and Cu(I) transport across the membrane. It has been shown that the cytoplasmic copper chaperone Atx1 can deliver Cu(I) to either the N-terminal MBD, which is not on-pathway for copper transfer, or the transmembrane site directly[61], the latter hypothesized to occur via docking to the positively charged platform region that surrounds the putative entry site for Cu transfer[67]. Thus, the negative electrostatic surface potential of sCupA is complementary to both the MBD and the platform region of CopA, and may facilitate transient docking and Cu delivery to either site (**Fig. 29**).

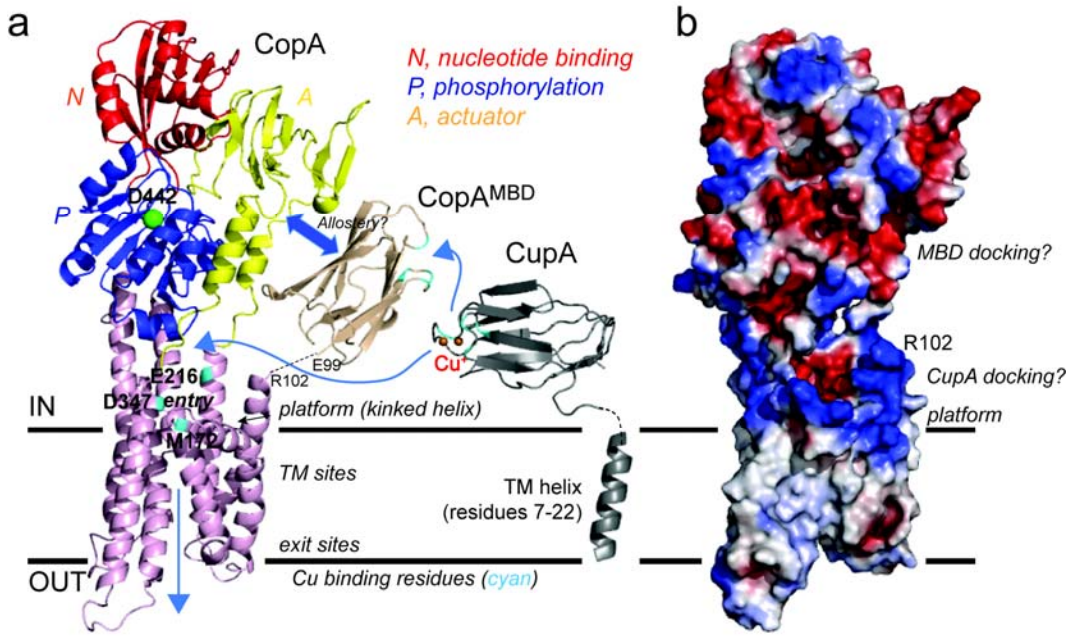

Figure 29: Cu(I) resistance mechanism proposed based on data in chapter II. (**a**) Homology model predicted by Swiss-Model[157,158] of *S. pneumoniae* CopA shown to scale with our structures of sCupA and CopA^{MBD}. R102 defines the N-terminus of the model based on *Lp*CopA structure[67], while E99 defines the most C-terminal residue visible in our CopA^{MBD} structure. This places the MBD in close proximity to the actuator domain (*yellow*) where it can influence the rate of hydrolysis of D442 in the phosphorylation domain (shaded *blue*). Possible paths of copper delivery by CupA are represented by the *cyan* arrows. (**b**) The electrostatic surface potential of the model of *Spn* CopA suggest that the positively charged MBD (**Fig. 17-18**) could preferentially dock against the negatively charged actuator domain region, while CupA could be electrostatically guided to the positively charged platform helix region in order to deliver Cu(I) directly to the entry site just above the transmembrane (TM) binding sites (not shown).

Table 1: Cu(I) binding affinities for sCupA and $CopA^{MBD}$ *

Protein	log K_{Cu1} (M^{-1})	log K_{Cu2} (M^{-1})	log $\beta_{2,Cu}$ (M^{-2})
sCupA	17.9 (±0.3)	14.8 (±0.2)[2]	32.6 (±0.3)
$CopA^{MBD}$	16.3 (±0.1)	13.4 (±0.3)	29.8 (±0.3)

* These parameters were measured via global analysis of multiple anaerobic CuCl titrations using BCA or BCS as a competitor Cu chelator (see **Figs. 15-16** for titrations) using a nonlinear least squares fit to a stepwise two-Cu(I) binding model in both cases. [2]Reflects the average value from BCA and BCS titrations. Conditions: 25 mM Hepes, 0.2 M NaCl, pH 7.0, 22 ºC).

Table 2: Crystallographic data collection and refinement statistics

	Cu_2 sCupA	Cu_2 $CopA^{MBD}$
Data collection		
Space group	$P2_12_12$	$P2_12_12_1$
Cell dimensions		
a, *b*, *c* (Å)	47.208, 78.647,23.455	35.455, 37.329, 69.294
α, β, γ (°)	90, 90, 90	90, 90, 90
Resolution (Å)[a]	50.00-1.45 (1.48-1.45)	50.00-1.45 (1.48-1.45)
R_{sym} or R_{merge}[a]	0.024 (0.183)	0.035 (0.363)
$I / \sigma I$[a]	46.5 (8.2)	43.0 (6.3)
Completeness (%)[a]	99.8 (99.5)	99.9 (100.0)
Redundancy[a]	6.6 (6.1)	11.4 (10.6)
Refinement[b,c]		
Resolution (Å)	21.00-1.45	20.00-1.50
No. reflections	16233	15410
R_{work} / R_{free}	0.1778/0.1998	0.2134/0.2430
No. atoms		
Protein	774	783
Ligand/ion	3	3
Water	192	122
B-factors		
Protein	14.73	23.37
Ligand/ion	12.44	20.59
Water	26.91	35.05
R.m.s. deviations		
Bond lengths (Å)	0.017	0.020
Bond angles (°)	0.913	0.766

[a]Values in parentheses are for highest-resolution shell.
[b]Structures have been deposited with Protein Data Bank under accession codes 4F2E (sCupA) and 4F2F ($CopA^{MBD}$), respectively.
[c]Two crystals were used to collect diffraction data for $CopA^{MBD}$. One crystal was used to collect diffraction data of sCupA.

Table 3: Crystallographically determined copper coordination bond lengths and bond angles for Cu_2 sCupA and Cu_2 $CopA^{MBD}$ [a]

Cu site	Bond Distance Å		Structure Angle °	
sCupA S1	Cu – C74 Sγ	2.16	C74 Sγ – Cu – C111 Sγ	157.31
	Cu – C111 Sγ	2.18		
sCupA S2	Cu – C74 Sγ	2.25	C74 Sγ – Cu – M115 Sδ	118.26
	Cu – M113 Sδ	2.31	C74 Sγ – Cu –M113 Sδ	128.66
	Cu – M115 Sδ	2.32	M113 Sδ – Cu – M115 Sδ	108.54
	Cu – Cl^-	2.33	C74 Sγ – Cu – Cl^-	100.06
			M113 Sδ – Cu – Cl^-	93.21
			M115 Sδ – Cu – Cl^-	97.67
$CopA^{MBD}$ S1	Cu – C49 Sγ	2.16	C49 Sγ – Cu – C86 Sγ	158.52
	Cu – C86 Sγ	2.15		
$CopA^{MBD}$ S2	Cu – C49 Sγ	2.23	C49 Sγ – Cu – M90 Sδ	118.52
	Cu – M88 Sδ	2.30	C49 Sγ – Cu –M88 Sδ	121.02
	Cu – M90 Sδ	2.24	M88 Sδ – Cu – M90 Sδ	114.64
	Cu – Cl^-	2.47	C49 Sγ – Cu – Cl^-	99.91
			M88 Sδ – Cu – Cl^-	90.92
			M90 Sδ – Cu – Cl^-	103.32

[a]See **Table 2** for crystallographic data collection and refinement statistics on which these data are based.

Table 4: Total cell-associated copper content (in ng/mg protein) of various *Spn* strains in the absence and presence of 0.2 mM added to the growth medium[a]

Strain	No Cu added[b]	0.2 mM Cu, 2 h[b]	0.2 mM Cu, 3 h[c]
WT (IU1781)	193 (±50)	285 (±32)	176 (±3)
Δ*cupA* (IU5971)	223 (±29)	906 (±402)[d]	889 (±168)[d]
cupA(C74S) (IU6050)	187 (±30)[c]	631 (±103)[d]	928 (±540)
Δ*copA* (IU5975)	162 (±16)	624 (±88)[d]	809 (±14)[d]

[a]Cells used for this experiment were obtained from 2 to 3 (*n*) experiments, derived from a representative growth curve like that shown in **Fig. 12e** for the Cu-containing samples. OD_{620} ranged from 0.1-0.3. [b]From *n*=3 biological replicates. Student's *t*-test shows that the differences in Cu content observed among the No Cu added samples are not significant. [c]From *n*=2 biological replicates. [d]Difference in Cu content between the WT strain vs. other strains for samples collected at 2 and 3 h post Cu addition is statistically significant ($p \leq 0.05$). Measurement was carried out by John P. Lisher from Giedroc lab.

CHAPTER III: Solution structure of apo-sCupA and the functional role of each Cu(I) binding site in CupA

3.1 Introduction

The physiological function of cytoplasmic copper chaperones has received considerable attention over the last several years. The early copper trafficking hypothesis proposed that the chaperone was responsible for delivering Cu(I) to its cellular target without dissociation into solvent, mitigating copper-mediated cellular damage.[123] However, in eukaryotic cells, there is no observable copper hypersensitivity for any of the mutants lacking copper chaperones in each of three major pathways: (1) to the *trans*-Golgi network; (2) to superoxide dismutase; and (3) to cytochrome c oxidase. In prokaryotes, CopZ-like copper chaperones were proposed to transfer Cu(I) either to the copper-responsive metallosensor leading to transcriptional derepression of the Cu resistance *cop* operon, and/or to the copper exporting ATPase that pumps Cu(I) out of the cytoplasm.[59,61] However, genomic deletion of *copZ* in *Listeria monocytogenes*, for example, was shown to have little effect on the transcription of the *cop* operon or on growth rate under copper stress[92], suggesting that the CopZ-like chaperone may not be playing an obligatory role in either proposed trafficking function. A subsequent model derived from studies of the cyanobacteria copper chaperone scAtx1 proposed that scAtx1 is not an obligatory player for copper delivery to cellular targets either; rather, scAtx1 alongside glutathione, buffers Cu(I) to very low "free" levels, by preventing Cu(I) from gaining access to other non-cognate metal sites, thereby preventing Cu(I) toxicity.[116]

Since Cu(I) binding by CupA was shown to be essential for Cu(I) resistance, how CupA functions in this process as well as the functional role played by each of the two

Cu(I) sites is not yet established. Further, a high resolution structure of apo-sCupA is not yet available. The essentiality of CupA in pneumococcal Cu(I) resistance thus provides an excellent system with which to discriminate between the two competing models of copper chaperone function: (1) the copper chaperone is on-route for cytoplasmic Cu(I) efflux, or (2) the copper chaperone is exclusively involved in buffering free Cu(I) to very low levels.

In this chapter, biophysical, biochemical and molecular microbiological approaches are employed to determine the solution structure of apo-sCupA and evaluate the functionality of each Cu(I) site in CupA *in vivo*. Our findings reveal the apo-sCupA adopts the same cupredoxin fold as Cu_2-CupA with a dynamic Cu(I) binding loop demonstrated by both backbone and side chain measurements. The side chains of coordinating residues in the S1 Cu site are pre-organized for Cu(I) binding while the S2-specific side chains (M113, M115) are highly dynamic. The high affinity S1 Cu(I) site is dispensable for cellular Cu(I) resistance, while the low affinity S2 Cu(I) binding site is essential for bacterial growth under copper stress. These growth phenotypes track with total cell associated Cu(I), consistent with the hypothesis that the S2 site in CupA delivers Cu(I) directly to the to CopA for export. A triple substitution of the proposed metal entry site (MBS) in CopA in abrogates Cu resistance, and a CopZ tethered to the plasma membrane via a cupA TM helix also fails to protect pneumococcus from Cu poisoning. These studies are consistent with a direct physical interaction of the CupA S2 Cu with the MBS of CopA that is on pathway for Cu(I) efflux.

3.2 Methods

3.2.1 Measurement of apo-sCupA backbone dynamics

^{15}N relaxation experiments were acquired using two-dimensional, proton-detected heteronuclear NMR experiments.[124] R_1 values were measured from the spectra recorded with ten different duration of delay T: T = 10, 50, 110, 190, 310, 500, 650, 1000, 1500 and 1900 ms. R_2 values were determined from the spectra recorded with ten different durations of the delay T: T = 10, 30, 50, 90, 110, 150, 190, 210, 230 and 250 ms. ^{1}H-^{15}N heteronuclear NOE values were determined from spectra recorded in the absence and presence of a 3 s ^{1}H pre-saturation period. The rotational correlation time (τ_c) of apo sCupA was estimated from the data analysis according to model-free formalism using Tensor V2.0[125].

3.2.2 Measurement of apo-sCupA side chain dynamics

To measure the intra-methyl ^{1}H-^{1}H dipole-dipole cross-correlated relaxation rate (η)[126,127], a set of pairs of experiments were recorded. The signal intensity (I_a) in the first experiment during a variable relaxation delay (T) depends on spin-dynamics in the I = 3/2 manifold of the Met ε methyl ^{1}H spin-system. The signal intensity (I_b) in the second experiment is determined by spin-dynamics in the I = 3/2 and I = 1/2 manifolds. The cross-correlated rate (η) is related to the intensity ratio (I_a/I_b) in the given equation at each time T:

$$\frac{I_a}{I_b} = \frac{-0.5\eta \tanh(\sqrt{\eta^2 + \delta^2}T)}{\sqrt{\eta^2 + \delta^2} - \delta \tanh(\sqrt{\eta^2 + \delta^2}T)} \quad (1)$$

Ten values of T = 2, 5, 8, 12, 17, 22, 27, 32, 37, 42 ms were used for both experiments. An η value was obtained by fitting the experimentally determined I_a/I_b ratio as a function

of *T* to eq (1) (see **Fig. 35** for representative fits). The axial order parameters (S^2_{axis}) were then calculated from eq (2) using the rotational correlation time (τ_c) of apo sCupA (determined above):

$$S^2_{axis} = \frac{10}{9}\frac{r^6_{HH}\eta}{\gamma^4_H \hbar^2 \tau_c P_2(\cos(\theta_{HH}))^2} \quad (2)$$
$$P_2(x) = \frac{(3x^2 - 1)}{2}$$

where r_{HH} = 1.813 Å, θ_{HH} = 90°.

3.2.3 Apo-sCupA structure calculation

Distance restraints were derived from 3D ^{15}N-edited NOESY-HSQC (m = 200 ms) and ^{13}C-edited NOESY-HSQC (m = 150 ms) experiments. Backbone dihedral angle restraints for three-dimensional structure calculation were generated from apo sCupA backbone assignments using TALOS$^+$.[128] Initial NOE cross-peak assignments were obtained using automatic NOE assignment and structure calculation algorithm implemented in CYANA 2.1.[129,130] Partial assigned peak lists were then further manually assigned and confirmed during subsequent CYANA calculations. In total, 100 structures were calculated using CYANA and subsequently refined using a simulated annealing protocol with Xplor-NIH.[131] After iterative refinement and editing of the distance restraints based on the NOESY spectra to remove incorrect and ambiguous assignments, a final ensemble of 18 structures with the lowest energies were chosen for analysis and were deposited in the Protein Data Bank (entry 2MRY). Substantially complete resonance assignments for apo-sCupA have been deposited in the BMRB under accession number 25098.

3.2.4 *In vitro* redox potential measurement

The assay is modified based on study of Atox1 in yeast.[2] Apo sCupA and $CopA^{MBD}$ were prepared as previously described[132] in the anaerobic glove box. A typical concentration of 30 μM proteins was used to perform the measurement to be incubated with a mixture of GSH and GSSG present at different ratios in 50 mM potassium phosphate, pH 7.0. Concentrations of [GSH] and [GSSG] were chosen so that: $[GSH]+2\times[GSSG]=10mM$. Incubation time was 2 hours. The reaction was quenched by adding 10 % (w/v) TCA. Followed by centrifugation at 10K for 30 min, the pellet was washed with ice-cold acetone twice and resuspended in Laemmli sample buffer containing 4 M urea. The protein was labeled with 5 mM EZ-link maleimide-PEG11-miotin at room temperature for 3 hours. The labeling was quenched by adding excessive amount of cysteine. The labeled protein was subject to 18 % SDS-PAGE to determine reduced vs. oxidized protein. Incorporation of EZ-Link maleimide-PEG11-biotin, indicating the presence of reduce cysteine, was identified by a mobility shift of labeled protein. Protein quantification in bands was done by densitometry using ImageJ. The ratio of reduced Cys residues to total was plotted against the redox potential of the GSH/GSSG pair and fit to the following Nernst equation:

$$E = E_0 - \frac{RT}{2F}\ln(\frac{f}{1-f})$$

f is fraction of reduced Cys residues. E is the redox potential of the GSH/GSSH pair in the solution and E_0 is the standard redox potential of the Cys pair in the protein. The fitting was done in Kaleidagraph. Redox potential of GSH/GSSG pair was calculated using the following equeation:

$$E = E_{GSH} - \frac{RT}{2F}\ln(\frac{[GSH]^2}{[GSSH]})$$

E_{GSH} is the standard redox potential of GSH/GSSG pair, which is -0.24 V. [2]

3.2.5 CupA oxidation by Cu(II)

Unlabeled apo sCupA was prepared in the anaerobic glove box in 25 mM Tris, pH 7.0 and 200 mM NaCl. A typical 5 or 10 μM concentration of protein was used in the assay. Protein was mixed with excessive amount of BCS (> 10 fold) followed by titration of $CuCl_2$ into the solution. Cu(II) reduction by sCupA was quantified by monitoring the absorption of BCS_2:Cu(I) complex at 483 nm. The reduced Cys residue in sCupA after titration was quantified by DTNB assay.

For NMR sample, ^{13}C, ^{15}N labeled sCupA was prepared in the anaerobic glove box in 25 mM Tris, pH 7.0 and 200 mM NaCl. A typical 400 μM concentration of protein was used and $CuCl_2$ was added to a final concentration of 800 μM to fully oxidize sCupA.

3.2.6 *In situ* thiol-labeling experiment

Strains subject to thiol-labeling were inoculated in 3 mL BHI and allowed to grow overnight at 37 °C and 5 % CO_2. Then cells were to diluted to OD 0.004 in 30 ml BHI from O/N cultures. The cells were allowed to grow till OD 0.25 for harvesting. If the effect of oxidative stress on CupA was assessed, various oxidants were added to each cell culture 30 min before harvesting. The cell pellet was washed twice using PBS buffer with 1 mM BCS to remove extracellular copper. The washed pellet was resuspended in the lysis buffer (100 mM Tris, pH 8.0, 1 mM $CaCl_2$, 3 mM EDTA, 18 % (w/v) sucrose, 1 mM BCS). The supernatant from cell lysate was treated with 20 mM AMS (100 mM

stock) to label reduced Cys residues. Reduced or oxidized CupA protein control was prepared by incubating supernant from cell lysate with 5 mM TCEP or 0.4 mM 4-DPS respectively. The labeled samples were subjected to 18 % SDS-PAGE. Incorporation of AMS to reduced Cys residues was shown as a shift in the gel band.

3.3 Results

3.3.1 Resonance Assignments and Solution Structure of apo CupA

Uniformly ^{13}C, ^{15}N labeled apo-sCupA (residues 26-123) was subjected to multidimensional NMR spectroscopy using standard methods to obtain ≈91.6% of all possible proton assignments in the ordered regions and 87.9% overall. Four residues, residues 113-116, were characterized by missing resonances in the ^{1}H, ^{15}N-heteronuclear single quantum coherence (HSQC) spectrum of apo-sCupA and include two Met residues, M113 and M115, that coordinate the S2 Cu(I) ion found in the loop containing three of the four Cu(I) binding residues, between the β7 and β8 (**Fig. 30**). The three-dimensional structure of apo-sCupA is well defined by the NMR data with 2201 NOE-based distance constraints, including 1067 long-range constraints, and 130 dihedral angle constraints (**Table 5**). The final bundle of 18 structures is characterizes by a pair-wise atomic rmsd values of 0.1 Å and 0.6 Å for the backbone and all heavy atoms, respectively (**Fig. 31**). Apo-sCupA in solution adopts the same cupredoxin-like fold as Cu_2-sCupA[132] where nearly all regions of the molecule are well defined, with the exception of the N-terminal region and the β7-β8 loop, from residues 112-116 (**Fig. 32**). The ordered regions of apo-sCupA superimpose extremely well on the structure of Cu_2-CupA (**Fig. 33a)**, fully consistent with previous chemical shift perturbation experiments.[132] The lack of constraints for the Cu(I) binding loop largely parallels the

missing of the cross-peaks in the ^{1}H, ^{15}N HSQC spectrum, indicating flexibility in the backbone of this region of the loop on the μs-ms timescale. In contrast, both the positions of the backbone and the side chain donor atoms of the high-affinity S1 Cu(I) ion, C74 in the β3-β4 loop and C111 in the β7-β8 loop, appear pre-organized for Cu(I) binding (**Fig. 33b**).

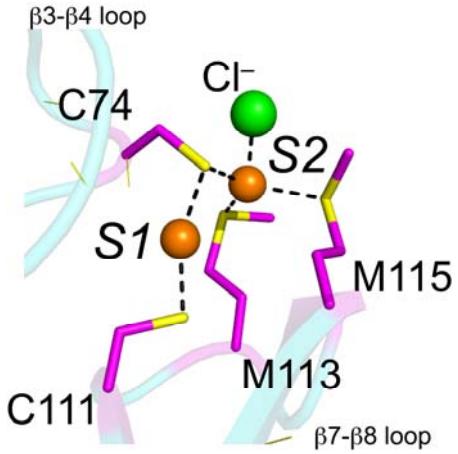

Figure 30: Close-up of the binuclear Cu(I) cluster in Cu_2-bound sCupA.
All the Cu(I) binding ligands reside on the two loops between β3-β4 and β7-β8. The loop between b7-b8 is disordered in the apo-sCupA solution structure (residue 112-116).

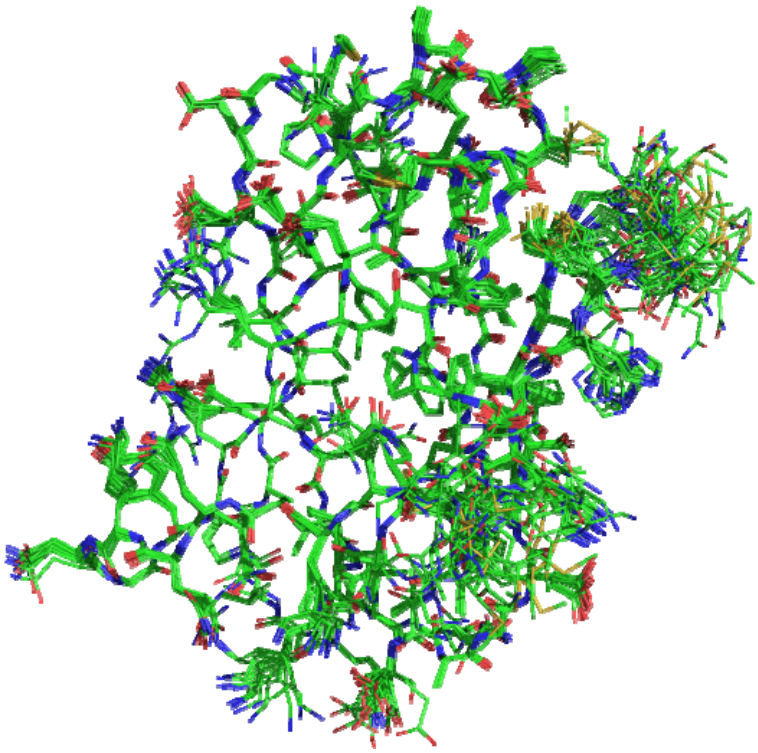

Figure 31: Solution structure ensemble of apo-sCupA.
All atom representation of the ensemble of the 18 lowest-energy models. Note the side chains of residues in the loop between β7-β8 are not converging due to dynamics.

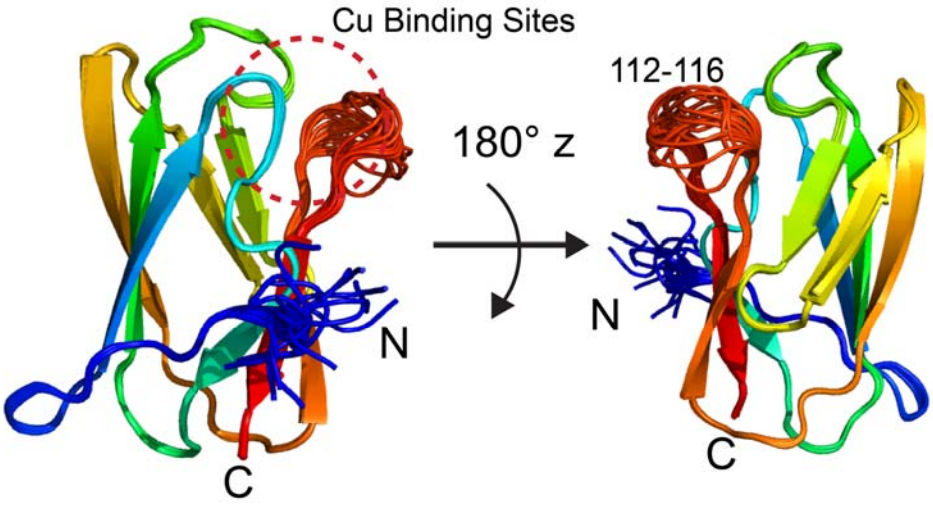

Figure 32: Cartoon representation of apo-sCupA solution structure.

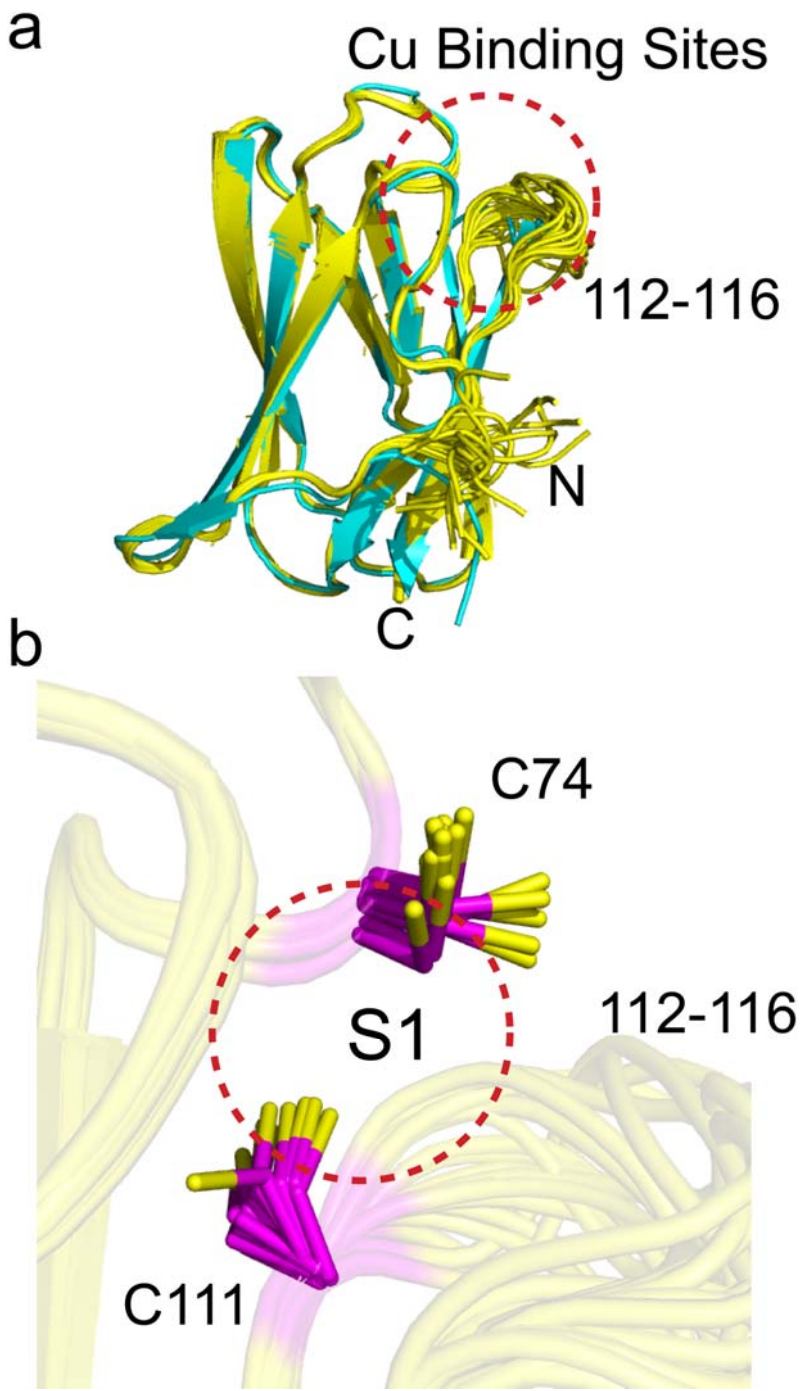

Figure 33: Structural overlay of apo and $Cu(I)_2$ form sCupA
(**a**) Cartoon representation of the ensemble of apo-sCupA overlay with Cu_2-sCupA. The overall fold is identical between apo and Cu_2 form. (**b**) Close-up of the side chains of C74 and C111 in apo-sCupA structure. The pre-organized side chains may facilitate in the high-affinity Cu(I) binding.

3.3.2 Dynamics of the Cu(I) Binding β7-β8 Loop.

The four residues with missing cross-peaks in the $^{1}H,^{15}N$-HSQC spectrum (residues 113-116) are likely due to intermediate chemical exchange broadening between two or more distinct conformations. Fast timescale (ps–ns) internal dynamical fluctuations can be approximated by the magnitude of ^{1}H-^{15}N hNOE[124], where a hNOE≥0.8 is considered rigid, and correspondingly smaller values increasingly dynamic on this fast timescale. This experiment provides insights to changes in backbone flexibility upon sequential Cu(I) loading of the high affinity S1 and low affinity S2 Cu(I) sites (**Fig. 34**). Inspection of these data reveals that Cu(I) binding to S1 site completely quenches backbone disorder in the C111 in the β7-β8 loop, while loading of the second Cu(I) into the S2 site has little or no effect on the hNOE values, and thus backbone flexibility.

Methyl groups are excellent reporters of side chain disorder on the ps-ns and μs-ms timescale.[126] Given the relatively high abundance and reasonably good distribution of methionine residues (7 total) in sCupA, particularly in the Cu(I) binding loop (M113, M115), we used the Met εCH_3 groups to compare the flexibility of the Cu(I) binding loop with the core of the protein.

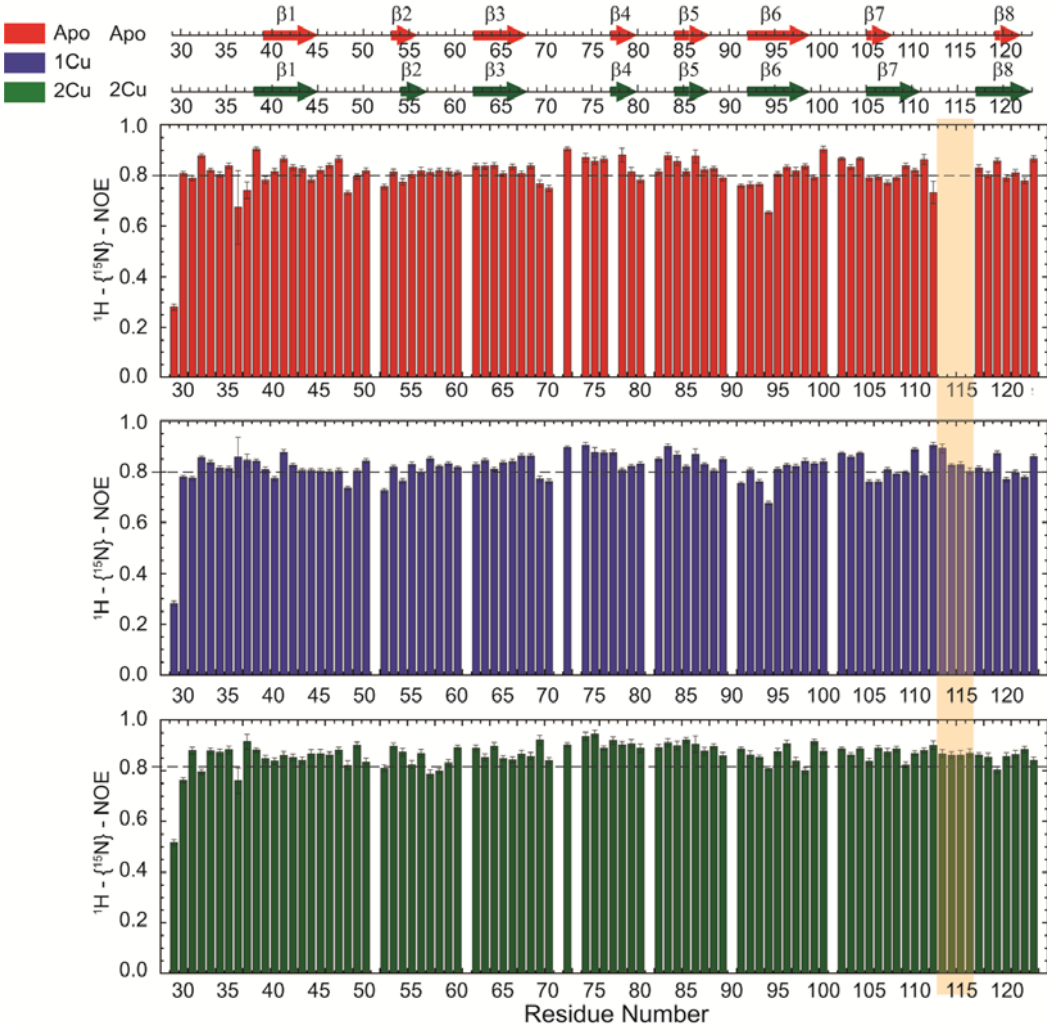

Figure 34: Plot of backbone ^{1}H-^{15}N heteronuclear NOE.
Coloring: apo (red), Cu_1 (blue) and Cu_2 (green) states of sCupA vs. residue number. Regions of significant difference among three states are colored with yellow box. Secondary structures based on apo-sCupA solution structure and Cu_2-sCupA crystal structures are depicted on the top.

Intra-methyl ^{1}H-^{1}H dipole-dipole cross-correlated relaxation rates (η) of the Met εCH_3 (**Fig. 35-36**) reports on the local dynamics on the ps-ns timescale from which one can calculate the axial order parameters of each side chain εCH_3 group (S^2_{axis}). For side chain methyls that are highly dynamic at the ps-ns timescale, the S^2_{axis} value is close to 0, while for residues that are ordered the value is close to 1. The S^2_{axis} values of the Met εCH_3 groups were measured in all three states: apo, Cu_1 (S1-bound), and Cu_2 states and compared with one another (**Fig. 36**).[126,127] M91, whose side chain is stabilized by interaction with neighboring residues in both the apo- and Cu_2-states, shows consistently larger S^2_{axis} values of ≈0.4 while M28, near the N-terminus, has S^2_{axis} values less than 0.05 for all three states. M46, solvent exposed and just C-terminal to the β1 strand generally gives low S^2_{axis} value as well. The two S2 ligands, M113 and M115, as well as M116 and M120 exhibit similar mobilities in the apo-state, with S^2_{axis}≈0.15, with the binding of the S1 and S2 Cu(I) ions inducing opposite effects. Filling of the S1 Cu(I) site detectably quenches motional disorder in M116 and M120, while significantly enhancing disorder in the two S2-Cu ligands, M113 and M115. While this disorder in M113 and M115 methyls is quenched in the Cu_2 state as a result of formation of Cu-S coordination bonds, rising to an S^2_{axis} comparable to that of M91, M116 positioned closest to the S1 Cu, and M120 are characterized by *increased* mobility in the fully Cu-loaded state. The origin of these latter effects is unknown, particularly since M120 is buried in the core in both the apo- and Cu_2 states, although inspection of the NMR ensemble of apo-sCupA (**Fig. 31**) reveals that rotation about the C^{γ}-S^{δ} bond is clearly possible.

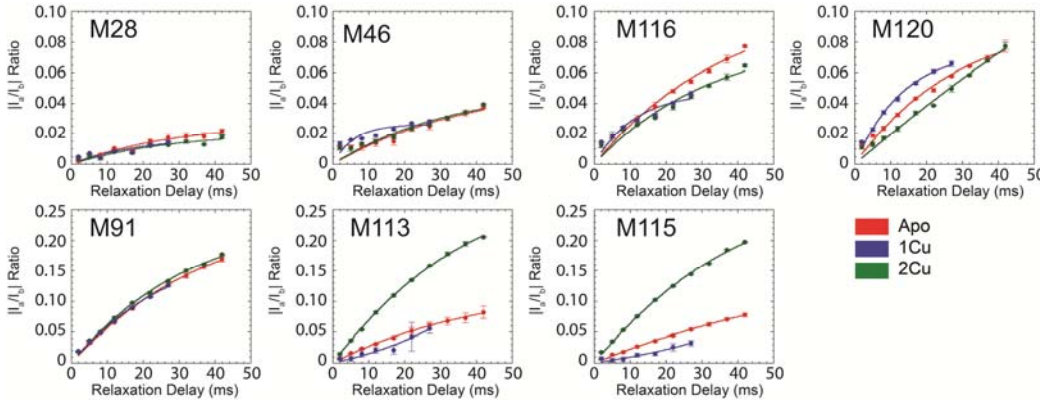

Figure 35: Build-up curves as a function of intensity ratio (I_a/I_b) used to determine the intra-methyl ^{1}H-^{1}H dipole-dipole cross-correlated relaxation rate (η).
For each of the seven Met εCH_3 groups in sCupA in each of three ligation states, apo (*red*), Cu(I) bound to the S1 sites (*blue*), and both S1 and S2 sites filled (*green*) are shown. η related to the axial order parameter, S^2_{axis} and the molecular rotational correlation time, τ_c.

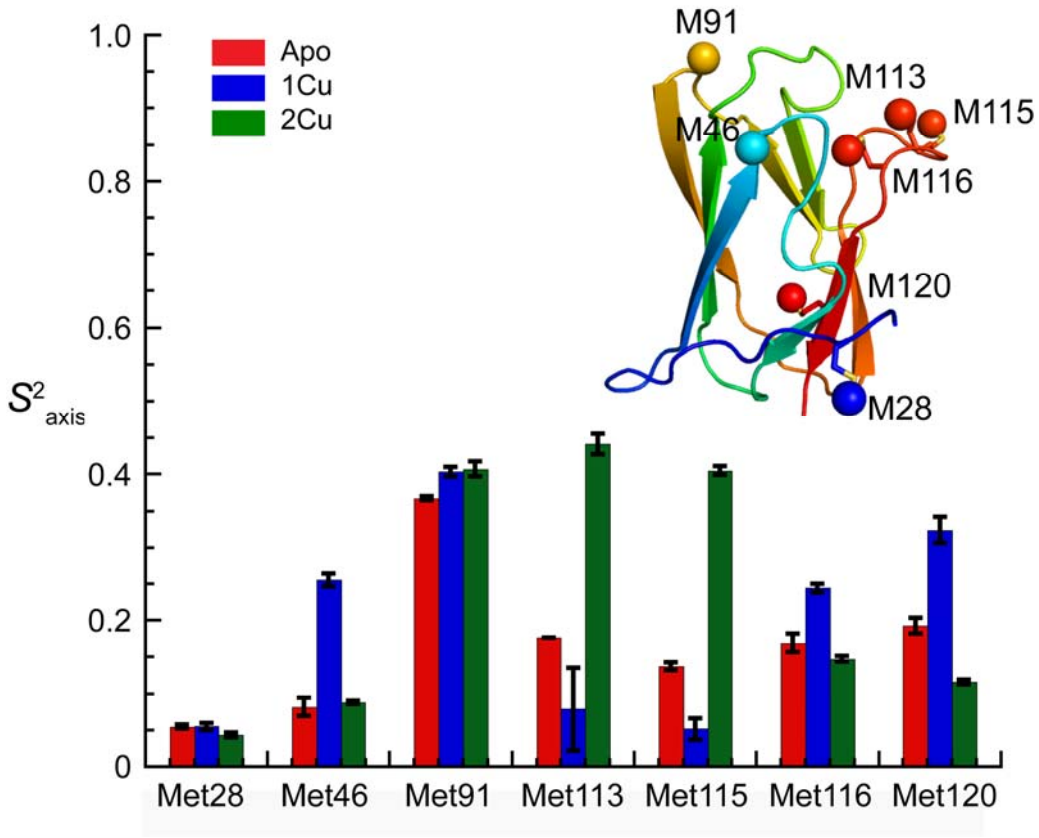

Figure 36: Plot of order parameters of each side chain εCH_3 group (S^2_{axis}) for three ligation states.
Coloring: apo (red), Cu_1 (blue) and Cu_2 (green). The position of each εCH_3 group is highlighted using a sphere on the apo-sCupA structure. M28, which is close to the N-terminus, is used as a proxy for disordered region while M91, which is stabilized by interactions with surrounding residues, is viewed as ordered regions.

These structural and dynamics studies reveal that the S1 and S2 Cu sites are characterized by distinct conformational dynamics, with the high affinity S1 site pre-organized to bind Cu, while the low affinity, more solvent exposed Met-rich S2 is highly mobile in the apo-state. Previous NMR studies show that the Cu bound to the S2 site is preferentially transferred to the S1 site of the $CopA^{MBD}$.[132] A pre-organized S1 site would lower the reorganizational energy likely resulting in a fast on-rate while prohibiting Cu(I) release. In contrast, Cu(I) binding to the S2 site would be entropically disfavored, perhaps contributing to the substantially lower affinity; on the other hand, the side chain dynamics of M113 and M115 are not entirely quenched, and these residual dynamics may well facilitate Cu transfer. These studies make the prediction that the S1 site may be principally involved in chelating Cu(I) at lower bioavailable [Cu], while S2 is largely responsible for transferring Cu(I) to CopA for export.

3.3.3 Differential biological functions for each Cu binding site in CupA

To test the hypothesis of the functionality of each Cu site in CupA, each Cu(I) site was disrupted by site directed mutagenesis, mutant bacterial strains prepared and tested for biological copper resistance. A C111S CupA substitution is postulated to abrogate Cu(I) binding to the S1 site, will maintain a functional S2 site. In contrast, the double mutant M113A/M115A CupA ($CupA^{2MA}$) was designed to block binding to the S2 site, without disruption of the S1 site. Anaerobic Cu(I) binding chelator competition experiments were carried out with each mutant to determine Cu(I) stoichiometry and affinity (**Table 6**). Both mutant CupAs bind a single mol•equivalent of Cu(I) with the results consistent with retention of the desired sites. In the case of $CupA^{2MA}$, log K_{Cu} is 17.2 (±0.1) or K_{Cu} within a factor of five of the S1 site in wild-type CupA. In contrast,

for C111S CupA, log K_{Cu} is 12.5 (±0.3) or K_{Cu} ≈200-fold weaker than for the S2 site in wild-type sCupA. This reveals that filling of the S1 site with Cu(I) clearly enhances the stability of the S2-Cu(I) complex. Interestingly, both $^{1}H,^{15}N$-HSQC and $^{1}H,^{13}C$-HSQC spectra in Cu(I)-loaded C111S sCupA exhibit features of chemical exchange broadening in the β7-β8 loop region and beyond, and thus do not provide clear evidence for Cu(I) ligation by M113 and M115 in the C111S mutant (**Fig. 37**). Substitution of immediately adjacent M116 and H117 with Ala does little to quench these dynamics, suggesting that non-native S2 Cu(I) coordination by these side chains is not the origin of this broadening (**Fig. 38**). Interestingly, it is possible to stoichiometrically oxidize the C74-C111 dithiol pair in apo-sCupA with two mol•equivalents of Cu(II) (**Fig. 39a**). In this case a downfield shift of the M113/M115 pair is observed (**Fig. 39b**). We conclude from these experiments taken collectively that C111 plays a structural role in stabilizing the structure and quenching conformational dynamics of the S2 site.

cupA^{C111S} and *cupA*^{2MA} mutants *S. pneumoniae* D39 strains were prepared next and the Cu(I)-sensitivity of these strains were compared relative to the wild-type and Δ*cupA* strains (**Fig. 40**). Previous studies showed that 0.2 mM Cu added to the BHI growth medium was sufficient to completely inhibit growth by the Δ*cupA* mutant (**Fig. 40**). Remarkably, the *cupA*^{C111S} strain is indistinguishable from the wild-type strain under these conditions revealing that the S1 site is dispensable for resistance of chronic Cu toxicity. In contrast, the *cupA*^{2MA} strain exhibits a severe growth phenotype, but grows slightly better than the Δ*cupA* strain under low copper stress (0.1 mM) (**Fig. 40**).

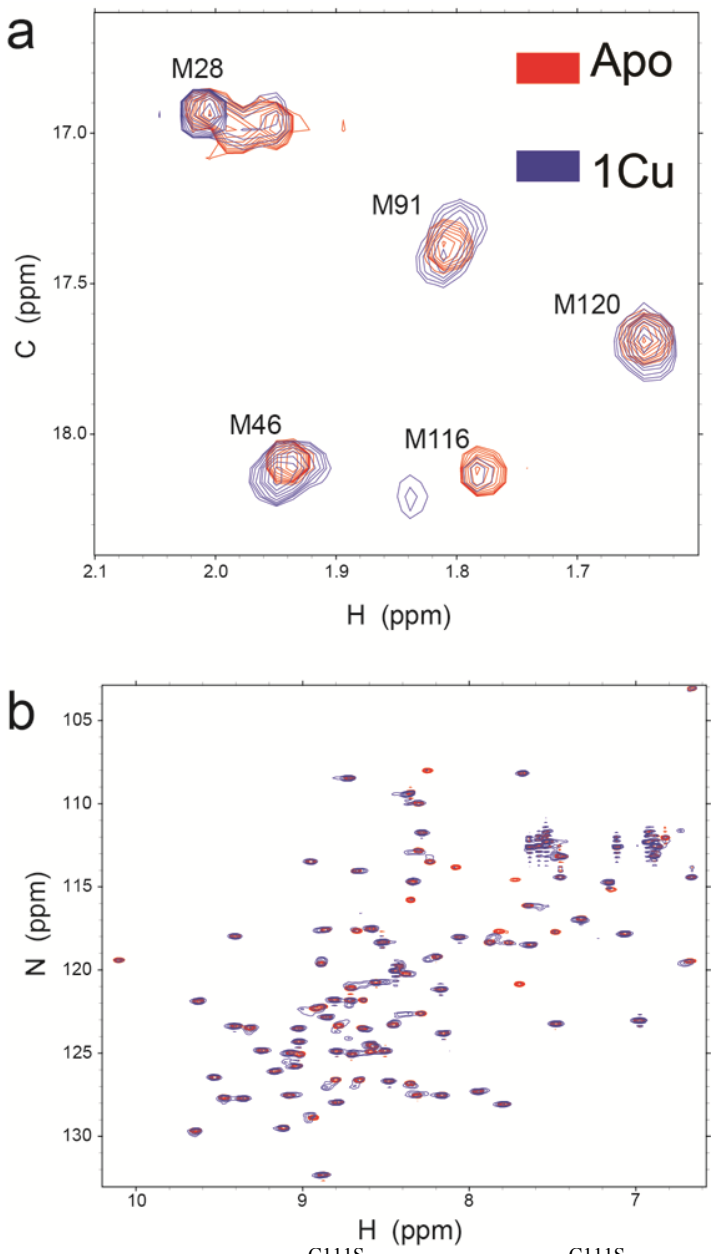

Figure 37: NMR spectra of apo-sCupA^{C111S} and Cu_1-sCupA^{C111S}.
(**a**) $^{1}H,^{13}C$-HMQC spectra overlay of apo-sCupA^{C111S} and Cu_1-sCupA^{C111S}. (**b**)^{1}H, ^{15}N-HSQC spectra overlay of apo-sCupA^{C111S} and Cu_1-sCupA^{C111S}.

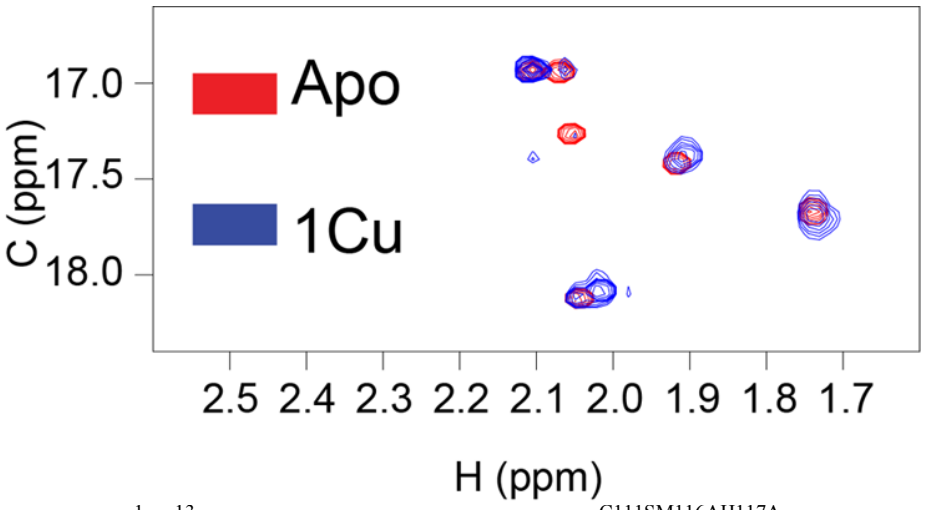

Figure 38: $^{1}H,^{13}C$-HMQC spectra of apo-sCupA^{C111SM116AH117A} and Cu_1-sCupA^{C111SM116AH117A}

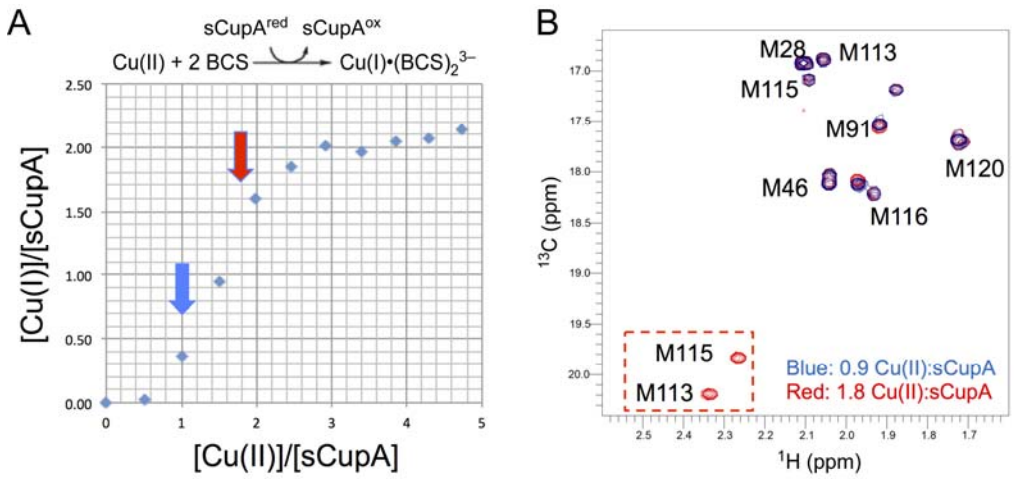

Figure 39: Apo-sCupA is stoichiometrically oxidized by two mol•equivalents Cu(II) concomitant with the binding of Cu(I) to the partially oxidized S2 metal site.

(**a**) Anaerobic titration of Cu(II) into apo-sCupA in the presence of excess BCS carried out essentialy as previously described for *E. coli* multiple antibiotic regulator (MarR).[159] Two mol•equiv of Cu(II) result in two mol•equiv of Cu(I) as detected by binding by BCS via absorbance at 483 nm and stoichiometric C74-C111 disulfide bond formation as determined by no residual reactivity toward dithiodinitrobenzoic acid (DTNB). The *blue* and *red* arrows represent samples subjected to $^{1}H,^{13}C$ HMQC analysis (**b**), and reveal that even under conditions in which all Cys are oxidized, sCupA is still capable of binding Cu(I) to the modified S2 site. As evidenced by the downfield shift in the Met methyl protons (red box).[132]

The reduced growth rate of the *cupA*^{2MA} strain is the result of copper toxicity as shown by elevated cell-associated copper, in contrast to the *cupA*^{C111S} strain which is characterized by similar total cell associated Cu under conditions of 0.2 mM Cu-shock, relative to the wild-type D39 strain (**Fig. 41**). These data reveal that the S2 Met-rich site Cu site is necessary and sufficient for cellular Cu resistance. In addition, they reveal that despite the fact that this S2 site in the *cupA*^{C111S} strain is of substantially lower Cu affinity and enhanced conformational dynamics, it is capable of functioning like a wild-type S2 chelate in cellular Cu resistance. These studies support the hypothesis that the S2 site of CupA is primarily involved in Cu transfer to CopA for efflux and thus is essential in Cu resistance. In contrast, the high affinity S1 site is only involved in chelating cellular Cu(I), and plays no role in mitigating the effects of Cu(I) toxicity. The S1 site may have a role in buffering low levels of free Cu, like previously attributed to other bacterial chaperones, thus effectively tuning the sensitivity of the cellular Cu response.[92]

3.3.4 Oxidation state of CupA in cells

One possible explanation for the fact that the S1 plays little if any role in Cu resistance is that the C74-C111 pair is oxidized under the microaerophilic growth conditions used here. Under these conditions, *S. pneumoniae* respires by generating millimolar hydrogen peroxide as a result of the action of two enzymes, lactate oxidase and pyruvate oxidase. A major modification of H_2O_2 is sulfenylation of cysteine thiols[133], which allowed to occur on CupA, would likely lead to C74-C111 disulfide bond formation. We first measured the redox potentials of both sCupA and the CopA^{MBD} using a simple GSH:GSSG titration and measured the extent of reduced thiols by reacting the

reaction mixture with EZ-link-PEG11 conjugate, and running the products on a denaturing, non-reducing polyacrylamide gel.

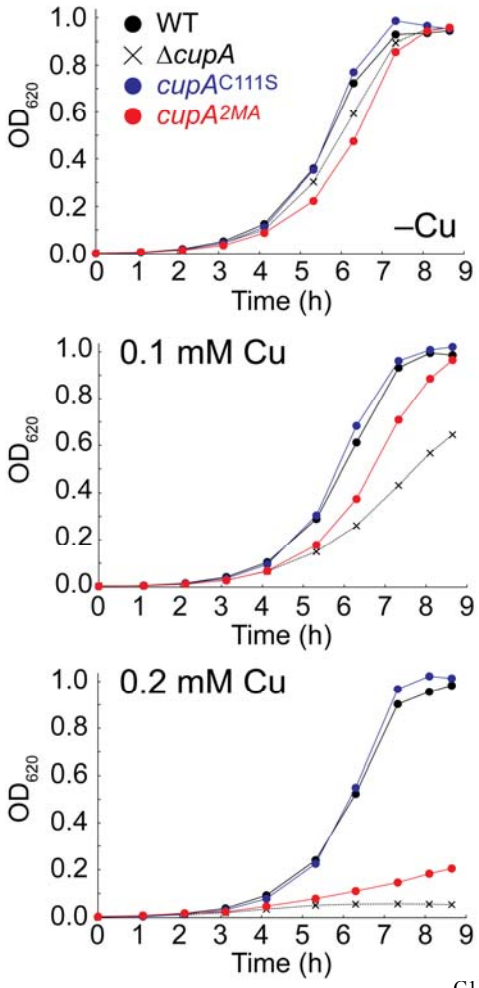

Figure 40: Growth rate analysis of strains encoding CupA^{C111S} or CupA^{2MA} in BHI media in various Cu stress conditions.
0.1 mM Cu is viewed as moderate level of stress and 0.2 mM is considered to be severe level of stress. Experiment was carried out by Yue Fu and Kevin Bruce from Winkler Lab in the Department of Biology.

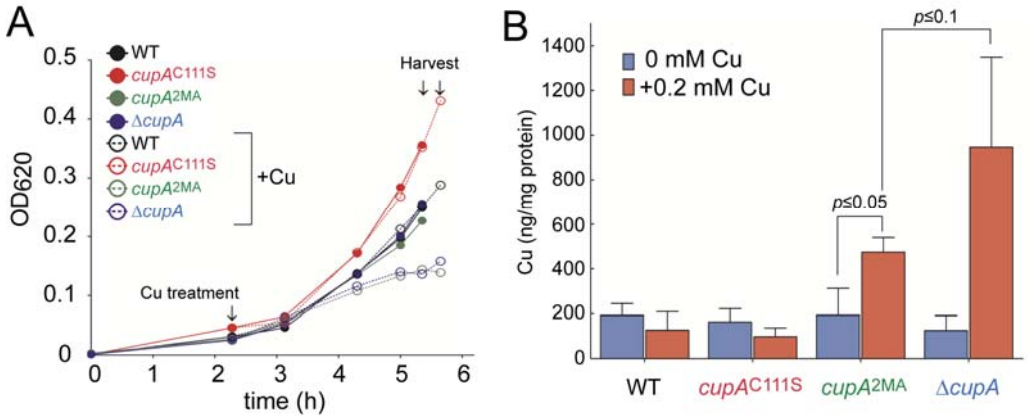

Figure 41: Total cell associated Cu measurement for different cupA WT and mutant strains.

(**a**) Cell growth scheme for Cu content measurement. (**b**) Total cell associated Cu content for each strain in the absence and presence of Cu stress. Cells subject to measurement were harvested as shown in (**a**). Experiment was carried out by Kevin Bruce from Winkler Lab in the Department of Biology.

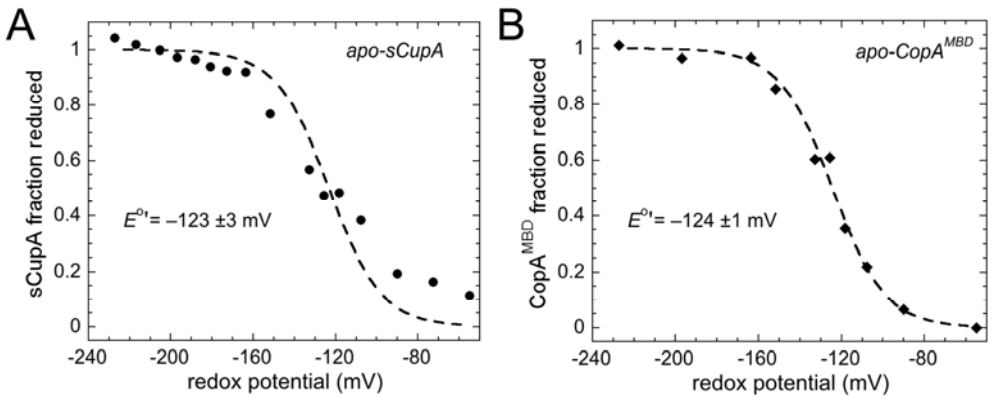

Figure 42: Redox potential measurement for (**a**) apo-sCupA and (**b**) apo-CopA^{MBD}.

Both sCupA and $CopA^{MBD}$ exhibit nearly identical redox potentials, $E^{o'}$, of ≈–123 mV (**Fig. 42**). Although the cytoplasmic redox potential of *S. pneumoniae* D39, or that close to the inner leaflet of the plasma membrane, are not known, each of these potentials is strongly positive relative to previously characterized copper chaperones, *e.g.,* human Atox1[134], consistent with the hypothesis that sCupA is likely to be fully reduced in pneumococcal cells.

To test this, a standard *in situ* thiol-labeling experiment was adapted by treating cell extracts derived from cells expressing FLAG-tagged CupA stressed with 0.2 mM Cu with 4-acetamido-4'-maleimidylstilbene-2,2'-disulfonic acid (AMS), running them out on gels and probing these gels with anti-FLAG antibodies (**Fig. 43**).[2] These experiments reveal that CupA is largely reduced in cells (ranging from 85-100% in multiple experiments) in the presence of Cu stress (0.2 mM Cu) (**Fig. 43, lane 3**), relative to controls for the reduced (pretreatment with the reducing agent, TCEP) (**Fig. 43, lane 4**) and oxidized (pretreatment with 0.2 mM 4,4'-dithiopyridine or 4,4'-DPS) (**Fig. 43**, **lane 5**) CupAs. Note that when wild-type cells are cultured with 0.2 mM DPS prior to harvest, this results in oxidation of ≈50% of the CupA under these conditions (**Fig. 44b**, insert last lane). This significant level of oxidation (50%) of CupA induces no growth phenotype (treatment with DPS alone also induces no growth phenotype under these conditions). In contrast, a strong growth phenotype is observed for the $cupA^{2MA}$ strain when subjected to the same copper shock with 0.2 mM Cu in the presence of DPS vs. Cu- or DPS-treatment alone (**Fig. 44a**).

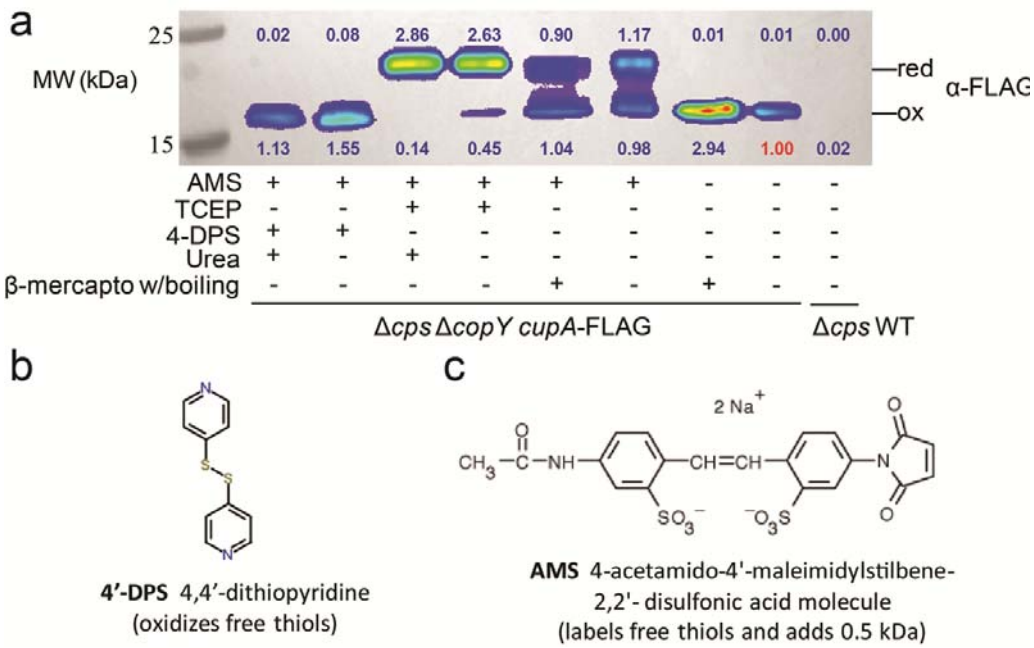

Figure 43: Free thiol labeling with CupA.
(**a**) *in situ* thiol-labeling experiment for CupA protein. Oxidized and reduced control were prepared using 4-DPS or TCEP treatment respectively. (**b**) and (**c**) chemical structure of DPS and AMS used in (**a**). Experiment was carried out by Yue Fu and Kevin Bruce from Winkler Lab in the Department of Biology.

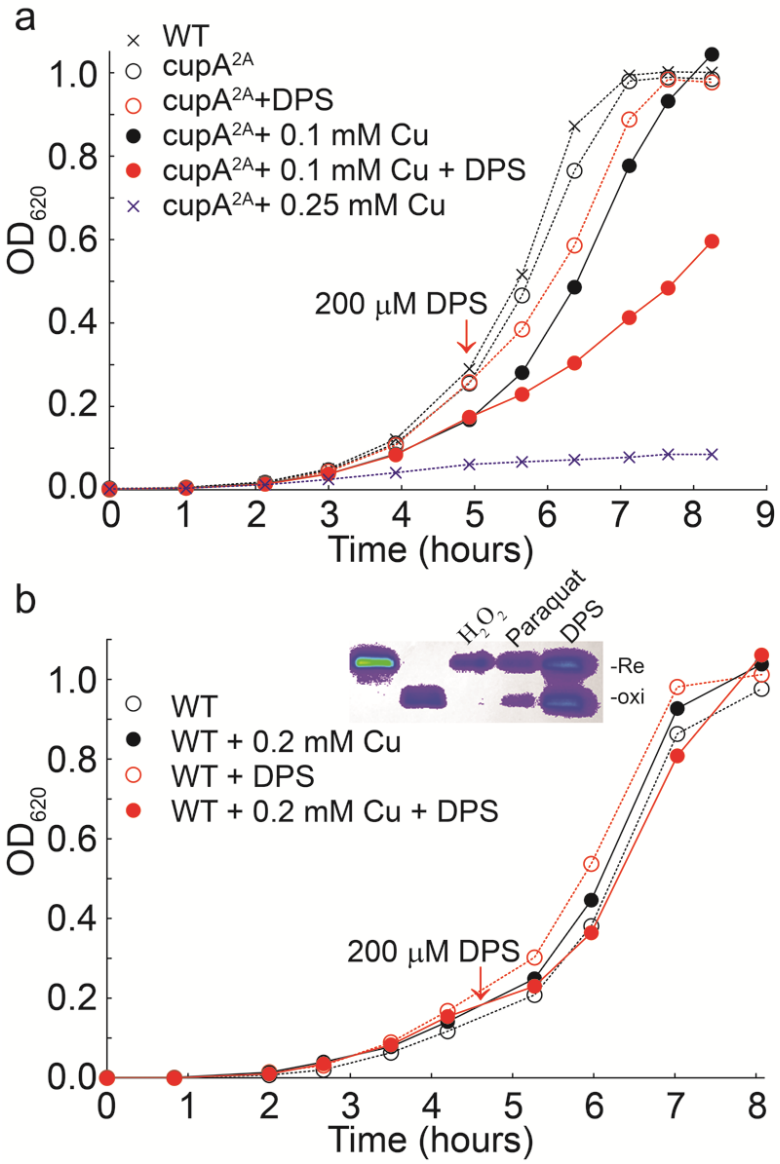

Figure 44: Growth rate analysis using copper and oxidative stress.
(**a**) Growth rate analysis of cupA^{2A} mutant strain in the presence of 4-DPS and Cu. (**b**) Growth rate analysis of cupA WT strain in the presence of 4-DPS treatment. *Insert*, *in situ* thiol-labeling experiment for CupA under oxidant treatment before harvesting. Experiment was carried out by Yue Fu and Kevin Bruce from Winkler Lab in the Department of Biology.

These findings taken together suggest that the CupA dithiol pair is not significantly oxidized in cells, but if this occurs by treatment with the strong oxidant DPS, cellular Cu resistance mediated by CupA is refractory to CupA oxidation, but only if a functional S2 site is lost. Further, these results are also consistent with a buffering role for the S1 site that only becomes apparent when the S2 site is inactivated (**Fig. 44a**).

3.3.5 A heterologous copper chaperone expressed and localized to the plasma membrane does not provide cellular copper resistance

The results above reveal the functional primacy of the CupA S2 site in mediating cellular Cu resistance, with the hypothesis that CupA transiently docks with CopA, and via intermolecular transfer mediated by ligand exchange, to facilitate Cu efflux from the cell. This protein-protein interaction model makes the prediction that a non-cognate Cu chaperone may not support robust cellular Cu resistance, and that there exists site on CopA that mediates intermolecular Cu transfer that is distinct from the N-terminal MBD. While $CopA^{MBD}$ is capable of stripping Cu from the S2 site of CupA, this transfer reaction is not required for cellular Cu resistance since the *copA*^{C49S} strain exhibits wild-type Cu resistance.[132] To test this, we first prepared a mutant strain designed to express a chimeric *Bacillus subtilis* CopZ ($CopZ_{Bsu}$), which harbors the N-terminal transmembrane helix of CupA and full-length $CopZ_{Bsu.}$ We note that $CopZ_{Bsu}$ is characterized by a high Cu(I) binding affinity comparable to S1 site of CupA.[28] Growth curves of the chimeric strain reveals a severe growth phenotype under 0.2 mM Cu stress, despite the fact that the CopZ chimera is expressed to high levels, localizes to the plasma membrane, and is fully reduced in cells and thus would be capable of binding intracellular Cu (**Fig. 45**). This mutant is functionally indistinguishable from the Δ*cupA* and *cupA*^{2MA} strains, which is in

consistent with the hypothesis that there is a specificity of Cu trafficking at the plasma membrane in *S. pneumoniae*.

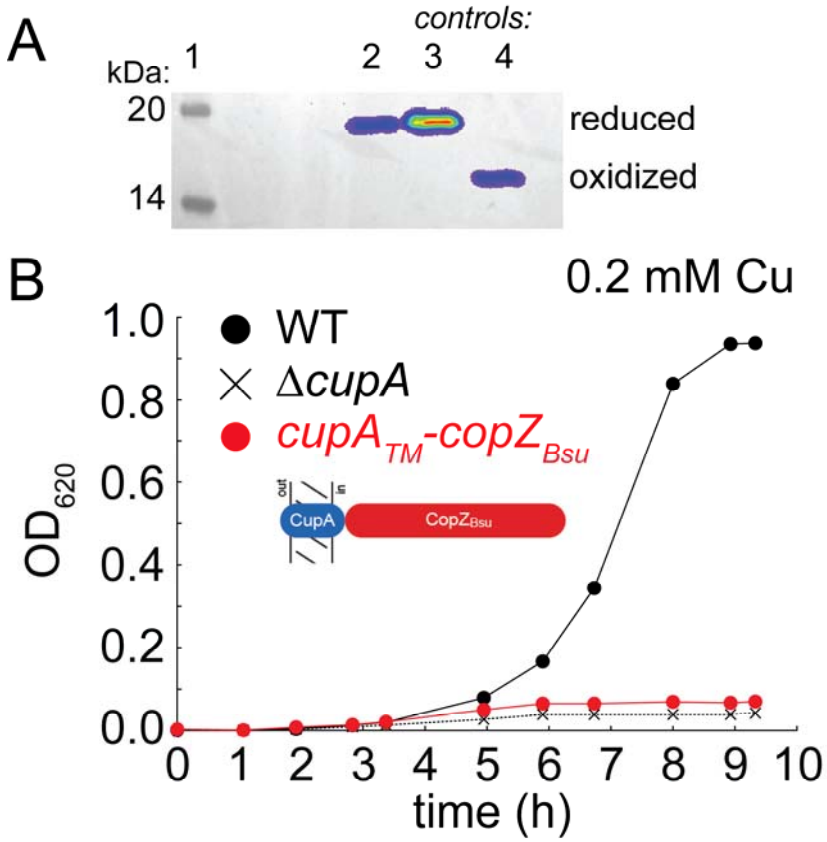

Figure 45: Growth rate analysis of *copZ* chimeric strain.
(**a**) *in situ* thiol-labeling experiment for TM_{cupA}-CopZ protein. (**b**) Growth rate analysis of TM_{cupA}-CopZ strain under Cu stress. The chimeric protein is illustrated in the cartoon representation. Although both Cys residues are reduced, the chimeric protein has little effect on copper resistance. Experiment was carried out by Kevin Bruce from Winkler Lab in the department of biology.

3.3.6 The metal binding site or entry site on CopA is required for Cu resistance at high Cu

Previous crystallographic studies of *Legionella pneumophila* CopA in the apo-state revealed a trio of highly conserved, cytoplasmic-facing residues corresponding to M172, E216 and D347 in *S. pneumoniae* CopA positioned just above the inner leaflet of the plasma membrane and the "platform helix", corresponding to the C-terminal half of kinked MB helix unique to Cu/Zn P_{1B} ATPase transporters.[67] In an archeal CopA, this entry metal binding site (MBS) was shown to be required for cognate Cu(I)-CopZ-stimulated CopA ATPase activity and Cu(I) transfer, but was not required for free Cu(I)-stimulated activity, consistent with the interpretation that the MBS specifically provides a docking site copper chaperone-mediated Cu delivery.[72] We therefore prepared a strain encoding a FLAG-tagged triple Ala substitution mutant of *copA*, M172A/E216A/D347A, denoted $copA^{\Delta MBS}$ in a C49S CopA background and tested the viability of this strain at 0, 0.2 and 0.5 mM Cu added to the BHI medium (**Fig. 46**). As can be seen, although this strain grows with no clear growth phenotype at 0.2 mM Cu relative to the parent $copA^{C49S}$ strain, it nearly fails to grow at 0.5 mM Cu. These data are consistent with the hypothesis that the MBS provides a docking site for CupA in mediated extracellular Cu(I) efflux.[72]

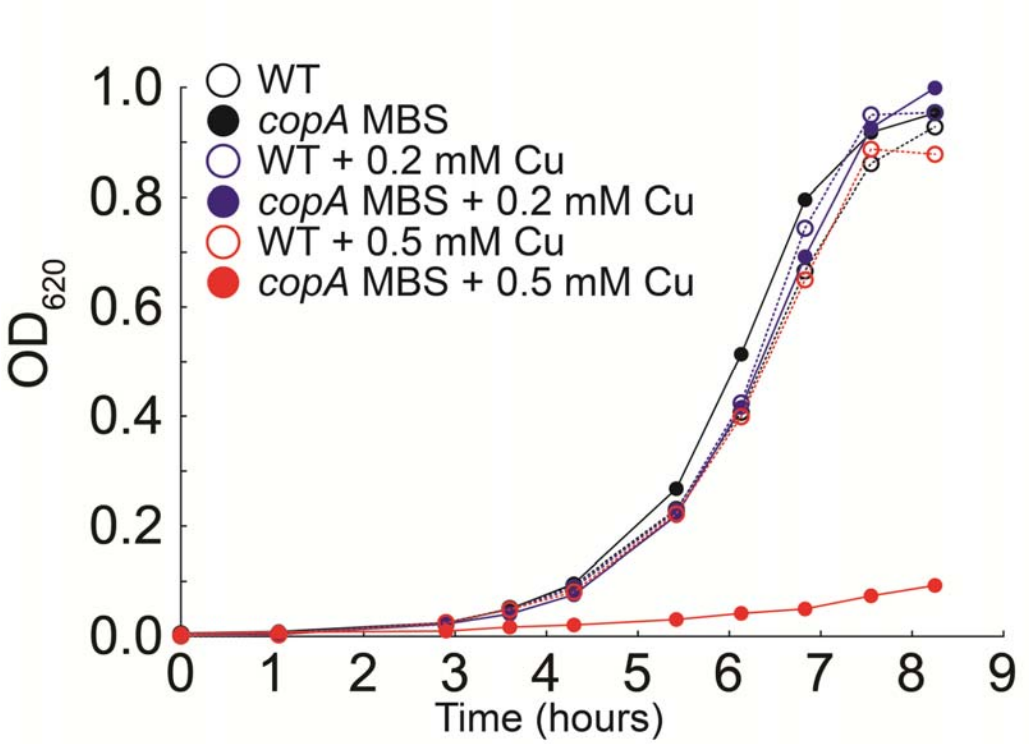

Figure 46: Growth rate analysis of $copA^{MBS}$ strain in various Cu stress conditions. Three different extracellular Cu concentration were used: 0 mM, 0.2 mM and 0.5 mM. $copA^{MBS}$ strain shows growth phenotype only under 0.5 mM Cu. Experiment was carried out by Kevin Bruce from Winkler Lab in the Department of Biology.

3.4 Implication of the work

This work provides new insights into the mechanism of cellular Cu resistance in the Gram-positive respiratory pathogen, *S. pneumoniae*, and builds on previous structural studies of the novel, membrane-anchored cupredoxin fold chaperone, CupA. We present the solution structure of metal-free apo-sCupA and show that it adopts a structure that is essentially identical to that of Cu_2-sCupA, with the exception of residues 112-116, which are highly dynamic in the both the backbone and the side methyl groups of the S2-coordinating methionines, M113 and M115. In contrast the high affinity S1 Cu site is essentially pre-organized, filling of which quenches backbone disorder but enhances side chain dynamics, which collectively increase the S2 site binding Cu(I) binding affinity. The S2 Cu site in CupA is necessary and sufficient for resistance against chronic Cu toxicity, while the S1 site is largely dispensable for this activity. Although the di-thiol C74-C111 pair in CupA is reduced in cells under Cu stress, oxidation to an intramolecular disulfide bond retains Cu(I) binding to the S2 site, and this oxidation in the cell has little effect on cellular Cu resistance provided a functional S2 site is present in CupA. The S1 site provides some protection against Cu toxicity, and may well function to buffer very low levels of Cu in the absence of significant Cu stress. Finally, two lines of evidence were presented which are in consistent, albeit not confirmatory, with the hypothesis that CupA S2-mediated Cu transfer to CopA is on pathway for Cu efflux, and this requires structural integrity of the CupA S2 and CopA MBS Cu sites, which is in contrast to the N-terminal MBD which is seemingly not required for this function.

There is speculation that the Cu(I) binding affinity of the copper-sensing repressor CopY and the copper chaperone CupA, when expressed as equilibrium dissociation constants, $1/K_{Cu}$, provide a threshold $[Cu]_{free}$, below which pneumococcal cells buffer free Cu, and above which, the CopY-induced expression of the *cop* operon is induced to effect cellular Cu(I)-resistance. In this model, this set point might be set to $\leq 10^{-16}$ M Cu, corresponding to the affinity of CopY for Cu(I) (see chapter IV, **Fig. 49**), which is then bound by both Cu sites in CupA as soon as $[Cu]_{free}$ exceeds $\approx 10^{-14}$ M, which corresponds to the Cu concentration where virtually all CupA sites would be bound, poised to facilitate Cu efflux from the cell. The characterization of the $cupA^{C111S}$ strain suggests that $[Cu]_{free}$ 100-fold higher provides full protection against Cu toxicity. Thus, based on K_{Cu} values measured for other bacterial Cu chaperones, *S. pneumoniae* would appear to be more tolerant of low levels of bioavailable Cu, and this might be the primary role played by the S1 Cu site in CupA. We emphasize, however, that a K_{Cu} of 10^{12} M^{-1} is clearly not all that is required since the C74S CupA mutant (which disrupts Cu binding to both S1 and S2 sites) retains a non-native Cu-binding site of 10^{12} M^{-1} affinity, but is as sensitive to Cu stress as a Δ*cupA* strain (table 6).

These findings suggest that the Met pair in the S2 Cu site optimizes the dynamics, rather than the stability, of the site in a way that kinetically facilitates intermolecular Cu transfer to the MBS, which is on pathway for Cu efflux.[61,72] Intermolecular Cu transfer via ligand exchange at the S2 site is plausible given the fact this site is at the protein surface, and is clearly capable of adding a fourth ligand from CopA to initiate Cu transfer, as exemplified by coordination of Cl^- or Br^- in NaCl or NaBr-containing solutions, respectively.[132] Although M116 is not conserved in CupAs, H117 is, which

suggests the possibility that residues beyond the S2 Mets and the CopA MBS are required for Cu transfer.

Table 5: NMR structural statistics for apo_sCupA.

Conformationally-restricting experimental constraints [a]			
NMR distance and dihedral constraints			
NOE-based distance constraints			
Total NOE		2201	
intra-residue (|i - j| = 0)		347	
sequential (|i – j| = 1)		539	
medium range (1 < |i – j| < 5)		248	
long range (|i – j| ≥ 5)		1067	
NOE constraints per restrained residue [b]		23.9	
Dihedral-angle constraints			
φ (°)		65	
ψ (°)		65	
Total no. of restricting constraints [b]		2331	
Total no. of restricting constraints per restrained residue [b]		25.3	
Restricting long-range constraints per restrained residue [b]		11.6	
Residual constraint violations [a, c]			
Average no. of distance violations per structure			
0.1 – 0.2 Å		5.5	
0.2 – 0.5 Å		0.44	
> 0.5 Å		0	
Maximum distance violation (Å) [d]		0.35	
Average no. of dihedral angle violations per structure			
1 – 10 °		0.83	
> 10 °		0	
Maximum dihedral angle violation (°) [d]		1.70	
RMSD Values			
Backbone atoms (Å) [e]		0.1	
Heavy atoms (Å) [e]		0.6	
Ramachandran plot statistics [e]			
Most favored regions (%)		90.7	
Allowed regions (%)		9.3	
Disallowed regions (%)		0	
Global quality scores			
	Mean score	SD	Z-score[f]
Procheck G-factor (φ/ψ) [e]	-0.66	N/A	-2.28
Procheck G-factor (all) [e]	-0.81	N/A	-4.79
Verify3D	0.43	0.0244	-0.48
ProsaII (-ve)	0.45	0.0315	-0.83
MolProbity clashscore	12.99	1.7223	-0.70
BMRB accession no.		25098	
PDB ID code		2MRY	

[a] Analysed for residue 26 to 123

[b] There are 92 residues with conformationally restricting constraints

[c] Calculated for all constraints using sum over r^{-6} (Generated using PSVS 1.5[135–140])
[d] Largest constraint violation among all the reported structures
[e] Ordered residue range 30 – 111, 117 – 122 [S(φ) + S (ψ) ≥ 1.8]
[f] With respect to mean and standard deviation for a set of 252 X-ray structures of < 500 residues with resolution ≤ 1.80 Å, *R* factor ≤ 0.25 and Rfree ≤0.28; a positive value indicates a 'better' score (Generated using PSVS 1.5)

Table 6: Cu(I) binding affinities of wild-type sCupA and sCupA mutants[a]

Protein	log K_{Cu1}^{S1} (M^{-1})	log K_{Cu2}^{S2} (M^{-1})
sCupA	17.9 (±0.3)	14.8 (±0.2)
C111S sCupA	–	12.5 (±0.3)
C74S sCupA	–	12.5 (±0.2)
M113A/M115A sCupA (2MA)	17.2 (±0.1)	–

[a]Measured using a global fit to a series of anaerobic chelator competition assays as described previously[132]. Conditions: 25 mM HEPES, pH 7.0, 200 mM NaCl, ambient temperature.

Chapter IV: Characterization of Cu(I)-specific regulator CopY in *S. pneumoniae*

4.1 Introduction

CupA and CopA from *S. pneumoniae* are under the regulation of the transcriptional regulator CopY. CopY represents a family of copper specific metalloregulatory proteins, founding member of which was characterized in *Enterococcus. hirae*.[47] CopY contains a N-terminal DNA binding domain and a C-terminal copper binding domain. Based on sequence similarity of the N-terminal DNA binding domain, it is proposed to be a member of MecI/BlaI family proteins.[86] In *E. hirae*, CopY regulates the *copYZBA* operon which encodes two Cu(I) specific P_{1B} type ATPase CopA and CopB, a cytoplamic Cu(I) chaperone CopZ and CopY itself. Zn(II) bound CopY was proposed to bind to the operator-promotor region of the *copYZBA* operon to repress the *transcription in vitro*.[89] CopZ in *E. hirae* has been proposed to deliver Cu(I) to Zn(II) bound CopY and convert it into Cu(I) bound CopY, which then dissociate from the DNA binding region (the cop box), allowing transcription of downstream genes in the *copYZBA* operon. Based on multiple sequence alignment (**Fig. 47**), most CopY proteins contain a CXXC…CXXC motif at the extreme of the C-terminal regulatory domain. This has been shown to form a highly luminescent binuclear S_4-Cu_2 cluster demonstrated in previous spectroscopic studies of *E. hirae* CopY[141], with the Cu(I) binding stoichiometry of 2Cu(I) per CopY. Howeer, the regulatory function of each Cys residue has not been clearly detailed. The NMR solution structure of the N-terminal DNA binding domain of CopR, a CopY family copper specific regulator found in *Lactococcus lactis IL1403*, provides insights into the structure of CopY family protein.[142] The monomer domain reveals a winged helix-turn-helix domain with high

structural similarity to the DNA binding domain of *S.aureus* MecI and BlaI.[86] However, there is yet little details on the structure of intact CopY.

In *Streptococcus pneumoniae*, CopY regulates the *cop* operon, encoding CopY, CupA and CopA.[132] Transcriptional analysis by real time quantitative qRT-PCR and assaying strains with *copY*-lacZ fusion demonstrate that the *cop* operon is autoregulated by copper-specific regulator CopY.[1] However, the details of regulatory mechanism of CopY in pneumococcus remain unclear. For example, whether Zn(II) functions as an co-repressor while Cu(I) functions as an allosteric inhibitor of DNA/protein binding is not clear. In this chapter, preliminary characterization of *Spn* CopY is presented, including Zn(II) and Cu(I) binding affinities of CopY and initial NMR study on apo, Zn and Cu(I) bound form of intact CopY/regulatory domain of CopY.

4.2 Methods

4.2.1 Protein expression and purification

The pHis plasmid was used to subclone CopY from *S.pneumoniae* D39 strain (SPD_0633). This vector encodes a His_6 tag and TEV protease cleavage site at the N terminus to yield, following cleavage, three non-native N-terminal amino acids of the sequence GAM for CopY as described for sCupA.[132] BL21 (DE3) competent cells were transformed with the resultant plasmid. For unlabeled proteins, an overnight culture of *E. coli.* cell was inoculated into Luria Broth (LB) media containing 100 μg/mL ampicillin. For the ^{13}C,^{15}N-labeled proteins, an overnight culture of *E. coli.* was inoculated into M9 minimal media (pH 7.4) containing 100 μg/mL ampicillin, supplemented with $^{15}NH_4Cl$ (1 g/L) (Cambridge Isotope Laboratories) and [$^{13}C_6$]-D-glucose (2.5 g/L) (Cambridge Isotope Laboratories). For both media, the cells were grown at 37 °C to OD_{600} = 0.6.

Isopropyl β-D-thiogalactopyranoside (IPTG) was then added to a final concentration of 1 mM and cultures were continued at 16 °C for 20 h. The cells were harvested by centrifuging and stored at -80 °C. All the buffers in the purification were degassed and refilled with Argon using a Schlenk line just prior to use. To break the cells, the cells were resuspended in buffer R (25 mM Tris, pH 8.0, 200 mM NaCl, 5 mM TCEP). The resuspended cells were lyzed by a sonic dismembrator (Fisher). The recombinant proteins were purified using HisTrap FF columns (GE Healthcare) using a gradient of imidazole from 10 mM to 300 mM in buffer R. The appropriate fractions were pooled and subjected to TEV protease cleavage at for 16 °C for 36 h. The proteins were further purified using HisTrap FF columns (GE healthcare) and Superdex 75 16/60 column (GE healthcare). The purity of the proteins was estimated to be >95 % as judeged by SDS-PAGE and ESI-MS. Protein concentration was determined by A_{280} with an extinction coefficient of 18240 $M^{-1}cm^{-1}$ on an UV-visible spectrometer (HP/Agilent 8453).

4.2.2 Cu(I) Binding Affinity Measurements

Bathocuproine disulfonate (BCS) was used for Cu(I) binding affinity determination of CopY. All proteins for binding experiments were buffer exchanged from protein stock to the degassed buffer B (25 mM HEPES, pH 7.0, 200 mM NaCl) in an anaerobic glove box. Cu(I) stock was prepared by taking the supernatant from the mixture of CuCl powder with fully degassed buffer B (25 mM HEPES, pH 7.0, 200 mM NaCl). The accurate concentration of Cu(I) stock was determined by Atomic Absorption Spectroscopy with a general concentration around 10 mM. The final titration solution contains 20 or 30 μM Cu(I) and 60 or 90 μM BCS in Buffer B. Each 120 μL aliquot of titration solution was mixed with increasing CopY titrant. Optical spectra of BCS were

recorded from 200 nm to 900 nm. Corrected spectra were obtained by subtracting baseline spectrum from each CopY-addition spectrum and then corrected for dilution. A_{483} was used to determine the concentration of Cu_2-BCS complex using an extinction coefficient of 13500 $M^{-1}cm^{-1}$. All the data were fitted to the appropriate competition model using Dynafit[113].

4.2.3 Intial NMR study on CopY

Typical NMR sample solution conditions were 300-600 μM CopY protomer, $^{15}N/^{13}C$-labeled CopY in 50 mM potassium phosphate pH 7.0, 200 mM NaCl, 0.02% (w/v) NaN_3 and 10% (v/v) ^2H_2O. All NMR samples were prepared in an anaerobic glove box. Apo-CopY was prepared with 5 mM TCEP. Varian DDR 800 and 600 MHz spectrometers equipped with cryogenic probes in the METACyt Biomolecular NMR Laboratory were used to acquire data for CopY samples. NMR data were processed using NMRPipe[103] and were analyzed using Sparky[104] and CcpNmr Analysis[105]. All spectra were acquired at 30 °C. Chemical shift is referenced relative to 2,2-dimethyl-2-silapentene-5-sulfonic acid (DSS).

4.3 Results

4.3.1 Copper and Zinc binding affinities of *Spn* CopY

A multiple sequence alignment shows CopY from *S. pneumoniae* has sequence similarity with characterized CopY from *E. hirae* and CopR from *L. lactis* (**Fig. 47**). However, *Spn* CopY only contains 2 of the 4 conserved Cys residues near the C terminus, which has been shown to form a highly luminescent binuclear S_4-Cu_2 cluster in other CopY proteins.[143] The impact of a lack of two of the four Cys residues on the metal binding affinities and geometry of *Spn* CopY was therefore of interest. *Spn* CopY still

binds Zn(II) with high affinity (**Fig. 49**) with the stoichiometry of $CopY_{dimer}$: Zn(II) to be 1:1. Only a lower affinity can be obtained for K_{zn} with this condition. With additional experiments using higher affinity chelators, detailed Zn binding affinities can be measured. A BCS competition assay was employed to measure the Cu(I) binding affinity of *Spn* CopY(**Fig. 48**). Based on three titrations, *Spn* CopY binds to Cu(I) with a stoichiometry of $CopY_{dimer}$:Cu(I) to be 1:2 with an affinity of $\log K_{Cu} = 16.6 \pm 0.1 M^{-1}$ (**Fig. 48).** The binding affinity for Cu(I) of CopY is about two magnitude lower than those previeously described Cu(I)-specific transcriptional regulators, CsoRs and CueR.[48,49]

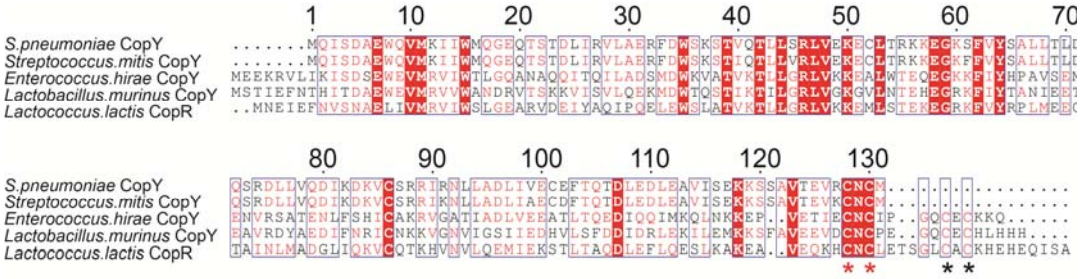

Figure 47: Multiple sequence alignment of CopY from different bacteria.
The conserved Cys residue proposed involved in copper and zinc binding are highlighted with asterisk. Note *S. pneumoniae* CopY only contains two of the four Cys residues near C terminus.

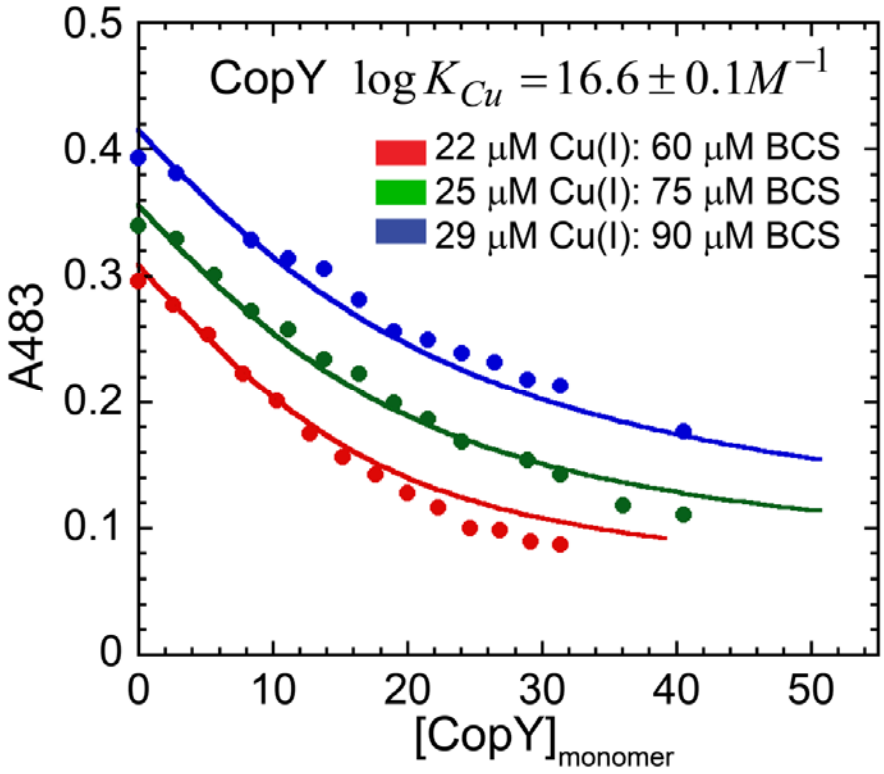

Figure 48: Binding curves obtained from anaerobic Cu(I) chelator competition to measure Cu(I) binding affinity of CopY.
The experiments were carried out by titrating apo CopY into a mixture of Cu(I) and BCS at pH 7.0. Three individual experiments were carried out for BCS assay. Closed symbols represent A_{483} values for the Cu(I)-$(BCS)_2$ complex. The continuous line represents the results of a global analysis of all experiments to the same model. *Red*: 22 μM CuCl and 60 μM BCS; *Green*: 25 μM CuCl and 75 μM BCS; *Blue*: 29 μM CuCl and 90 μM BCS. Cu(I) binding affinity of CopY was extracted from all three experiments and is shown at the top of the figure. Hendrik Glauninger performed the titrations shown in this figure under the instruction of Yue Fu.

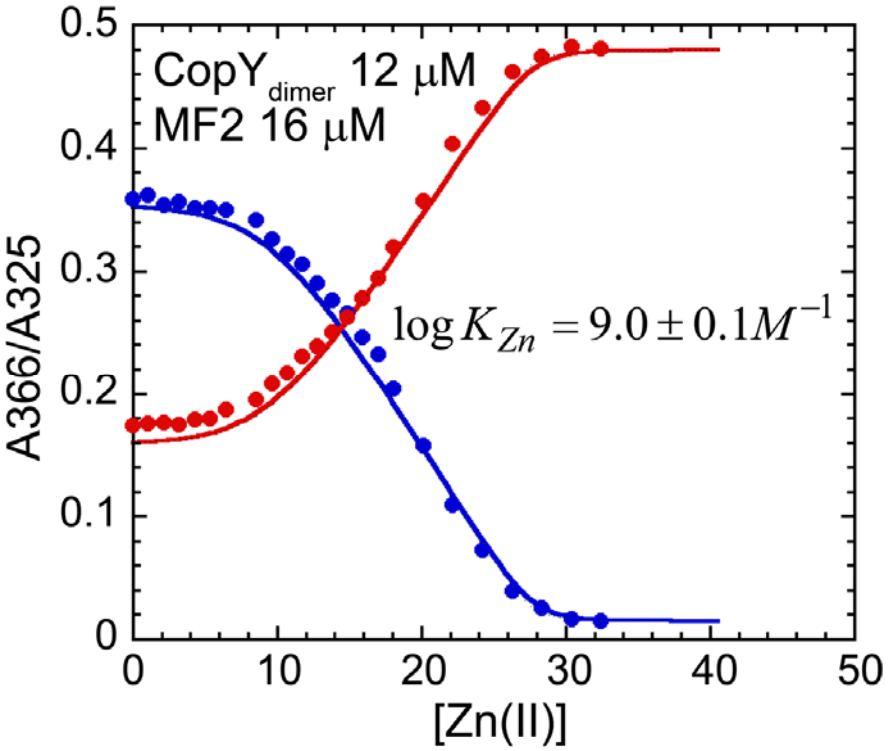

Figure 49: Binding curves obtained from zinc chelator competition to measure Zn(II) binding affinity of CopY.

The experiments were carried out by titrating Zn(II) into a mixture of apo CopY and MF2 at pH 7.0. Closed symbols represent A_{366} or A_{325} values for the Zn(II)-MF2 complex. The continuous line represents the results of the analysis of the experiments to the binding model. *Red*: A_{325} values; *Blue*: A_{366} values; For the experiment in the figure, the mixture contains 12 μM $CopY_{dimer}$ and 16 μM MF2. Zn(II) binding affinity of CopY was extracted from the experiment and is shown in the figure.

4.3.2 Initial NMR study on *Spn* CopY

There are no structures available for any full length CopY, with the only high solution resolution structure of the N-terminal DNA binding domain of *L .lactis* CopR.[142] Efforts were made towards characterizing the C-terminal metal binding domain (residue 68-131) as well as full length *Spn* CopY structurally using NMR spectroscopy. ^{1}H, ^{15}N-HSQC spectra of apo, Zn(II) loaded and Cu(I) loaded $CopY^{68-131}$ reveal far few cross-peaks than expected based on the actual number of residues in $CopY^{68-131}$, thus giving little structural information (**Fig. 50**). ^{1}H, ^{15}N-HSQC spectra of full length *Spn* CopY in the Zn(II)-loaded state gives by far the most cross-peaks (**Fig. 51b**), but the relative intensity of the cross peaks vary substantially, indicative of conformational dynamics in certain regions of the molecule. One possibility is that the conformational dynamics would be quenched further by forming Zn(II)-CopY: DNA complex. However, a preliminary experiment shows that the complex gives far few cross peaks compared to Zn state CopY. Given that, it is difficult to extract useful structure data from NMR based experiment.

4.4 Summary

We characterized the copper and zinc binding affinities of *Spn* CopY. *Spn* CopY binds up to one molar equivalent of Zn(II) or up to two molar equivalents of Cu(I) per dimer, respectively. The Cu(I) binding affinity of *Spn* CopY, although lower than the affinities measured in other Cu(I)-specific regulators, agrees with the "threshold" model proposed in Chapter III. Work is underway to characterize the DNA binding properties of apo, Zn(II) or Cu(I) loaded *Spn* CopY as well as various mutants, which will provide information about the mechanism of transcriptional regulation by CopY.

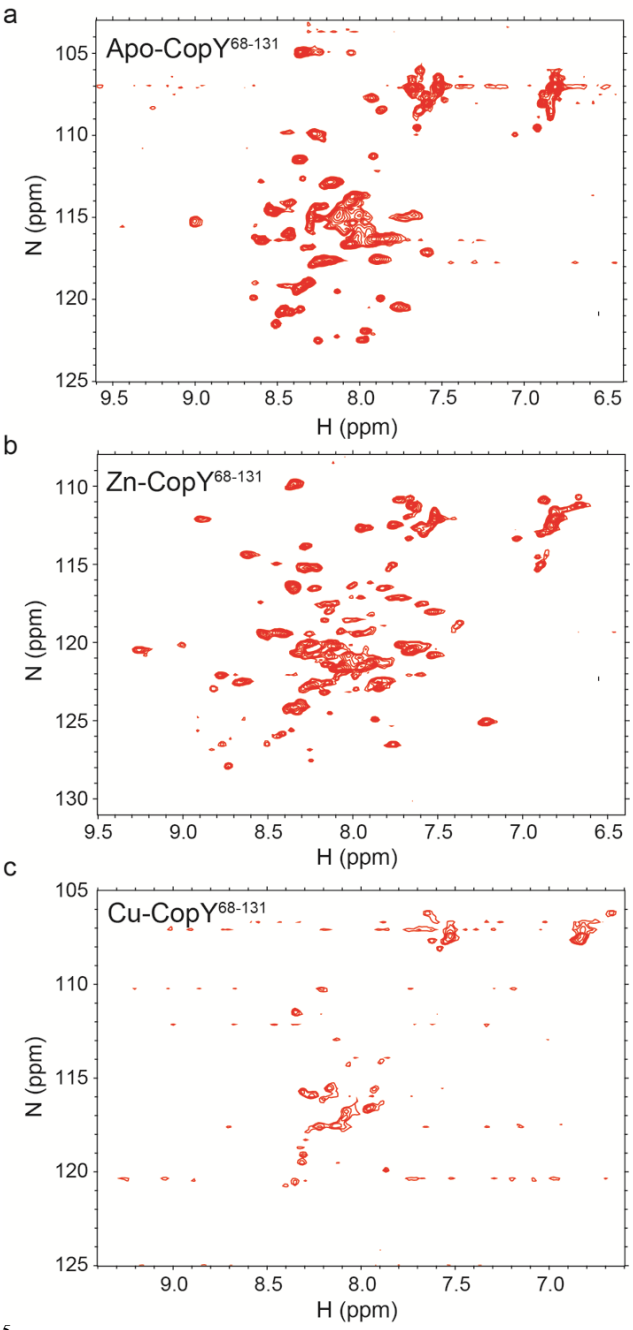

Figure 50: ^{1}H, ^{15}N-HSQC spectra of different metallated states of the C-terminal metal binding domain of CopY ($CopY^{68-131}$). Protein concentration ~ 300 µM. nt =16, ni =128. Buffer as described in the material and methods.
(**a**) ^{1}H, ^{15}N-HSQC spectra of apo $CopY^{68-131}$; (**b**) ^{1}H, ^{15}N-HSQC of fully Zn(II) loaded $CopY^{68-131}$; (**c**) ^{1}H, ^{15}N-HSQC spectra of fully Cu(I) loaded $CopY^{68-131}$.

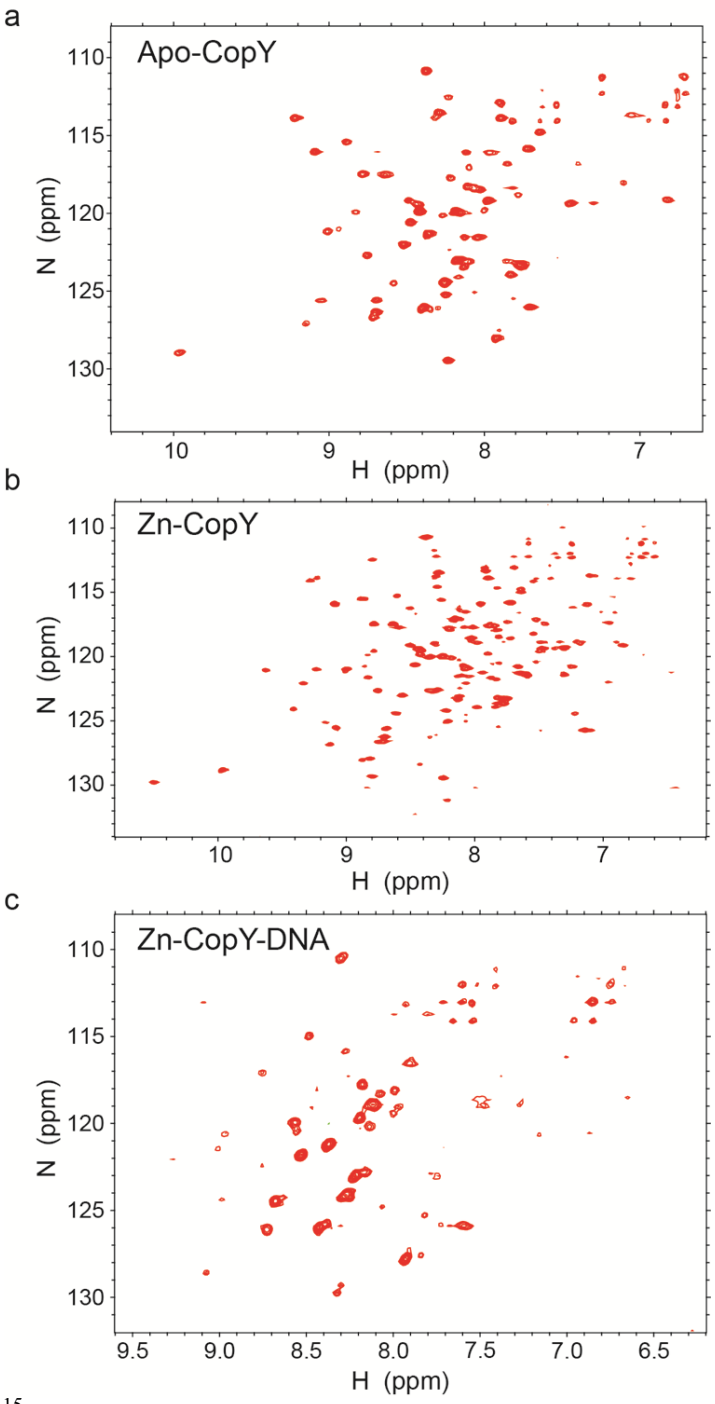

Figure 51: ^{1}H, ^{15}N-HSQC spectra of different states of CopY. Protein concentration ~ 400 µM. nt =16, ni =128. Buffer as described in the material and methods. The DNA promoter sequence is 5'-GTTCTATAATT TACA AT TGTA AATTATAGAAC-3'. (**a**) ^{1}H, ^{15}N-HSQC spectra of apo CopY; (**b**) ^{1}H, ^{15}N-HSQC of fully Zn(II) loaded CopY; (**c**) ^{1}H, ^{15}N-HSQC spectra of fully Zn(II) loaded CopY-DNA promoter ternary complex.

Chapter V: Future work and Perspectives

There are two major unsolved issues regarding the mechanisms of the copper resistance in pneumococcus and in bacteria as a whole. The first one is the understanding of the details on copper transfer mechanism from copper chaperone to exporting P_{1B} type ATPase. The CupA-CopA system in pneumococcus provides an ideal platform for investigating the transfer mechanism. The initial question we have to address is that whether there is direct protein-protein interaction between CupA and CopA in the cell membrane. One hypothesis is that the interaction is dependent upon the charge complementarities between regions around S2 site in CupA and the regions around the putative Cu entry site in CopA. Potential charged residues around Cu entry site in CopA are proposed to be involved in facilitating protein-protein interaction between CupA and CopA, which may be essential for the productive Cu transfer. Based on the homology model of CopA from the known CopA crystal structure, the potential Cu entry site for Spn CopA is composed of M172, E216 and D347. There is a ring of positively charged K and R residues around the entry site including: R102, K103, and R110 from the N-terminus of CopA; K155, K166 and K167 from the platform helix of CopA; K221, K229, K333, K334 and R339 from the Nucleotide binding domain (N domain) of CopA. Pneumococcal strains with CopA charge residue mutant can be constructed and growth rates analyzed will be performed in the absence and presence of Cu stress to test the essentiality of these electrostatic interactions. Efforts are also underway in an effort to trap wild-type and potentially longer-lived CupA-CopA complexes by covalent crosslinking *in vivo*.

Once an physical interaction between CupA and CopA is demonstrated, the next question of interest would be the factors that influence the Cu transfer rate between CupA and CopA. The most fruitful would be to biochemical purify full length CupA and CopA and reconstitute them into liposome to enable either ATPase activity measurement or fluorescent based Cu transfer rate analysis across the membrane.

The second major question remaining is whether there is interplay between Cu resistance system and bacterial cellular redox homeostasis system, which are intrinsically linked by sulfur chemistry.[2,144] Glutathione and perhaps other related low molecular weight thiols (LMWTs) in bacterial pathogens that lack glutathione, *e.g.,* bacillithiol and mycothiol in *S. aureus* and *M. tuberculosis*, respectively, likely help to buffer "free" Cu(I) to very low levels given their high affinity for Cu(I)[27], since in some[116] but not all[57] cases, crippling glutathione biosynthesis is synergistic with the deletion of the copper chaperone with respect to Cu(I) stress resistance. Likewise, in *S. pneumoniae*, abrogation of the ability to uptake glutathione (pneumococcus does not biosynthesize GSH) gives rise to a severe growth defect under copper stress.[58] These studies thus generally link the redox status of the cytoplasmic compartment as defined by the GSH/GSSG couple to copper homeostasis and resistance.[144]

Further, in mammalian cells, it has been demonstrated that the reduced cysteines in Atox1 are responsible for coordinating Cu(I), the redox state of those cysteines is also maintained through equilibrium with GSH/GSSG pair in human cells.[2] Atox1, in turn, may functionally replace GSH under conditions of low total glutathione, consistent with the original functional description of Atox1 as an antioxidant protein.[2] Further, human glutaredoxin 1 (hGrx1) has been shown to catalyze the interchange between disulfide-

oxidized and reduced Atox1 as a function of the GSH/GSSG ratio.[144] *In vitro* experiments also demonstrate that hGrx1 binds Cu(I) with high affinity, indicating a potential role in Cu(I) buffering.[144] The dual roles of GSH, Atox1 and Grx1 in cellular redox and copper homeostasis strongly suggest a functional linkage between these two systems in higher eukaryotes. Future studies that define the chemical and physical origins of this linkage and more generally, how copper stress impacts other kinds of thiol chemistry in bacteria that might be manifest in a typical antimicrobial host response, promises new surprises at the host-pathogen interface.

Appendix

Appendix I Assignments of backbone resonances of extracellular loop 1 of FtsX ($FtsX^{ECL1}$) from *S. pneumoniae*

Methods

Protein expression and purification The pHis plasmid was used to subclone $FtsX^{ECL1}$ (residues 47-168 of full-length FtsX) This vector encodes a His6 tag and TEV protease cleavage site at the N terminus to yield, following cleavage, three non-native N-terminal amino acids of the sequence GAM for $FtsX^{ECL1}$ (denoted residues 26-28 in the structure). BL21 (DE3) competent cells were transformed with the resultant plasmids. For unlabeled proteins, an overnight culture of *E. coli*. cell was inoculated into Luria Broth (LB) media containing 100 μg/mL ampicillin. For the $^{15}N/^{13}C$ labeled proteins, an overnight culture of *E.coli*. cells was inoculated into M9 minimal media (pH 7.4) containing 100 μg/mL ampicillin, supplemented with $^{15}NH_4Cl$ (1 g/L) (Cambridge Isotope Laboratories) and [$^{13}C_6$]-D-glucose (2.5 g/L) (Cambridge Isotope Laboratories). For both media, the cells were grown at 37 °C to OD600 = 0.6. Isopropyl β-d-thiogalactopyranoside (IPTG) was then added to a final concentration of 0.4 mM and cultures were continued at 16 °C for 20 h. The cells were harvested by centrifuging and kept at -80 °C. All the buffers in the purification were degassed and refilled with Argon using a Schlenk line right before use. To break the cells, the cells were resuspended in buffer R (25 mM Tris, pH 8.0, 200 mM NaCl, 5 mM TCEP). The resuspended cells were lyzed by a sonic dismembrator (Fisher). The recombinant proteins were purified using HisTrap FF columns (GE Healthcare) using a gradient of imidazole from 10 mM to 300 mM in buffer R. The appropriate fractions were pooled and subjected to TEV protease

cleavage at for 16 °C for 36 h. The proteins were further purified using HisTrap FF columns (GE healthcare) and Superdex 75 16/60 column (GE healthcare). The purity of the proteins was estimated to be >95 % as judeged by SDS-PAGE and ESI-MS. Protein concentration was determined by A280 with an extinction coefficient of 14440 $M^{-1}cm^{-1}$ on an UV-VIS spectrometer (HP/Agilent8453).

FtsxECL1 resonance assignment Typical NMR sample solution conditions were 500-600 μM, $^{15}N/^{13}C$-labeled $FtsX^{ECL1}$, pH 7.0, 50 mM potassium phosphate, 50 mM NaCl, 0.02% (w/v) NaN_3 and 10% (v/v) ^2H_2O. Varian 600 MHz spectrometers equipped with cryogenic probes in the METACyt Biomolecular NMR Laboratory were used to acquire data for $FtsX^{ECL1}$ samples. NMR spectra were referenced to H_2O. NMR data were processed using NMRPipe and was analyzed using Sparky and CcpNmr Analysis. All spectra were acquired at 25 °C. Sequential resonance assignments of $FtsX^{ECL1}$ were obtained using ^1H-^{15}N heteronuclear single quantum coherence (HSQC) spectra, along with triple resonance CBCA(CO)NH, NHCACB, HNCO, HNCA and HN(CO)CA spectra. Automatically backbone assignment server PINE[108] was employed to help with the assignment.

Results

Complete backbone assignments of $FtsX^{ECL1}$ construct

FtsX in involved in cell division complex formation in *S. pneumoniae*. Complete backbone H, N, CO, CA, CB resonance assignments were made for extracellular loop 1 of FtsX ($FtsX^{ECL1}$) by using a series of triple resonance spectra (see methods for details). After obtaining full backbone assignment other than residue N85, Talos+ was used to

predict secondary structure of FtsX^{ECL1} based on chemical shift and structure data in the database (**Fig. 52**).

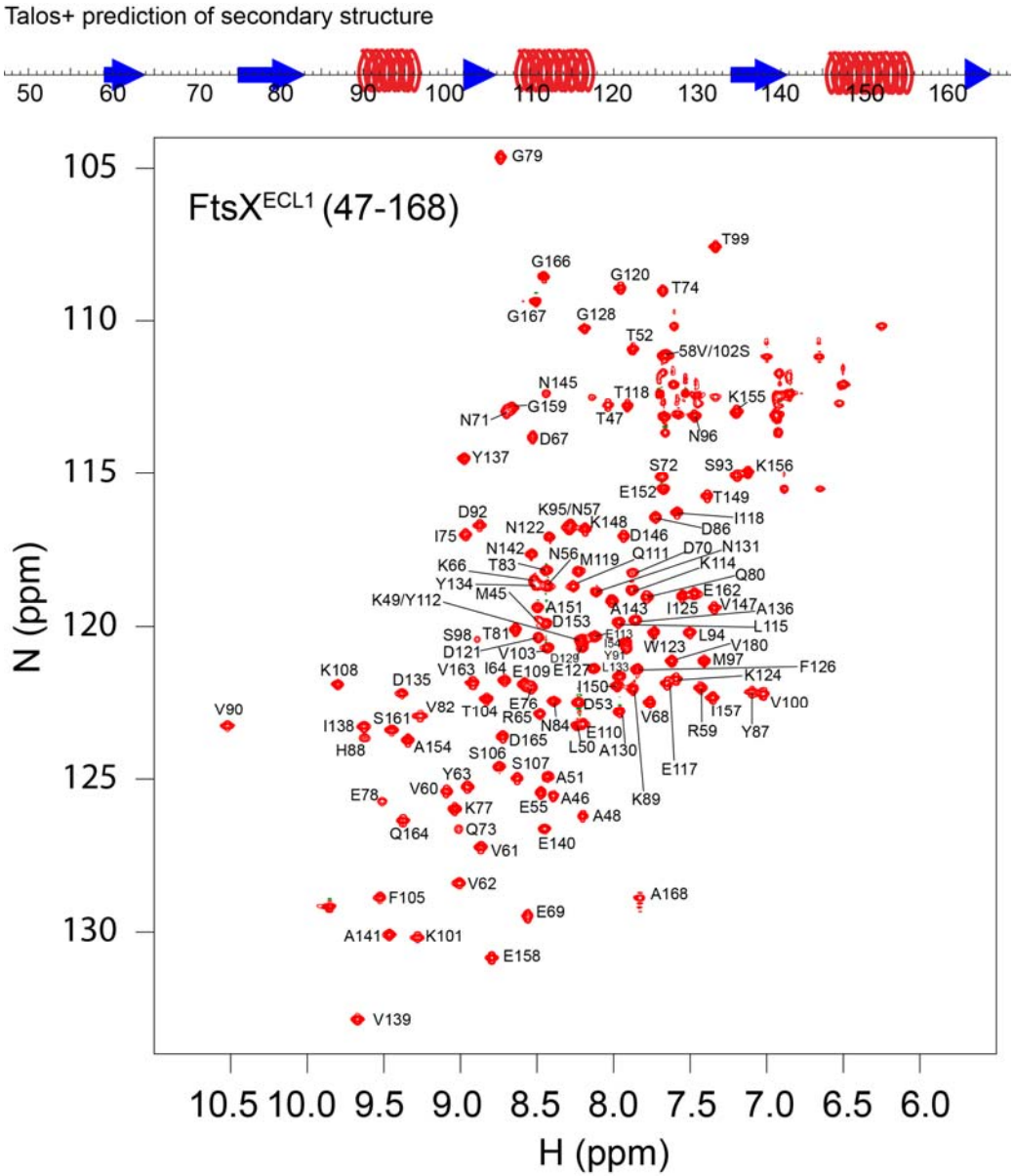

Figure 52: Backbone assignments labeled on ^{1}H, ^{15}N-HSQC spectra of FtsXECL1. Talos+ predicted secondary structure is plotted on the top.

Appendix II Backbone assignments of each metallation states

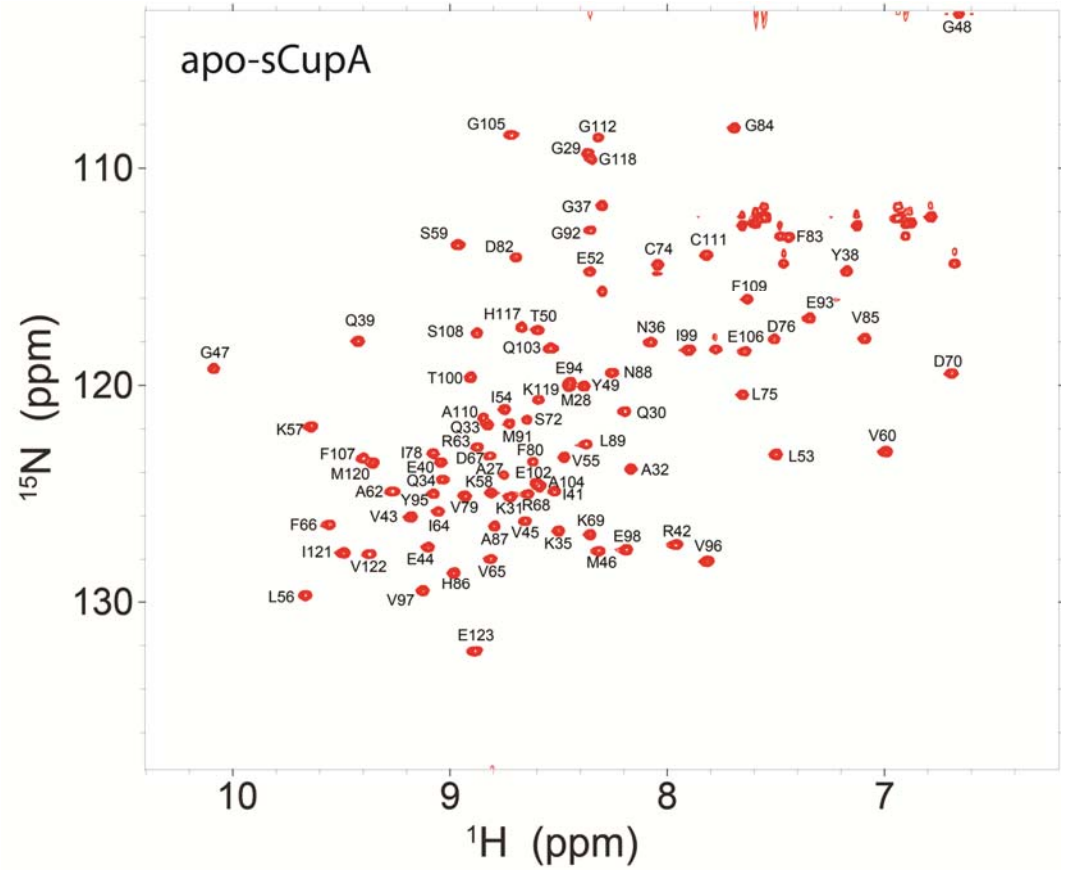

Figure 53: Backbone assignment labeled on ^{1}H, ^{15}N-HSQC spectra of apo-sCupA.

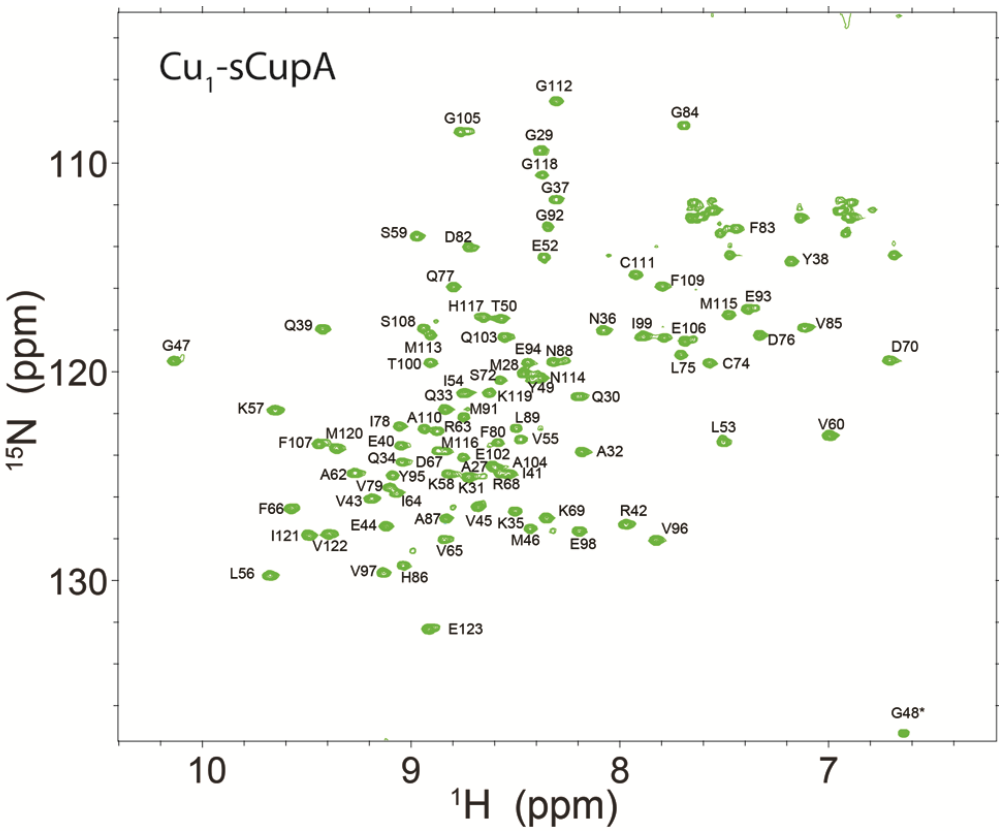

Figure 54: Backbone assignment labeled on ^{1}H, ^{15}N-HSQC spectra of Cu_1-sCupA.

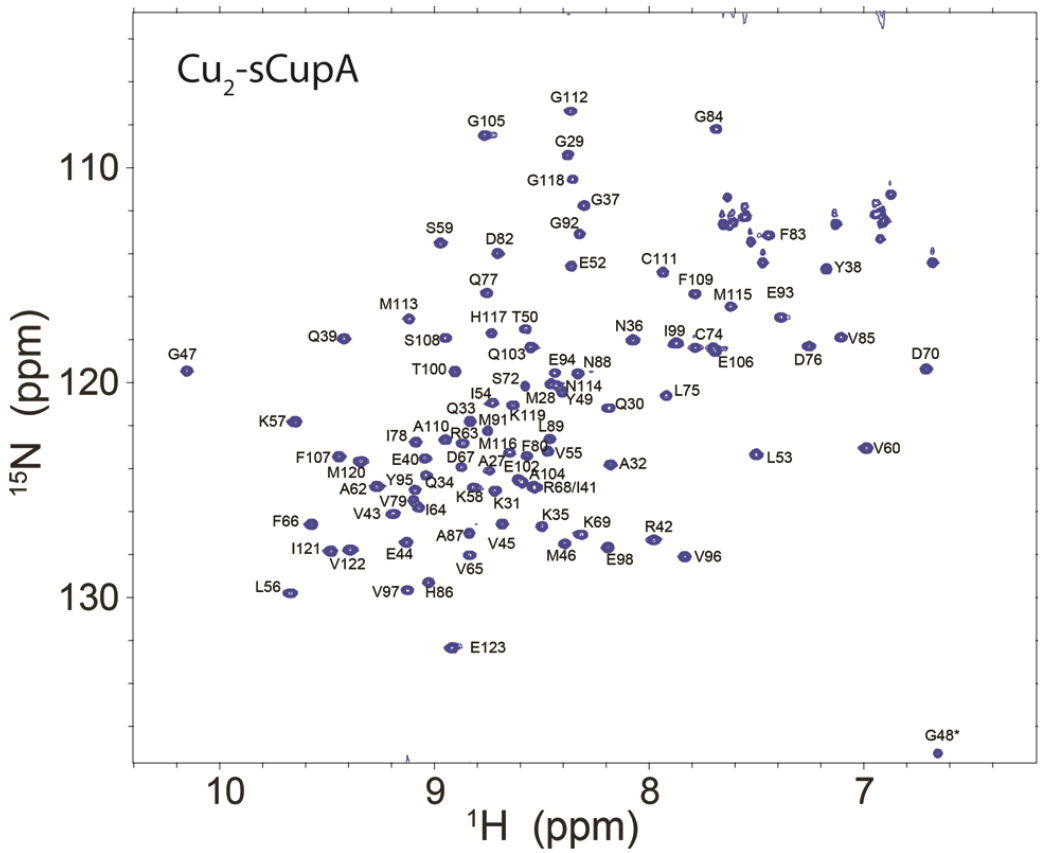

Figure 55: Backbone assignment labeled on ^{1}H, ^{15}N-HSQC spectra of Cu_1-sCupA.

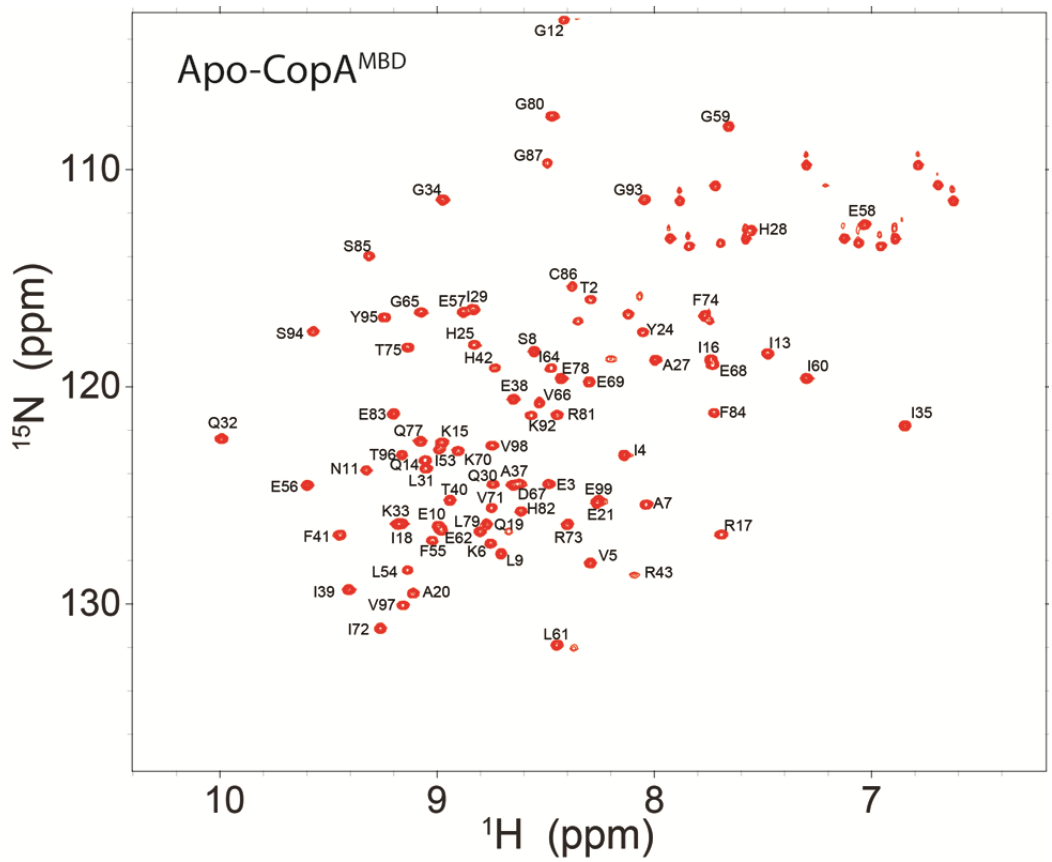

Figure 56: Backbone assignment labeled on ^{1}H, ^{15}N-HSQC spectra of apo-CopA^{MBD}.

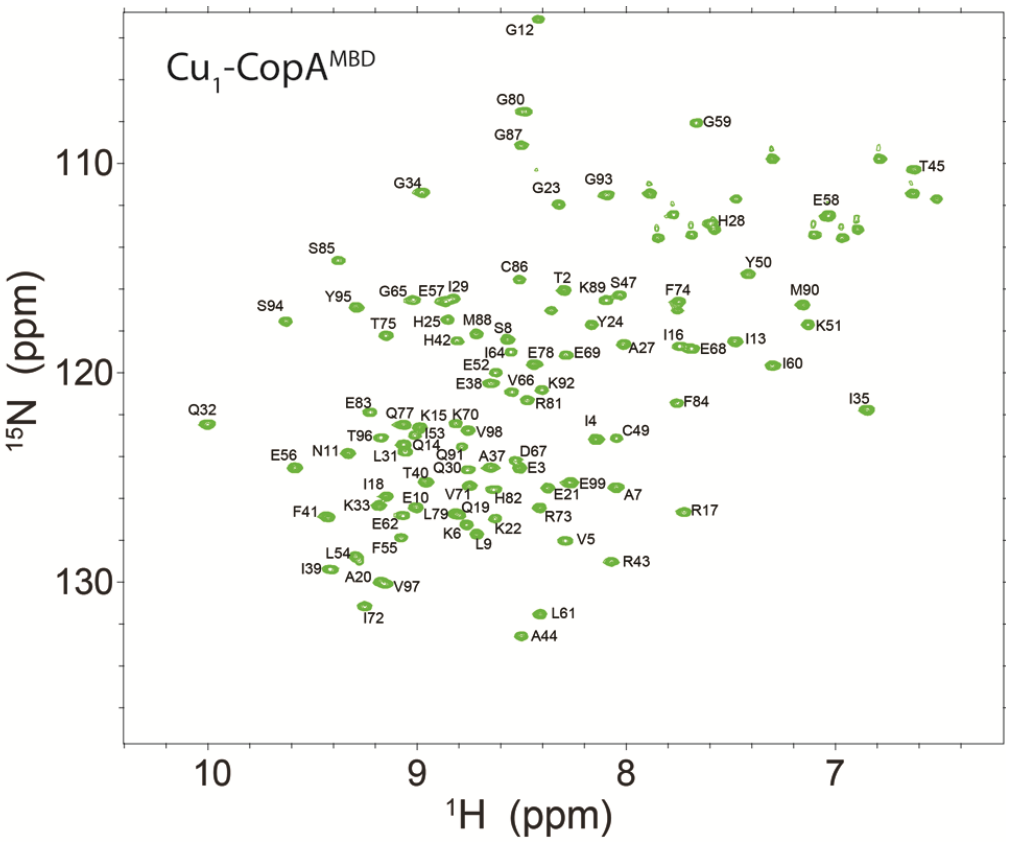

Figure 57: Backbone assignment labeled on ^{1}H, ^{15}N-HSQC spectra of Cu_1-$CopA^{MBD}$.

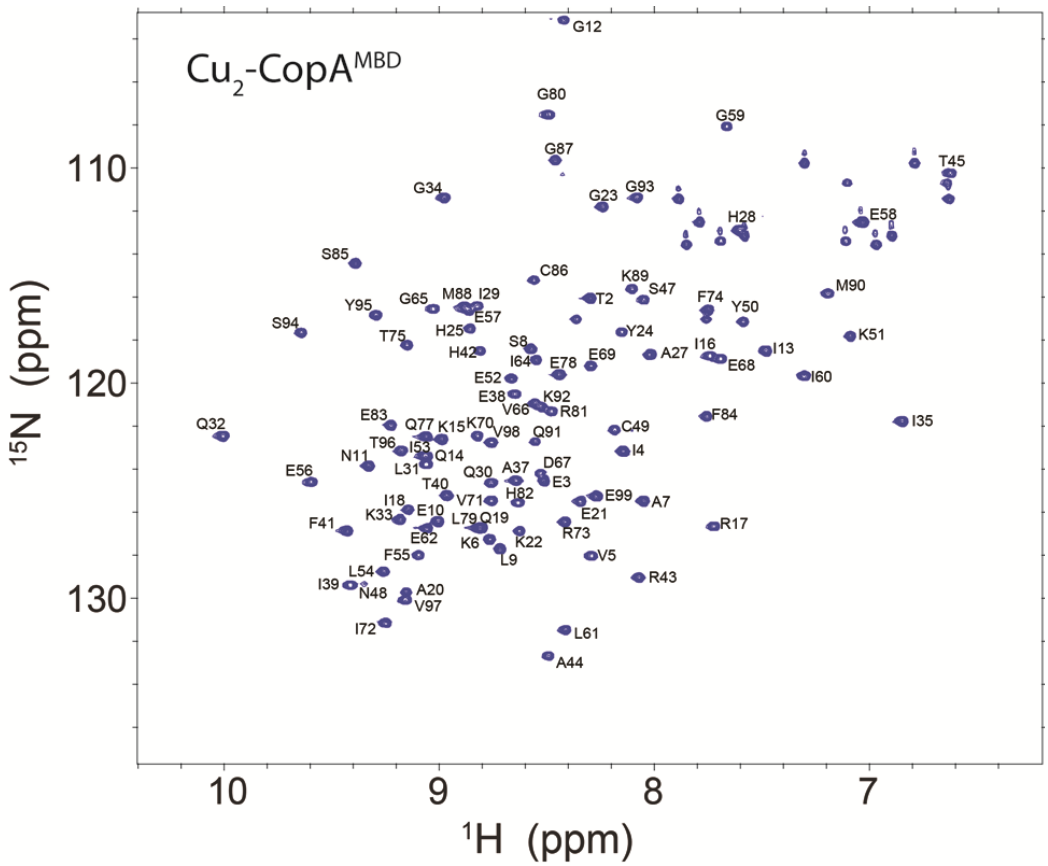

Figure 58: Backbone assignment labeled on ^{1}H, ^{15}N-HSQC spectra of Cu_2-$CopA^{MBD}$.

Appendix III Sample Dyanfit script for Cu(I) binding affinity measurement.

BCA binding experiments

```
[task]
data = equilibria
task = fit
[mechanism]
cupa + cu <==> cupa.cu : k1 assoc.
bca + bca + cu <==> bca2.cu : k2 assoc.
[concentrations]
[constants]
k1 = 1e+3?
k2 = 1.585e+5
[responses]
bca = 5.7e-5?
bca2.cu = 0.0077
[equilibria]
variable cupa
file ./data/CupAC111S/20131010.txt |concentration cu = 21, bca = 50
file ./data/CupAC111S/20131010_30.txt |concentration cu = 30, bca = 70
[output]
directory ./output/CupAC111S/20131010_combine
```

BCS binding experiments

[task]

data = equilibria

task = fit

[mechanism]

cupa + cu <==> cupa.cu : k1 assoc.

bcs + bcs + cu <==> bcs2.cu : k2 assoc.

[concentrations]

cu = 37

bcs = 200?

[constants]

k1 = 1e+7?

k2 = 6.31e+7

[responses]

bcs = 5.7e-5?

bcs2.cu = 0.0135

[equilibria]

variable cupa

file ./data/CupAM113AM115A/20130415.txt

[output]

directory ./output/CupAM113AM115A/20130415

Appendix IV XAS study of Cu(I) coordination geometry

Sample preparation done by Yue Fu. Professor Khadine Higgins performed XAS data reduction and analysis for various metallated sCupA and $CopA^{MBD}$. Heidi Hu from University of Massachusetts, Amherst collected XAS data.

Methods

X-ray Absorption Spectroscopy (XAS) sCupA and MBD were concentrated to 2 mM and 1.2 mM respectively in 25 mM Hepes (pH 7.0) and 200 mM NaCl or NaBr. 0.8 molar equivalent of CuCl or CuBr was added to both MBD and CupA under anaerobic conditions. 30 μL of each sample was syringed into polycarbonate XAS holders that were wrapped in kapton tape and frozen in liquid nitrogen. XAS data were collected at beamline 7-3 at the Stanford Synchrotron Radiation Laboratory (SSRL). Data were collected at 10 K using a liquid helium cryostat (Oxford Instruments). The ring conditions were 3GeV and 80-100mA. Beamline optics consisted of a Si(220) double-crystal monochromator and two rhodium-coated mirrors. X-ray fluorescence was collected using a 30-element Ge detector (Canberra). Scattering was minimized using Soller slits and placing a Z-1 filter between the sample chamber and the detector. XANES was collected from ± 200 eV relative to the metal edge. The X-ray energy for the Cu metal K_α-edge was internally calibrated to the first inflection point, 8980.3 eV. EXAFS was collected to 15 *k* above the edge energy (E_o).

XAS Data Reduction and Analysis The XAS data shown (*vide infra*) are the average of 8 scans. XAS data was analyzed using SixPack[145]. The SixPack fitting software builds on the ifeffit engine[146,147]. Each data set was background-corrected and normalized. For EXAFS analysis each data set was converted to *k*-space using the relationship

$$k = \left[2m_e(E - E_o)/\hbar^2\right]^{1/2}$$

where m_e is the mass of the electron, $\hbar$ is Plank's constant divided by 2π, and E_o is the threshold energy of the absorption edge. The threshold energy chosen for copper is 8990 eV[148]. The best fits for the data sets were obtained using a Fourier-transform of the data was produced using data over the range k = 2-14 Å^{-1}, where the upper limit was determined by the signal:noise ratio. Scattering parameters were generated using FEFF 8[147]. The first coordination sphere was determined by setting the number of scattering atoms in each shell to integer values and systematically varying the combination of N/O and S-donors. To compare different models of the same data set, ifeffit utilizes three goodness of fit parameters: χ^2, reduced χ^2, and the R-factor. χ^2 is given by equation 1, where N_{idp} is the number of independent data points, N_{ε^2} is the number of uncertainties to minimize, $\mathrm{Re}(f_i)$ is the real part of the EXAFS function, and $\mathrm{Im}(f_i)$ is the imaginary part of the EXAFS fitting function (eq. 1)

$$\chi^2 = \frac{N_{idp}}{N_{\varepsilon^2}} \sum_{i=1}^{N} \left\{ [\mathrm{Re}(f_i)]^2 + [\mathrm{Im}(f_i)]^2 \right\} \qquad (1)$$

Reduced $\chi^2 = \chi^2 / \left(N_{ind} - N_{\mathrm{var}ys}\right)$ where N_{varys} is the number of refining parameters and represents the degrees of freedom in the fit. Additionally ifeffit calculates the R-factor for the fit, which is given by equation 2, and is scaled to the magnitude of the data making it proportional to χ^2 (eq. 2)

$$R = \frac{\sum_{i=1}^{N} \left\{ [\mathrm{Re}(f_i)]^2 + [\mathrm{Im}(f_i)]^2 \right\}}{\sum_{i=1}^{N} \left\{ [\mathrm{Re}(\tilde{x}data_i)]^2 + [\mathrm{Im}(\tilde{x}data_i)]^2 \right\}} \qquad (2)$$

In comparing different models, the R-factor and reduced χ^2 parameter were used to determine which model was the best fit for the data. The R-factor will always generally improve with an increasing number of adjustable parameters, while reduced χ^2 will go through a minimum and then increase, indicating that the model is over fitting the data[149].

Results

The addition of substoichiometric Cu(I) to sCupA and $CopA^{MBD}$ gives rise to Cu(I) near-edge feature in the XANES spectrum whose intensity is consistent with a low-coordination number complex, either *n*=2 or *n*=3 (**Fig. 59**). For Cu_1 $CopA^{MBD}$, a best-fit of the EXAFS spectrum (as judged by minimizing %R, minimizing reduced χ^2, and obtaining acceptable σ^2 values) is a model corresponding to a digonal *bis*-thiolato (2S) complex in NaBr; in NaCl, a three-coordinate 2S-Cl^- fit with a long Cu-Cl^- bond (2.42 Å) is the best fit. These data and accompanying Cu(I)-S^- bond distances (2.18 Å) are consistent with Cu(I) binding to the two S1 site thiolate ligands Cys49 and Cys86 (**Fig. 59**). For Cu_1 sCupA, the spectra in both NaBr and NaCl are consistent with an *n*=3 complex, with a best fit 2S, 1N/O complex, consistent, for example, with recruitment of a solvent molecule into the anticipated 2S (Cys74, Cys111) complex (**Table 8**). As expected, XAS analysis of a Cu_2 sCupA sample in NaBr gives rise to an average Cu(I) coordination environment that is consistent with the crystal structure, including the presence of bound Br^- anion (**Table 9**).

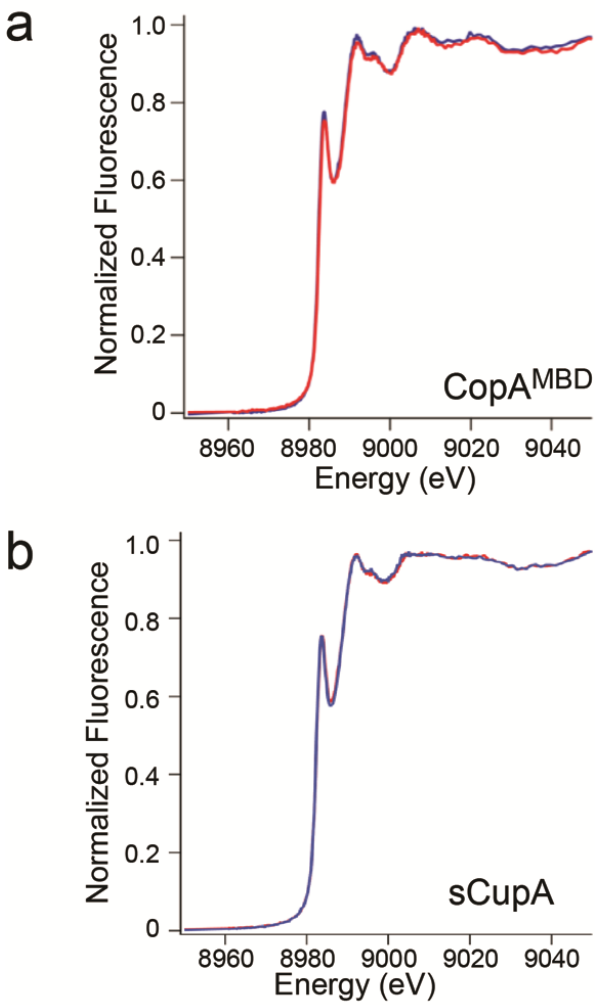

Figure 59: X-ray absorption near-edge spectra (XANES) of sCupA and $CopA^{MBD}$. XANES of Cu_1 $CopA^{MBD}$ (**a**) and Cu_1 sCupA (**b**) in the presence of 0.2 M NaBr (*red trace*) or 0.2 M NaCl (*blue trace*).

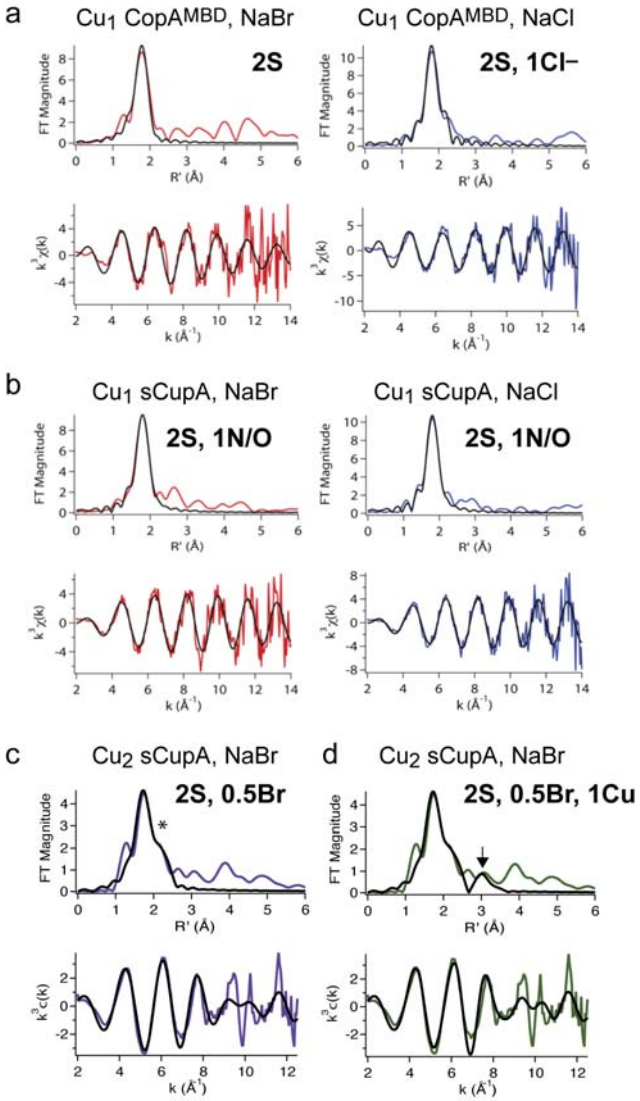

Figure 60: X-ray absorption spectroscopy for $Cu_{0.8}$ $CopA^{MBD}$.
(**a**), $Cu_{0.8}$ sCupA (**b**) and $Cu_{1.8}$ sCupA (**c-d**) in the presence of 0.2 M NaBr or NaCl as indicated, to assess the potential influence of a weakly bound anion (Br^- or Cl^-) on the fits. Both unfiltered k^3-weighted EXAFS spectra and Fourier-transformed EXAFS data are shown (*colored* lines) in addition to best fits to each of coordination model which results the parameters compiled in **Tables 7-9** (*black* lines). The coordination model with the statistically best-fit of the EXAFS data is shown in **bold-face** in each case. XANES spectra for the samples shown in panels a-b are shown in **Fig. 59**. Two fits are shown for $Cu_{1.8}$ sCupA which correspond to the statistically best-fit (**c**) and an alternative fit that includes a Cu-Cu vector at 3.4 Å (**d**). In panel c, the asterisk marks the strong feature associated with Cu-Br^- coordination bond, while in panel d, the arrow marks the fitted Cu–Cu scattering vector (**Table 9**). A significant Cu-Cu interaction can not be unequivocally extracted from these data, given a comparison of the reduced χ^2 values for these two fits (**Table 9**).

Table 7: EXAFS fits for $Cu_{0.8}$-$CopA^{MBD}$.
Data were fit from k = 2-14 $Å^{-1}$ and R = 1–2.5 Å.[a]

	N	r (Å)	σ^2 (x10^{-3} $Å^2$)	ΔE_o (eV)	% R	Reduced χ^2
NaBr	1N/O	2.05(4)	0(3)	8(7)	45.47	25.46
	2N/O	2.06(1)	0(0.1)	10.37(5)	26.76	15.00
	3N/O	2.05(2)	2(2)	7(3)	34.79	22.82
	4N/O	2.04(2)	4(2)	4(3)	49.12	27.50
	1S	2.18(2)	0.7(8)	-2(5)	13.69	7.66
	2S	**2.175(9)**	**3.9(6)**	**-3(2)**	**5.68**	**3.18**
	3S	2.17(2)	7(1)	-5(3)	13.31	7.45
	4S	2.17(2)	9(2)	-6(4)	25.67	14.37
	1S	2.12(2)	1(2)			
	1S	2.22(2)	0.4(2)	-4(3)	5.31	3.93
	2S	2.18(1)	3(1)			
	1N/O	2.2(2)	8(20)	-2(7)	2.30	3.25
	2S	2.18(1)	3.3(5)			
	2N/O	2.2(1)	20(20)	-1(4)	2.21	3.13
	2S	2.18(2)	5(2)			
	1Br	2.26(4)	11(6)	5(2)	4.54	3.36
	2S	2.18(1)	3.9(6)			
	1Br	2.62(4)	13(5)	-3(2)	4.63	3.43
	1N/O	2.01(6)	4(5)			
	1S	2.19(1)	0(1)	1(4)	3.09	4.36
	2N/O	2.0(1)	20(10)			
	1S	2.18(2)	0(0.9)	1(6)	4.76	6.73
	3N/O	2.1(2)	30(20)			
	1S	2.18(2)	0(0.8)	0(9)	6.65	9.40
NaCl	1N/O	2.06(5)	0(4)	9(9)	52.38	62.21
	2N/O	2.08(2)	0(2)	13.75(6)	29.51	35.04
	3N/O	2.08(1)	0.3(11)	9.75(5)	30.77	36.53
	4N/O	2.06(2)	2(2)	6(3)	46.66	55.41
	1S	2.18(2)	0.7(8)	-2(5)	13.69	7.66
	2S	2.177(9)	2.1(5)	-3(2)	6.95	8.26
	3S	2.17(2)	5(1)	-4(3)	19.06	22.63
	4S	2.17(2)	7(2)	-6(4)	34.08	40.47
	1S	2.18(2)	0(0.8)			
	1S	2.3(2)	20(30)	0(9)	8.22	12.91

2S	2.18(1)	2(2)			
1N/O	2.28(8)	0(4)	-3(5)	2.04	6.60
2S	2.180(9)	1(1)			
2N/O	2.21(5)	5(10)	1(4)	2.53	8.19
2S	**2.193(9)**	**1.8(5)**			
1Cl	**2.42(2)**	**6(3)**	**2(2)**	**3.97**	**6.23**
1N/O	2.04(4)	1(7)			
1S	2.18(2)	0(2)	1(4)	2.85	9.22
2N/O	2.04(7)	7(8)			
1S	2.18(1)	0(2)	1(5)	5.52	17.83
3N/O	2.0(1)	10(10)			
1S	2.18(1)	0(1)	1(7)	9.51	30.72

[a]Data collected on samples containing 0.2 M NaBr or 0.2 M NaCl as indicated. The best-fit is shown in *red*, bold-face type.

Table 8: EXAFS fits for $Cu_{0.8}$-sCupA.
Data were fit from k = 2-14 $Å^{-1}$ and R = 1–2.5 Å.[a]

	N	r (Å)	σ^2 (x10^{-3} $Å^2$)	ΔE_o (eV)	% R	Reduced χ^2
NaBr	1N/O	2.05(4)	0(3)	7(8)	45.07	36.95
	2N/O	2.07(1)	0(1)	11.67(5)	20.72	16.99
	3N/O	2.06(1)	1(1)	7(2)	28.36	23.25
	4N/O	2.05(2)	3(2)	5(3)	44.67	36.62
	1S	2.17(1)	0(0.5)	-3(3)	6.47	5.30
	2S	2.170(8)	3.0(4)	-5(2)	4.31	3.54
	3S	2.17(2)	6(1)	-6(3)	15.79	12.95
	4S	2.17(2)	9(2)	-7(4)	30.52	25.02
	1S	2.170(8)	0.5(6)	-6(4)	3.20	3.47
	1S	2.15(7)	9(5)			
	2S	**2.18(1)**	**3(1)**			
	1N/O	**2.29(3)**	**0(2)**	**-5(3)**	**1.90**	**2.06**
	2S	2.18(1)	2.7(4)			
	2N/O	2.24(9)	16(9)	-2(4)	2.50	2.71
	2S	2.173(9)	2.9(5)			
	1Br	2.52(6)	16(7)	-4(2)	4.05	4.39
	1N/O	2.02(4)	2(3)			
	1S	2.19(1)	0.5(8)	1(3)	2.48	2.69
	2N/O	2.09(5)	9(8)			
	1S	2.183(8)	0.4(7)	2(4)	4.38	4.75
	3N/O	2.1(2)	40(30)			
	1S	2.17(2)	0(1)	-1(6)	6.35	6.89
NaCl	1N/O	2.05(5)	0(4)	8(9)	49.22	56.70
	2N/O	2.06(2)	0(1)	7(4)	25.91	29.85
	3N/O	2.07(1)	0(1)	9.15(5)	27.12	31.24
	4N/O	2.06(2)	2(2)	5(3)	44.02	50.71
	1S	2.17(1)	0(1)	-2(3)	6.38	7.35
	2S	2.174(7)	2.4(4)	-4(2)	4.70	5.42
	3S	2.17(2)	5.0(9)	-6(3)	17.27	19.90
	4S	2.17(2)	8(2)	-7(4)	32.60	37.55
	1S	2.18(1)	0(1)			
	1S	2.18(1)	0(1)	-2(8)	4.00	6.09
	2S	**2.186(8)**	**2.4(8)**			
	1N/O	**2.29(3)**	**0(2)**	**-4(2)**	**1.12**	**1.71**

2S	2.184(6)	1.6(7)			
2N/O	2.21(4)	6(6)	0(3)	1.81	2.76
2S	2.185(8)	2.0(4)			
1Cl	2.41(3)	9(4)	-1(2)	3.49	5.32
1N/O	2.04(4)	3(4)			
1S	2.187(8)	0(0.6)	2(3)	1.65	2.52
2N/O	2.07(6)	11(8)			
1S	2.185(8)	0(0.6)	1(2)	3.40	5.18
3N/O	2.07(8)	20(10)			
1S	2.18(1)	0(0.6)	1(5)	6.13	9.34

[a]Data collected on samples containing 0.2 M NaBr or 0.2 M NaCl as indicated. The best-fit is shown in *red*, bold-face type.

Table 9: EXAFS fits for $Cu_{1.8}$-sCupA in 0.2 M NaBr.
Data were fit from k = 2-14 $Å^{-1}$ and R = 1–2.5 Å (*top*) or R = 1–4.0 Å (*bottom*).[a]

	N	r (Å)	σ^2 (x10^{-3} $Å^2$)	ΔE_o (eV)	% R	Reduced χ^2
1–2.5 Å	1N/O	2.11(4)	0(3)	5(6)	41.89	443.21
	2N/O	2.11(3)	4(3)	4(3)	31.41	332.35
	3N/O	2.11(3)	8(4)	3(3)	36.62	387.47
	4N/O	2.10(5)	12(5)	2(3)	48.38	511.87
	1S	2.17(1)	2.25(5)	5(3)	-6(9)	32.93
	2S	2.26(3)	10(2)	-5(4)	17.30	183.04
	3S	2.27(3)	14(2)	-6(4)	15.47	163.69
	4S	2.26(3)	17(2)	-7(4)	19.32	204.41
	1S	2.36(2)	1(2)	-3(3)	8.00	119.95
	1S	2.21(2)	1(1)			
	2S	2.30(6)	13(5)			
	1N/O	2.09(6)	4(6)	0(5)	14.35	215.18
	2S	2.28(5)	11(8)			
	2N/O	2.2(1)	18(76)	0(12)	16.11	241.62
	2S	2.23(2)	8(1)			
	0.5Br	2.49(2)	5(2)	-9(3)	5.84	87.58
	2S	2.21(2)	9(2)			
	1Br	2.48(3)	9(2)	-10(3)	6.51	97.73
	2S	2.09(5)	9(8)			
	2Br	2.183(8)	0.4(7)	-11(4)	7.47	112.07
	1N/O	2.08(3)	0(2)			
	1S	2.35(3)	6(3)	3(3)	11.12	166.73
	2N/O	2.11(8)	9(8)			
	1S	2.31(6)	10(9)	2(5)	19.22	288.13
1-4.0 Å	2S	2.26(2)	10(2)	-6(4)	26.33	114.44
	3S	2.26(2)	13(2)	-6(3)	24.81	120.33
	2S	2.21(2)	8(1)			
	1Br	2.48(2)	9(2)	-10(3)	16.20	89.20
	2S	2.21(2)	8(1)			
	1Br	2.48(3)	9(2)			
	1Cu	3.41(6)	12(6)	-10(3)	15.90	101.24
	2S	**2.23(2)**	**8(1)**			

0.5Br	**2.49(2)**	**4(1)**	**-9(3)**	**14.81**	**81.56**
2S	*2.23(2)*	*8(1)*			
0.5Br	*2.49(2)*	*4(1)*			
1Cu	*3.41(5)*	*12(6)*	*-8(3)*	*14.39*	*91.63*

[a]Data collected on samples containing 0.2 M NaBr or 0.2 M NaCl as indicated. The best-fit is shown in *red*, bold-face type (see **Fig. AIII.2c** for data and fit). An alternative fit with statistics close to the best-fit is highlighted in *green*, italic type (see **Fig. AIII.2d** for data and fit).

Appendix V. Strain used in the work

Table 10: Strain table

Strain number	Genotype (description)[a]	Antibiotic resistance[b]
K643	D39 Δ*cps* Δ*copA*:: P_c-[*kan*^{R}-*rpsL*$^+$] (IU1945 transformed with Δ*copA* :: P_c-[*kan*^{R}-*rpsL*$^+$] amplicon)	Str^S Kan^R
K645	D39 Δ*cps* Δ*cupA*:: P_c-[*kan*^{R}-*rpsL*$^+$] (IU1945 transformed with Δ*cupA* :: P_c-[*kan*^{R}-*rpsL*$^+$] amplicon)	Str^S Kan^R
IU1690	D39 (Single colony isolate of serotype 2 strain encapsulated D39 NCTC 7466)	None
IU1781	D39 *rpsL1* (IU1690 transformed with *pulA-rpsL1-rpsG-fusA* amplicon)	Str^R
IU1945	D39 Δ*cps*	None
IU3525	D39 *rpsL1* Δ*copY*:: P_c-[*kan*^{R}-*rpsL*$^+$] (IU1781 transformed with Δ*copY* :: P_c-[*kan*^{R}-*rpsL*$^+$] amplicon)	Str^S Kan^R
IU3566	D39 *rpsL1* Δ*copY* (IU3525 transformed with Δ*copY* amplicon)	Str^R
IU5921	D39 *rpsL1* Δ*cupA*:: P_c-[*kan*^{R}-*rpsL*$^+$] (IU1781 transformed with Δ*cupA* :: P_c-[*kan*^{R}-*rpsL*$^+$] amplicon from K645)	Str^S Kan^R
IU5923	D39 *rpsL1* Δ*copA*:: P_c-[*kan*^{R}-*rpsL*$^+$] (IU1781 transformed with Δ*copA* :: P_c-[*kan*^{R}-*rpsL*$^+$] amplicon from K643)	Str^S Kan^R
IU5971	D39 *rpsL1* Δ*cupA* (IU5921 transformed with Δ*cupA* amplicon)	Str^R
IU5975	D39 *rpsL1* Δ*copA* (IU5923 transformed with Δ*copA* amplicon)	Str^R
IU6015	D39 *rpsL1 cupA* (C111A; M113A; M115A) ≡ *cupA* (3A) (IU5921 transformed with *cupA* (3A) amplicon)	Str^R
IU6017	*D39 rpsL1* Δ*cupA//*Δ*bgaA′*::P_c-*kan* t1t2-P_{fcsk}-*cupA* (IU5971 transformed with Δ*bgaA′*::P_c-*kan* t1t2-P_{fcsk}-*cupA* amplicon)	Str^R Kan^R
IU6041	D39 *rpsL1 cupA*-(C)-FLAG (IU5921 transformed with *cupA*-(C)-FLAG amplicon)	Str^R
IU6044	D39 *rpsL1 copA*-(C)-FLAG (IU5923 transformed with *copA*-(C)-FLAG amplicon)	Str^R
IU6050	D39 *rpsL1 cupA* (C74S) (IU5921 transformed with *cupA* (C74S) amplicon)	Str^R
IU6052	D39 *rpsL1 cupA* (C74S; C111A; M113A; M115A)) ≡ *cupA* (C74S,3A) (IU5921) transformed with *cupA* (C74S,3A) amplicon)	Str^R
IU6054	D39 *rpsL1 copA* (D442A) (IU5923 transformed with *copA* (D442A) amplicon)	Str^R
IU6084	D39 *rpsL1 cupA* (Δ(2-28)) (IU5921 transformed with *cupA* Δ(2-28) amplicon)	Str^R
IU6086	D39 *rpsL1 cupA* (Δ(2-28)-(C)-FLAG (IU5921 transformed with *cupA* (Δ(2-28)-(C)-FLAG amplicon)	Str^R

IU6210	D39 *rpsL1 cupA* (C74S)-(C)-FLAG (IU5921 transformed with *cupA* (C74S)-(C)-FLAG amplicon)	Str^R
IU6212	D39 *rpsL1 cupA* (3A)-(C)-FLAG (IU5921 transformed with *cupA* (3A)-(C)-FLAG amplicon)	Str^R
IU6215	D39 *rpsL1 cupA* (C74S,3A)-(C)-FLAG (IU5921 transformed with *cupA* (C74S,3A)-(C)-FLAG amplicon)	Str^R
IU6216	D39 *rpsL1* Δ*cupA*-(33-aa remnant)-(C)-FLAG) (IU5921 transformed with Δ*cupA*-(C)-$FLAG^C$ amplicon)	Str^R
IU6240	D39 *rpsL1 copA* (D442A)-(C)-FLAG (IU5923 transformed with *copA* (D442A)-(C)-FLAG amplicon)	Str^R
IU6245	D39 *rpsL1 copA* (C49S)-(C)-FLAG (IU5923 transformed with *copA* (D442A)-(C)-FLAG amplicon)	Str^R
IU6260	D39 *rpsL1* Δ*copA*-(39-aa remnant)-(C)-FLAG (IU5923 transformed with Δ*copA*-(C)-FLAG amplicon)	Str^R
IU6307	D39 *rpsL1 cupA* (C74S) *copA*-(C)-FLAG (IU5923 transformed with *cupA* (C74S) *copA*-(C)- FLAG amplicon)	Str^R
IU6308	D39 *rpsL1* Δ*cupA copA*-(C)-FLAG (IU 5923 transformed with fusion Δ*cupA copA*-(C)-FLAG amplicon)	Str^R
IU6585	D39 *rpsL1 cupA* (M113A; M115A) ≡ *cupA* (2A) (IU5921 transformed with *cupA* (2A) amplicon)	Str^R

All FLAG-tagged fusions ((C)-FLAG) were made to the carboxyl end (C) of reading frames. The amino acid sequence for the FLAG epitope is DYKDDDDK[14,150]. aa = amino acids. [b]Antibiotic resistance markers: Kan^R, kanamycin; Str^R, streptomycin, Concentrations of antibiotics used for *S. pneumoniae* strains: 250 μg Str per mL (Sigma S6501) and 250 μg Kan per mL (Sigma K0254).

Reference

1. Shafeeq, S. *et al.* The cop operon is required for copper homeostasis and contributes to virulence in Streptococcus pneumoniae. *Mol Microbiol* **81,** 1255–1270 (2011).

2. Hatori, Y., Clasen, S., Hasan, N. M., Barry, A. N. & Lutsenko, S. Functional partnership of the copper export machinery and glutathione balance in human cells. *J Biol Chem* **287,** 26678–26687 (2012).

3. Rubino, J. T. & Franz, K. J. Coordination chemistry of copper proteins: how nature handles a toxic cargo for essential function. *J Inorg Biochem* **107,** 129–143 (2012).

4. Tottey, S. *et al.* Protein-folding location can regulate manganese-binding versus copper- or zinc-binding. *Nature* **455,** 1138–1142 (2008).

5. Braymer, J. J. & Giedroc, D. P. Recent developments in copper and zinc homeostasis in bacterial pathogens. *Curr Opin Chem Biol* **19,** 59–66 (2014).

6. Macomber, L., Rensing, C. & Imlay, J. A. Intracellular copper does not catalyze the formation of oxidative DNA damage in Escherichia coli. *J Bacteriol* **189,** 1616–1626 (2007).

7. Imlay, J. A., Chin, S. M. & Linn, S. Toxic DNA damage by hydrogen peroxide through the Fenton reaction in vivo and in vitro. *Science (80-)* **240,** 640–642 (1988).

8. White, C., Lee, J., Kambe, T., Fritsche, K. & Petris, M. J. A role for the ATP7A copper-transporting ATPase in macrophage bactericidal activity. *J Biol Chem* **284,** 33949–33956 (2009).

9. Yoon, B. Y. *et al.* Direct ROS scavenging activity of CueP from Salmonella enterica serovar Typhimurium. *Mol Cells* **37,** 100–108 (2014).

10. Macomber, L. & Imlay, J. A. The iron-sulfur clusters of dehydratases are primary intracellular targets of copper toxicity. *Proc Natl Acad Sci* **106,** 8344–8349 (2009).

11. Chillappagari, S. *et al.* Copper stress affects iron homeostasis by destabilizing iron-sulfur cluster formation in Bacillus subtilis. *J Bacteriol* **192,** 2512–2524 (2010).

12. Azzouzi, A. *et al.* Coproporphyrin III excretion identifies the anaerobic coproporphyrinogen III oxidase HemN as a copper target in the Cu(+)-ATPase mutant copA(-) of Rubrivivax gelatinosus. *Mol Microbiol* **88,** 339–351 (2013).

13. Djoko, K. Y. & McEwan, A. G. Antimicrobial Action of Copper Is Amplified via Inhibition of Heme Biosynthesis. *ACS Chem Biol* **8,** 2217–2223 (2013).

14. Ramos-Montanez, S., Kazmierczak, K. M., Hentchel, K. L. & Winkler, M. E. Instability of ackA (acetate kinase) mutations and their effects on acetyl phosphate and ATP amounts in Streptococcus pneumoniae D39. *J Bacteriol* **192,** 6390–6400 (2010).

15. Lutsenko, S. Human copper homeostasis: a network of interconnected pathways. *Curr Opin Chem Biol* **14,** 211–217 (2010).

16. Lee, J., Pena, M. M., Nose, Y. & Thiele, D. J. Biochemical characterization of the human copper transporter Ctr1. *J Biol Chem* **277,** 4380–4387 (2002).

17. Aller, S. G. & Unger, V. M. Projection structure of the human copper transporter CTR1 at 6-A resolution reveals a compact trimer with a novel channel-like architecture. *Proc Natl Acad Sci U S A* **103,** 3627–3632 (2006).

18. Tsigelny, I. *et al.* An All-Atom Model of the Structure of Human Copper Transporter 1. *Cell Biochem Biophys* **63,** 223–234 (2012).

19. Xiao, Z., Loughlin, F., George, G. N., Howlett, G. J. & Wedd, A. G. C-terminal domain of the membrane copper transporter Ctr1 from Saccharomyces cerevisiae binds four Cu(I) ions as a cuprous-thiolate polynuclear cluster: sub-femtomolar Cu(I) affinity of three proteins involved in copper trafficking. *J Am Chem Soc* **126,** 3081–3090 (2004).

20. Xiao, Z. & Wedd, A. G. A C-terminal domain of the membrane copper pump Ctr1 exchanges copper(i) with the copper chaperone Atx1. *Chem Commun* 588–589 (2002). doi:10.1039/B111180A

21. Maryon, E. B., Molloy, S. A., Ivy, K., Yu, H. & Kaplan, J. H. Rate and regulation of copper transport by human copper transporter 1 (hCTR1). *J Biol Chem* **288,** 18035–18046 (2013).

22. Rae, T. D., Schmidt, P. J., Pufahl, R. A., Culotta, V. C. & V. O'Halloran, T. Undetectable Intracellular Free Copper: The Requirement of a Copper Chaperone for Superoxide Dismutase. *Science (80-)* **284,** 805–808 (1999).

23. Anastassopoulou, I. *et al.* Solution Structure of the Apo and Copper(I)-Loaded Human Metallochaperone HAH1†. *Biochemistry* **43,** 13046–13053 (2004).

24. Ralle, M., Lutsenko, S. & Blackburn, N. J. X-ray Absorption Spectroscopy of the Copper Chaperone HAH1 Reveals a Linear Two-coordinate Cu(I) Center Capable of Adduct Formation with Exogenous Thiols and Phosphines. *J Biol Chem* **278,** 23163–23170 (2003).

25. Maryon, E. B. M. S. A. K. J. H. Cellular glutathione plays a key role in copper uptake mediated by human copper transporter 1. *Am J Physiol - Cell Physiol* **304,** C768–C779 (2013).

26. Flores, A. & Unger, V. Atox1 Contains Positive Residues that Mediate Membrane Association and Aid Subsequent Copper Loading. *J Membr Biol* **246,** 903–913 (2013).

27. Banci, L. *et al.* Affinity gradients drive copper to cellular destinations. *Nature* **465,** 645–648 (2010).

28. Xiao, Z. *et al.* Unification of the copper(I) binding affinities of the metallo-chaperones Atx1, Atox1, and related proteins: detection probes and affinity standards. *J Biol Chem* **286,** 11047–11055 (2011).

29. Xiao, Z. & Wedd, A. G. The challenges of determining metal-protein affinities. *Nat Prod Rep* **27,** 768–789 (2010).

30. Eisses, J. F. & Kaplan, J. H. The mechanism of copper uptake mediated by human CTR1: a mutational analysis. *J Biol Chem* **280,** 37159–37168 (2005).

31. Wolschendorf, F. *et al.* Copper resistance is essential for virulence of Mycobacterium tuberculosis. *Proc Natl Acad Sci U S A* **108,** 1621–1626 (2011).

32. Cavet, J. S., Borrelly, G. P. & Robinson, N. J. Zn, Cu and Co in cyanobacteria: selective control of metal availability. *FEMS Microbiol Rev* **27,** 165–181 (2003).

33. Cha, J. S. & Cooksey, D. A. Copper Hypersensitivity and Uptake in Pseudomonas syringae Containing Cloned Components of the Copper Resistance Operon. *Appl Env Microbiol* **59,** 1671–1674 (1993).

34. Arnesano, F., Banci, L., Bertini, I., Mangani, S. & Thompsett, A. R. A redox switch in CopC: an intriguing copper trafficking protein that binds copper(I) and copper(II) at different sites. *Proc Natl Acad Sci U S A* **100,** 3814–3819 (2003).

35. Chillappagari, S., Miethke, M., Trip, H., Kuipers, O. P. & Marahiel, M. A. Copper acquisition is mediated by YcnJ and regulated by YcnK and CsoR in Bacillus subtilis. *J Bacteriol* **191,** 2362–2370 (2009).

36. Dupont, C. L., Grass, G. & Rensing, C. Copper toxicity and the origin of bacterial resistance-new insights and applications. *Metallomics* **3,** 1109–1118 (2011).

37. Chaturvedi, K. S. & Henderson, J. P. Pathogenic adaptations to host-derived antibacterial copper. *Front Cell Infect Microbiol* **4,** 3 (2014).

38. Fang, F. C. Antimicrobial reactive oxygen and nitrogen species: concepts and controversies. *Nat Rev Microbiol* **2,** 820–832 (2004).

39. Gleason, J. E. *et al.* Candida albicans SOD5 represents the prototype of an unprecedented class of Cu-only superoxide dismutases required for pathogen defense. *Proc Natl Acad Sci U S A* **111,** 5866–5871 (2014).

40. Ma, Z., Jacobsen, F. E. & Giedroc, D. P. Coordination chemistry of bacterial metal transport and sensing. *Chem Rev* **109,** 4644–4681 (2009).

41. Ramos, J. L. *et al.* The TetR family of transcriptional repressors. *Microbiol Mol Biol Rev* **69,** 326–356 (2005).

42. Yu, Z., Reichheld, S. E., Savchenko, A., Parkinson, J. & Davidson, A. R. A comprehensive analysis of structural and sequence conservation in the TetR family transcriptional regulators. *J Mol Biol* **400,** 847–864 (2010).

43. Ellison, D. W. & Miller, V. L. Regulation of virulence by members of the MarR/SlyA family. *Curr Opin Microbiol* **9,** 153–159 (2006).

44. Schell, M. A. Molecular biology of the LysR family of transcriptional regulators. *Annu Rev Microbiol* **47,** 597–626 (1993).

45. Wang, Y., Hemmingsen, L. & Giedroc, D. P. Structural and functional characterization of Mycobacterium tuberculosis CmtR, a PbII/CdII-sensing SmtB/ArsR metalloregulatory repressor. *Biochemistry* **44,** 8976–8988 (2005).

46. Changela, A. *et al.* Molecular basis of metal-ion selectivity and zeptomolar sensitivity by CueR. *Science (80-)* **301,** 1383–1387 (2003).

47. Strausak, D. & Solioz, M. CopY is a copper-inducible repressor of the Enterococcus hirae copper ATPases. *J Biol Chem* **272,** 8932–8936 (1997).

48. Liu, T. *et al.* CsoR is a novel Mycobacterium tuberculosis copper-sensing transcriptional regulator. *Nat Chem Biol* **3,** 60–68 (2007).

49. Chang, F. M. *et al.* Cu(I)-mediated Allosteric Switching in a Copper-sensing Operon Repressor (CsoR). *J Biol Chem* **289,** 19204–19217 (2014).

50. Brown, N. L., Stoyanov, J. V, Kidd, S. P. & Hobman, J. L. The MerR family of transcriptional regulators. *FEMS Microbiol Rev* **27,** 145–163 (2003).

51. Frantz, B. & O'Halloran, T. V. DNA distortion accompanies transcriptional activation by the metal-responsive gene-regulatory protein MerR. *Biochemistry* **29,** 4747–4751 (1990).

52. Banci, L. *et al.* The Atx1-Ccc2 complex is a metal-mediated protein-protein interaction. *Nat Chem Biol* **2,** 367–368 (2006).

53. Joshi, C. P. *et al.* Direct substitution and assisted dissociation pathways for turning off transcription by a MerR-family metalloregulator. *Proc Natl Acad Sci* **109,** 15121–15126 (2012).

54. Grass, G. & Rensing, C. CueO is a multi-copper oxidase that confers copper tolerance in Escherichia coli. *Biochem Biophys Res Commun* **286,** 902–908 (2001).

55. Mealman, T. D., Blackburn, N. J. & McEvoy, M. M. Metal export by CusCFBA, the periplasmic Cu(I)/Ag(I) transport system of Escherichia coli. *Curr Top Membr* **69,** 163–196 (2012).

56. Gudipaty, S. A. & McEvoy, M. M. The histidine kinase CusS senses silver ions through direct binding by its sensor domain. *Biochim Biophys Acta* **1844,** 1656–1661 (2014).

57. Helbig, K., Bleuel, C., Krauss, G. J. & Nies, D. H. Glutathione and transition-metal homeostasis in Escherichia coli. *J Bacteriol* **190,** 5431–5438 (2008).

58. Potter, A. J., Trappetti, C. & Paton, J. C. Streptococcus pneumoniae uses glutathione to defend against oxidative stress and metal ion toxicity. *J Bacteriol* **194,** 6248–6254 (2012).

59. Cobine, P. *et al.* The Enterococcus hirae copper chaperone CopZ delivers copper(I) to the CopY repressor. *FEBS Lett* **445,** 27–30 (1999).

60. Banci, L., Bertini, I., Del Conte, R., Markey, J. & Ruiz-Dueñas, F. J. Copper Trafficking: the Solution Structure of Bacillus subtilis CopZ†. *Biochemistry* **40,** 15660–15668 (2001).

61. Gonzalez-Guerrero, M. & Arguello, J. M. Mechanism of Cu+-transporting ATPases: soluble Cu+ chaperones directly transfer Cu+ to transmembrane transport sites. *Proc Natl Acad Sci U S A* **105,** 5992–5997 (2008).

62. Banci, L. *et al.* Solution Structures of a Cyanobacterial Metallochaperone: INSIGHT INTO AN ATYPICAL COPPER-BINDING MOTIF. *J Biol Chem* **279,** 27502–27510 (2004).

63. Borrelly, G. P. M. *et al.* A novel copper site in a cyanobacterial metallochaperone. *Biochem J* **378,** 293–297 (2004).

64. Banci, L. *et al.* The delivery of copper for thylakoid import observed by NMR. *Proc Natl Acad Sci* **103,** 8320–8325 (2006).

65. Argüello, J., Eren, E. & González-Guerrero, M. The structure and function of heavy metal transport P1B-ATPases. *BioMetals* **20,** 233–248 (2007).

66. Smith, A. T., Smith, K. P. & Rosenzweig, A. C. Diversity of the metal-transporting P-type ATPases. *J Biol Inorg Chem* (2014). doi:10.1007/s00775-014-1129-2

67. Gourdon, P. *et al.* Crystal structure of a copper-transporting PIB-type ATPase. *Nature* **475,** 59–64 (2011).

68. Argüello, J. M. Identification of Ion-Selectivity Determinants in Heavy-Metal Transport P1B-type ATPases. *J Membr Biol* **195,** 93–108 (2003).

69. Albers, R. W. Biochemical aspects of active transport. *Annu Rev Biochem* **36,** 727–756 (1967).

70. Post, R. L., Hegyvary, C. & Kume, S. Activation by adenosine triphosphate in the phosphorylation kinetics of sodium and potassium ion transport adenosine triphosphatase. *J Biol Chem* **247,** 6530–6540 (1972).

71. Kuhlbrandt, W. Biology, structure and mechanism of P-type ATPases. *Nat Rev Mol Cell Biol* **5,** 282–295 (2004).

72. Padilla-Benavides, T., McCann, C. J. & Argüello, J. M. The Mechanism of Cu+ Transport ATPases: interaction with Cu chaperone and the role of transient metal-binding sties. *J Biol Chem* **288,** 69–78 (2013).

73. Andersson, M. *et al.* Copper-transporting P-type ATPases use a unique ion-release pathway. *Nat Struct Mol Biol* **21,** 43–48 (2014).

74. Gonzalez-Guerrero, M., Eren, E., Rawat, S., Stemmler, T. L. & Arguello, J. M. Structure of the two transmembrane Cu+ transport sites of the Cu+ -ATPases. *J Biol Chem* **283,** 29753–29759 (2008).

75. Franke, S., Grass, G., Rensing, C. & Nies, D. H. Molecular analysis of the copper-transporting efflux system CusCFBA of Escherichia coli. *J Bacteriol* **185,** 3804–3812 (2003).

76. Xue, Y. *et al.* Cu(I) recognition via cation-pi and methionine interactions in CusF. *Nat Chem Biol* **4,** 107–109 (2008).

77. Padilla-Benavides, T., George Thompson, A. M., McEvoy, M. M. & Arguello, J. M. Mechanism of ATPase-Mediated Cu+ Export and Delivery to Periplasmic Chaperones: The Interaction of Escherichia coli CopA and CusF. *J Biol Chem* (2014).

78. Mealman, T. D. *et al.* Interactions between CusF and CusB identified by NMR spectroscopy and chemical cross-linking coupled to mass spectrometry. *Biochemistry* **50,** 2559–2566 (2011).

79. Bagai, I., Rensing, C., Blackburn, N. J. & McEvoy, M. M. Direct Metal Transfer between Periplasmic Proteins Identifies a Bacterial Copper Chaperone†. *Biochemistry* **47,** 11408–11414 (2008).

80. Long, F. *et al.* Crystal structures of the CusA efflux pump suggest methionine-mediated metal transport. *Nature* **467,** 484–488 (2010).

81. Su, C.-C. *et al.* Crystal structure of the CusBA heavy-metal efflux complex of Escherichia coli. *Nature* **470,** 558–562 (2011).

82. Kelly N. Chacon Megan M. McEvoy, Ninian J. Blackburn, T. D. M., Chacón, K. N., Mealman, T. D., McEvoy, M. M. & Blackburn, N. J. Tracking metal ions through a Cu/Ag efflux pump assigns the functional roles of the periplasmic proteins. *Proc Natl Acad Sci U S A* **111,** 15373–15378 (2014).

83. Long, F. *et al.* Structure and mechanism of the tripartite CusCBA heavy-metal efflux complex. *Philos Trans R Soc L B Biol Sci* **367,** 1047–1058 (2012).

84. Hood, M. I. & Skaar, E. P. Nutritional immunity: transition metals at the pathogen–host interface. *Nat Rev Micro* **10,** 525–537 (2012).

85. Kim, D.-K. *et al.* Inverse agonist of estrogen-related receptor γ controls Salmonella typhimurium infection by modulating host iron homeostasis. *Nat Med* **20,** 419–424 (2014).

86. Portmann, R., Poulsen, K., Wimmer, R. & Solioz, M. CopY-like Copper Inducible Repressors are Putative “Winged Helix” Proteins. *BioMetals* **19,** 61–70 (2006).

87. Li, Y. J., Du, J. M., Zhang, P. & Ding, J. P. Crystal structure of human copper homeostasis protein CutC reveals a potential copper-binding site. *J Struct Biol* **169,** 399–405 (2010).

88. Latorre, M., Olivares, F., Reyes-Jara, A., Lopez, G. & Gonzalez, M. CutC is induced late during copper exposure and can modify intracellular copper content in Enterococcus faecalis. *Biochem Biophys Res Commun* **406,** 633–637 (2011).

89. Solioz, M. & Stoyanov, J. V. Copper homeostasis in Enterococcus hirae. *FEMS Microbiol Rev* **27,** 183–195 (2003).

90. Festa, R. A. *et al.* A novel copper-responsive regulon in Mycobacterium tuberculosis. *Mol Microbiol* **79,** 133–148 (2011).

91. Grossoehme, N. *et al.* Control of copper resistance and inorganic sulfur metabolism by paralogous regulators in Staphylococcus aureus. *J Biol Chem* **286,** 13522–13531 (2011).

92. Corbett, D. *et al.* The combined actions of the copper-responsive repressor CsoR and copper-metallochaperone CopZ modulate CopA-mediated copper efflux in the intracellular pathogen Listeria monocytogenes. *Mol Microbiol* **81,** 457–472 (2011).

93. Kazmierczak, K. M., Wayne, K. J., Rechtsteiner, A. & Winkler, M. E. Roles of rel(Spn) in stringent response, global regulation and virulence of serotype 2 Streptococcus pneumoniae D39. *Mol Microbiol* **72,** 590–611 (2009).

94. Jacobsen, F. E., Kazmierczak, K. M., Lisher, J. P., Winkler, M. E. & Giedroc, D. P. Interplay between manganese and zinc homeostasis in the human pathogen Streptococcus pneumoniae. *Metallomics* **3,** 38–41 (2011).

95. Hava, D. L. & Camilli, A. Large-scale identification of serotype 4 Streptococcus pneumoniae virulence factors. *Mol Microbiol* **45,** 1389–1406 (2002).

96. Banci, L. *et al.* A copper(I) protein possibly involved in the assembly of CuA center of bacterial cytochrome c oxidase. *Proc Natl Acad Sci U S A* **102,** 3994–3999 (2005).

97. Williams, P. A. *et al.* The CuA domain of Thermus thermophilus ba3-type cytochrome c oxidase at 1.6 A resolution. *Nat Struct Biol* **6,** 509–516 (1999).

98. Abriata, L. A. *et al.* Mechanism of Cu(A) assembly. *Nat Chem Biol* **4,** 599–601 (2008).

99. Sheffield, P., Garrard, S. & Derewenda, Z. Overcoming Expression and Purification Problems of RhoGDI Using a Family of "Parallel" Expression Vectors. *Protein Expr Purif* **15,** 34–39 (1999).

100. Otwinowski, Z. & Minor, W. Processing of X-ray diffraction data collected in oscillation mode. *Macromol Crystallogr Pt A* **276,** 307–326 (1997).

101. Adams, P. D. *et al.* PHENIX: a comprehensive Python-based system for macromolecular structure solution. *Acta Crystallogr D Biol Crystallogr* **66,** 213–221 (2010).

102. Emsley, P. & Cowtan, K. Coot: model-building tools for molecular graphics. *Acta Crystallogr D Biol Crystallogr* **60,** 2126–2132 (2004).

103. Delaglio, F. *et al.* NMRPipe: A multidimensional spectral processing system based on UNIX pipes. *J Biomol NMR* **6,** 277–293 (1995).

104. T. D. Goddard, D. G. K. Sparky3.

105. Vranken, W. F. *et al.* The CCPN data model for NMR spectroscopy: Development of a software pipeline. *Proteins Struct Funct Bioinforma* **59,** 687–696 (2005).

106. Lescop, E., Rasia, R. & Brutscher, B. Hadamard amino-acid-type edited NMR experiment for fast protein resonance assignment. *J Am Chem Soc* **130,** 5014–5015 (2008).

107. Lescop, E., Schanda, P. & Brutscher, B. A set of BEST triple-resonance experiments for time-optimized protein resonance assignment. *J Magn Reson* **187,** 163–169 (2007).

108. Bahrami, A., Assadi, A. H., Markley, J. L. & Eghbalnia, H. R. Probabilistic interaction network of evidence algorithm and its application to complete labeling of peak lists from protein NMR spectroscopy. *PLoS Comput Biol* **5,** e1000307 (2009).

109. Grzesiek, S., Anglister, J. & Bax, A. Correlation of Backbone Amide and Aliphatic Side-Chain Resonances in 13C/15N-Enriched Proteins by Isotropic Mixing of 13C Magnetization. *J Magn Reson Ser B* **101,** 114–119 (1993).

110. Montelione, G. T., Lyons, B. A., Emerson, S. D. & Tashiro, M. An efficient triple resonance experiment using carbon-13 isotropic mixing for determining sequence-specific resonance assignments of isotopically-enriched proteins. *J Am Chem Soc* **114,** 10974–10975 (1992).

111. Bax, A., Clore, G. M. & Gronenborn, A. M. 1H 1H correlation via isotropic mixing of 13C magnetization, a new three-dimensional approach for assigning 1H and 13C spectra of 13C-enriched proteins. *J Magn Reson* **88,** 425–431 (1990).

112. Kay, L. E., Ikura, M. & Bax, A. Proton-proton correlation via carbon-carbon couplings: a three-dimensional NMR approach for the assignment of aliphatic resonances in proteins labeled with carbon-13. *J Am Chem Soc* **112,** 888–889 (1990).

113. Kuzmic, P. DynaFit--a software package for enzymology. *Methods Enzym* **467,** 247–280 (2009).

114. Rosenzweig, A. C. Copper delivery by metallochaperone proteins. *Acc Chem Res* **34,** 119–128 (2001).

115. Wu, C. C., Rice, W. J. & Stokes, D. L. Structure of a copper pump suggests a regulatory role for its metal-binding domain. *Structure* **16,** 976–985 (2008).

116. Tottey, S. *et al.* Cyanobacterial metallochaperone inhibits deleterious side reactions of copper. *Proc Natl Acad Sci U S A* **109,** 95–100 (2012).

117. Pufahl, R. A. *et al.* Metal ion chaperone function of the soluble Cu(I) receptor Atx1. *Science (80-)* **278,** 853–856 (1997).

118. Badarau, A. & Dennison, C. Thermodynamics of copper and zinc distribution in the cyanobacterium Synechocystis PCC 6803. *Proc Natl Acad Sci U S A* **108,** 13007–13012 (2011).

119. Zaballa, M.-E., Abriata, L. A., Donaire, A. & Vila, A. J. Flexibility of the metal-binding region in apo-cupredoxins. *Proc Natl Acad Sci* **109,** 9254–9259 (2012).

120. Bersch, B. *et al.* Structural and metal binding characterization of the C-terminal metallochaperone domain of membrane fusion protein SilB from Cupriavidus metallidurans CH34. *Biochemistry* **50,** 2194–2204 (2011).

121. Badarau, A. & Dennison, C. Copper Trafficking Mechanism of CXXC-Containing Domains: Insight from the pH-Dependence of Their Cu(I) Affinities. *J Am Chem Soc* **133,** 2983–2988 (2011).

122. Rosenzweig, A. C. & O'Halloran, T. V. Structure and chemistry of the copper chaperone proteins. *Curr Opin Chem Biol* **4,** 140–147 (2000).

123. Banci, L., Bertini, I., Ciofi-Baffoni, S., Del Conte, R. & Gonnelli, L. Understanding copper trafficking in bacteria: interaction between the copper transport protein CopZ and the N-terminal domain of the copper ATPase CopA from Bacillus subtilis. *Biochemistry* **42,** 1939–1949 (2003).

124. Farrow, N. A. *et al.* Backbone Dynamics of a Free and a Phosphopeptide-Complexed Src Homology 2 Domain Studied by 15N NMR Relaxation. *Biochemistry* **33,** 5984–6003 (1994).

125. Dosset, P., Hus, J. C., Blackledge, M. & Marion, D. Efficient analysis of macromolecular rotational diffusion from heteronuclear relaxation data. *J Biomol NMR* **16,** 23–28 (2000).

126. Tugarinov, V. & Kay, L. E. Relaxation Rates of Degenerate 1H Transitions in Methyl Groups of Proteins as Reporters of Side-Chain Dynamics. *J Am Chem Soc* **128,** 7299–7308 (2006).

127. Tugarinov, V., Sprangers, R. & Kay, L. E. Probing Side-Chain Dynamics in the Proteasome by Relaxation Violated Coherence Transfer NMR Spectroscopy. *J Am Chem Soc* **129,** 1743–1750 (2007).

128. Shen, Y., Delaglio, F., Cornilescu, G. & Bax, A. TALOS+: a hybrid method for predicting protein backbone torsion angles from NMR chemical shifts. *J Biomol NMR* **44,** 213–223 (2009).

129. Güntert, P., Mumenthaler, C. & Wüthrich, K. Torsion angle dynamics for NMR structure calculation with the new program Dyana. *J Mol Biol* **273,** 283–298 (1997).

130. Herrmann, T., Güntert, P. & Wüthrich, K. Protein NMR Structure Determination with Automated NOE Assignment Using the New Software CANDID and the Torsion Angle Dynamics Algorithm DYANA. *J Mol Biol* **319,** 209–227 (2002).

131. Schwieters, C. D., Kuszewski, J. J., Tjandra, N. & Marius Clore, G. The Xplor-NIH NMR molecular structure determination package. *J Magn Reson* **160,** 65–73 (2003).

132. Fu, Y. *et al.* A new structural paradigm in copper resistance in Streptococcus pneumoniae. *Nat Chem Biol* **9,** 177–183 (2013).

133. Pan, J. & Carroll, K. S. Chemical biology approaches to study protein cysteine sulfenylation. *Biopolymers* **101,** 165–172 (2014).

134. Hatori, Y. & Lutsenko, S. An expanding range of functions for the copper chaperone/antioxidant protein Atox1. *Antioxid Redox Signal* **19,** 945–957 (2013).

135. Bhattacharya, A., Tejero, R. & Montelione, G. T. Evaluating protein structures determined by structural genomics consortia. *Proteins* **66,** 778–795 (2007).

136. Huang, Y. J., Powers, R. & Montelione, G. T. Protein NMR recall, precision, and F-measure scores (RPF scores): structure quality assessment measures based on information retrieval statistics. *J Am Chem Soc* **127,** 1665–1674 (2005).

137. Laskowski, R. A., Macarthur, M. W., Moss, D. S. & Thornton, J. M. Procheck - a Program to Check the Stereochemical Quality of Protein Structures. *J Appl Crystallogr* **26,** 283–291 (1993).

138. Lovell, S. C. *et al.* Structure validation by Calpha geometry: phi,psi and Cbeta deviation. *Proteins* **50,** 437–450 (2003).

139. Luthy, R., Bowie, J. U. & Eisenberg, D. Assessment of protein models with three-dimensional profiles. *Nature* **356,** 83–85 (1992).

140. Sippl, M. J. Recognition of errors in three-dimensional structures of proteins. *Proteins* **17,** 355–362 (1993).

141. Cobine, P. A. *et al.* Copper Transfer from the Cu(I) Chaperone, CopZ, to the Repressor, Zn(II)CopY: Metal Coordination Environments and Protein Interactions†. *Biochemistry* **41,** 5822–5829 (2002).

142. Cantini, F., Banci, L. & Solioz, M. The copper-responsive repressor CopR of Lactococcus lactis is a "winged helix" protein. *Biochem J* **417,** 493–499 (2009).

143. Cobine, P. A. *et al.* Copper transfer from the Cu(I) chaperone, CopZ, to the repressor, Zn(II)CopY: Metal coordination environments and protein interactions. *Biochemistry* **41,** 5822–5829 (2002).

144. Brose, J., La Fontaine, S., Wedd, A. G. & Xiao, Z. Redox sulfur chemistry of the copper chaperone Atox1 is regulated by the enzyme glutaredoxin 1, the reduction potential of the glutathione couple GSSG/2GSH and the availability of Cu(I). *Metallomics* **6,** 793–808 (2014).

145. Webb, S. M. SIXpack: a graphical user interface for XAS analysis using IFEFFIT. *Phys Scr* **2005,** 1011 (2005).

146. Zabinsky, S. I., Rehr, J. J., Ankudinov, A., Albers, R. C. & Eller, M. J. Multiple-scattering calculations of x-ray-absorption spectra. *Phys Rev B* **52,** 2995–3009 (1995).

147. Ankudinov, A. L., Ravel, B., Rehr, J. J. & Conradson, S. D. Real-space multiple-scattering calculation and interpretation of x-ray-absorption near-edge structure. *Phys Rev B* **58,** 7565–7576 (1998).

148. Leitch, S., Bradley, M. J., Rowe, J. L., Chivers, P. T. & Maroney, M. J. Nickel-specific response in the transcriptional regulator, Escherichia coli NikR. *J Am Chem Soc* **129,** 5085–5095 (2007).

149. Herbst, R. W. *et al.* Role of conserved tyrosine residues in NiSOD catalysis: a case of convergent evolution. *Biochemistry* **48,** 3354–3369 (2009).

150. Wayne, K. J. *et al.* Localization and cellular amounts of the WalRKJ (VicRKX) two-component regulatory system proteins in serotype 2 Streptococcus pneumoniae. *J Bacteriol* **192,** 4388–4394 (2010).

151. Rowland, J. L. & Niederweis, M. A Multicopper Oxidase Is Required for Copper Resistance in Mycobacterium tuberculosis. *J Bacteriol* **195,** 3724–3733 (2013).

152. Ward, S. K., Abomoelak, B., Hoye, E. A., Steinberg, H. & Talaat, A. M. CtpV: a putative copper exporter required for full virulence of Mycobacterium tuberculosis. *Mol Microbiol* **77,** 1096–1110 (2010).

153. Speer, A., Rowland, J. L., Haeili, M., Niederweis, M. & Wolschendorf, F. Porins Increase Copper Susceptibility of Mycobacterium tuberculosis. *J Bacteriol* **195,** 5133–5140 (2013).

154. Shi, X. *et al.* The Copper-Responsive RicR Regulon Contributes to Mycobacterium tuberculosis Virulence. *MBio* **5,** (2014).

155. Zhang, L., Koay, M., Maher, M. J., Xiao, Z. & Wedd, A. G. Intermolecular transfer of copper ions from the CopC protein of Pseudomonas syringae. Crystal structures of fully loaded Cu(I)Cu(II) forms. *J Am Chem Soc* **128,** 5834–5850 (2006).

156. Holm, L. & Rosenstrom, P. Dali server: conservation mapping in 3D. *Nucleic Acids Res* **38,** W545–9 (2010).

157. Kiefer, F., Arnold, K., Kunzli, M., Bordoli, L. & Schwede, T. The SWISS-MODEL Repository and associated resources. *Nucleic Acids Res* **37,** D387–92 (2009).

158. Arnold, K., Bordoli, L., Kopp, J. & Schwede, T. The SWISS-MODEL workspace: a web-based environment for protein structure homology modelling. *Bioinformatics* **22,** 195–201 (2006).

159. Hao, Z. *et al.* The multiple antibiotic resistance regulator MarR is a copper sensor in Escherichia coli. *Nat Chem Biol* **10,** 21–28 (2014).

Curriculum vitae

Yue Fu
Molecular and Cellular Biochemistry Department
Indiana University Bloomington
Bloomington, IN, 47405
Cell (812)606-7643 bionmrFu@gmail.com

EDUCATION

Ph. D in Biochemistry, Indiana University Bloomington, IN, 2009 – Feb, 2015

- Thesis: Copper Resistance Mechanism in *Streptococcus pneumoniae*
- Advisor: Professor and Chair David P. Giedroc

B.S. in Biological Science, University of Science and Technology of China, 2009

- Thesis: Oxidative Stress Response in *Saccharomyces cerevisiae*
- Advisor: Professor Congzhao Zhou

RESEARCH EXPERIENCE

Doctoral Thesis Research, Indiana University Bloomington, IN, 2009 – present

- Identified the first cell membrane–anchored Cu(I) chaperone CupA in bacteria and demonstrated that CupA is obligatory for copper resistance. CupA has two Cu(I) binding sites: S1 site with high affinity for Cu(I) and S2 site with low affinity. The S1 site functions as Cu(I) buffering site, while the S2 site primarily transfers Cu(I) to the Cu(I)-effluxing P_{1B}-type ATPase CopA.
- Using NMR and X-ray crystallography to determine the structures of apo-CupA, Cu(I)-CupA and the metal binding domain of CopA (PDB ID: 2MRY, 4F2E,4F2F), which revealed each protein adopts a common cupredoxin-like fold containing a binuclear Cu(I) cluster that is unprecedented in bacteria.

Graduate Research, Indiana University Bloomington, IN, 2012 – present

- Using NMR to study the dynamics and structure of the extracellular domain of FtsX, which is a transmembrane peptidoglycan hydrolase regulator essential in bacterial cell division.

Undergrad Research, University of Science and Technology of China, 2007 – 2009

- Identified important cysteine residues in peroxiredoxin-1 (Prx1), which is involved in oxidative stress response in *Saccharomyces cerevisiae* using biochemical approaches.

TEACHING EXPERIENCE

Undergraduate Student Mentor, David Giedroc's Lab, IUB, 2013 – 2014

- Overseeing and designing research projects for freshman student

Associate Instructor, Molecular and Cellular Biochemistry Department, IUB, 2013

- B530 Macromolecular Structure and Function (graduate course)

Associate Instructor, Department of Chemistry, IUB, 2011

- C487 Biochemistry Laboratory (upper level undergraduate course)

Associate Instructor, Department of Biology, IUB, 2010

- L313 Cell Biology Laboratory (upper level undergraduate course)

AWARDS AND HONORS

2011 Best Poster Award, Gordon Research Conference: Cell Biology of Metals
2009 - 2010 University Fellowship, Indiana University Bloomington

SPECIAL SKILLS

Molecular Biology: general cloning techniques, PCR, plasmid construction, site directed mutagenesis, western blotting, strain construction using Janus cassette

Bacteria Physiology: growth analysis, glutathione measurement

Protein Expression and Purification: *E.coli* expression system, Waters™ HPLC system, ÄKTA® FPLC system, various affinity tags for purification, ion exchange chromatography, size exclusion chromatography, reverse phase chromatography, control of anaerobic environment for oxygen sensitive proteins

Protein Biochemical Characterization: fluorescence spectrophotometer, UV-VIS, Atomic Absorption Spectrometry, Isothermal Titration Calorimetry(ITC), Mass Spectrometry (LC-ESI MS, MALDI for both proteins and peptides)

Protein NMR: linux working station and Python programming, data collection on Varian DDR 800MHz and 600MHz spectrometers with cryogenic-probes, data analysis using Sparky and CCPNmr analysis, protein dynamic study at various time scale, structure calculation using Cyana, model refinement using NIH-Xplor and PSVS 1.5

Protein X-ray Crystallography: crystal condition screening, diffraction data collection using Rigaku R-AXIS IV+ detector and detector at Advance Light Source in Lawrence Berkley National Laboratory (A.L.S. 4.2.2), phasing, model building and refinement using Pymol, Coot and Phenix

PRESENTATIONS

Oral Seminar

- 246th American Chemical Society National Meeting. (2013) Indianapolis, IN

Poster

- Gordon Research Seminar. (2013) Ventura, CA
- Watanabe Symposium in Chemical Biotechnology. (2012) Bloomington, IN
- Gordon Research Conference. (2011) Newport, RI
- American Chemical Society Central Regional Meeting. (2011) Indianapolis, IN

PUBLICATIONS

Yue Fu, Ho-Ching Tiffany Tsui, Kevin E. Bruce, Lok-To Sham, Khadine A. Higgins, John P. Lisher, Krystyna M. Kazmierczak, Michael J. Maroney, Charles E. Dann III, Malcolm E. Winkler & David P. Giedroc. A new structural paradigm in copper resistance in *Streptococcus pneumoniae. Nature Chemical Biology* 9, 177-183 (2013)

Yue Fu, Feng-Ming Chang & David P. Giedroc. Copper transport and trafficking at the host-pathogen interface. *Accounts of Chemical Research*, Accepted (2014)

Yue Fu, Hongwei Wu, Kevin E. Bruce & David P. Giedroc. Solution structure and functional study of the copper chaperone CupA. In preparation for *ACS Chemical Biology*